EXPERIMENTAL INVESTIGATION OF ENERGY DISSIPATION THROUGH TRIANGULAR SCREENS

A THESIS SUBMITTED TO
THE GRADUATE SCHOOL OF NATURAL AND APPLIED SCIENCES
OF
MIDDLE EAST TECHNICAL UNIVERSITY

BY

ENDAM GÜNGÖR

IN PARTIAL FULFILLMENT OF THE REQUIREMENTS
FOR
THE DEGREE OF MASTER OF SCIENCE
IN
CIVIL ENGINEERING

MAY 2005

Approval of the Graduate School of Natural and Applied Sciences

Prof. Dr. Canan ÖZGEN
Director

I certify that this thesis satisfies all the requirements as a thesis for the degree of Master of Science.

Prof. Dr. Erdal ÇOKÇA
Head of Department

This is to certify that we have read this thesis and that in our opinion it is fully adequate, in scope and quality, as a thesis for the degree of Master of Science.

Prof. Dr. Metin Ger
Co-Supervisor

Assoc. Prof. Dr. Zafer Bozkuş
Supervisor

Examining Committee Members

Prof. Dr. Doğan ALTINBİLEK	(METU, CE)	
Assoc. Prof. Dr. Zafer BOZKUŞ	(METU, CE)	
Prof. Dr. Metin GER	(METU, CE)	
Assist. Prof. Dr. Şahnaz TİĞREK	(METU, CE)	
Dr. Yakup DARAMA	(DSİ)	

I hereby declare that all information in this document has been obtained and presented in accordance with academic rules and ethical conduct. I also declare that, as required by these rules and conduct, I have fully cited and referenced all material and results that are not original to this work.

Name, Last name :Endam GÜNGÖR

Signature :

ABSTRACT

EXPERIMENTAL INVESTIGATION OF ENERGY DISSIPATION THROUGH TRIANGULAR SCREENS

Güngör, Endam
M.Sc., Department of Civil Engineering
Supervisor: Assoc. Prof. Dr. Zafer Bozkuş
Co-Supervisor: Prof. Dr. Metin Ger

May 2005, 82 pages

For the present study, a series of experimental works are executed to dissipate energy through triangular screens. Recent studies have shown that the implementation of the screen for energy dissipation is an effective way to extract out the excessive energy of water downstream of small hydraulic structures located in rivers of relatively negligible sediment content. In the present study, double screen arrangement with a porosity of 40% is used. The inclination angle of the screens is opted as 60 degree. The major parameters for the present study are upstream flow depth, location of the screen together with the supercritical upstream flow Froude number for a range covering from 7.5 to 25.5. The gate opening simulating a hydraulic structure is adjusted with various heights of 1 cm, 1.25 cm, 1.6 cm, 1.7 cm, 2 cm, 2.5 cm, 2.7 cm, 3.2 cm and 3.3 cm during the study. The results of the experiments show that the triangular screen configuration with the same pore geometry has no significant additional contribution on the energy dissipation as compared to vertically placed screens.

Keywords: Screen, energy dissipation, triangular configuration, porosity, hydraulic jump, supercritical flow.

ÖZ

ÜÇGEN ELEKLERLE ENERJİ KIRILIMININ DENEYSEL OLARAK ARAŞTIRILMASI

Güngör, Endam
Yüksek Lisans, İnşaat Mühendisliği Bölümü
Tez Danışmanı: Doç. Dr. Zafer Bozkuş
Yardımcı Tez Danışmanı: Prof. Dr. Metin Ger

Mayıs 2005, 82 sayfa

Bu çalışma için, üçgen eleklerdeki enerji kırılımını göstermek amacıyla bir dizi deney yapılmıştır. Yakın geçmişte yapılan araştırmalar sediment içeriği ihmal edilebilir oranda olan nehirlerdeki küçük hidrolik yapıların mansabında elek kullanılmasının suyun fazla enerjisini sönümlemek için etkili bir yol olduğunu göstermiştir. Bu çalışmada ikili elek düzenlemesi %40'lık boşluk oranıyla kullanılmıştır. Eleklerin eğim açısı 60 derece olarak seçilmiştir. Bu çalışmanın ana parametreleri menba su derinliği, eleğin yeri ve eleğin menbasındaki akımın Froude sayısıdır. Menba akımının Froude sayıları 7.5 ile 25.5 arasında değişmektedir. Araştırma süresince hidrolik bir yapının benzeşimini sağlayan bir kapağın çeşitli açıklık değerleri 1 cm, 1.25 cm, 1.6 cm, 1.7 cm, 2 cm, 2.5 cm, 2.7 cm, 3.2 cm and 3.3 cm olarak kullanılmıştır. Deney sonuçları, üçgen elek geometrisinin aynı boşluk geometrisi uygulandığında dik koyulan eleklere kıyasla, enerji kırılımı üzerine artı bir etkisi olmadığını göstermektedir.

Keywords: Elek, enerji kırılımı, üçgen elek geometrisi, boşluk oranı, hidrolik sıçrama, süperkritik akım

To my mother, Saadet Güngör…

ACKNOWLEDGMENTS

I wish to express my heartfelt gratitude and appreciation to Assoc. Prof. Dr. Zafer Bozkuş for his substantial support, tolerance and guidance during my research and thesis work.

I would like to express my deepest gratitude to Prof. Dr. Metin Ger for his guidance, encouragement and support throughout the entire process of researching and writing this work.

I owe special thanks to Dr. Erhan Karaesmen for his academic and non-academic guidance, trust and genuine concern.

Finally, I would like to express my deepest gratitude to my parents and my sister for their love, sensibility, trust and invaluable support throughout my whole life. I cannot possibly begin to describe how much their love meant to me.

TABLE OF CONTENTS

LIST OF TABLES

LIST OF FIGURES

LIST OF SYMBOLS

A_0	area of Section 0 of the orifice-meter
A_1	area of Section 1 of the orifice-meter
A_2	area of Section 2 of the orifice-meter
C_0	discharge coefficient of the orifice-meter
C_C	contraction coefficient of the orifice-meter
C_V	contraction coefficient of vena contracta
d	gate opening
D	a symbol to denote double screen configuration
D_0	orifice throat diameter
D_1	pipe diameter in which the orifice meter is mounted
D_{hole}	diameters of the screen holes
E_G	energy at section G
Fr_A	Froude number at Section A
Fr_C	Froude number at Section C
Fr_G	Froude number at Section G
g	gravitational acceleration
h_L	head loss through the orifice-meter
k	distance between the screens of the double screen
L	theoretical length of a full jump
p	porosity of the screen
p_1	pressure at Section 1 of the orifice-meter
p_2	pressure at Section 2 of the orifice-meter
Q	flow rate
Q_{ideal}	ideal discharge for the orifice-meter
rms	root mean square
Re	Reynold's number
S	energy dissipated due to screen

t	thickness of the screen
V_1	velocity at Section 1 of the orifice-meter
V_2	velocity at Section 2 of the orifice-meter
V_A	average velocity at Section A
V_C	average velocity at Section C
w	width of the channel
X	distance between the screen and the gate
x	distance from the upstream end of the pseudo-jump to the screen
y_A	water depth at Section A
y_{A2}	conjugate depth of y_A
y_C	water depth at Section C
y_G	water depth at Section G
ΔE_{AB}	energy loss between Sections A and B
ΔE_{AC}	energy loss between Sections A and C
ΔE_{GC}	energy loss between Sections G and C
ΔE_{jA}	energy loss due to a full jump at Section A
ΔE_{jG}	energy loss due to a full jump at Section G
α	a non-dimensional parameter defined in Equation 3.3
β	a non-dimensional parameter defined in Equation 3.2
ϕ	diameter ratio of the Sections 0 and 1 for the orifice-meter
γ	specific weight of water
η_{scr}	screen efficiency
η_{sys}	system efficiency
μ	dynamic viscosity of water
ρ	density of water
θ	inclination angle of screen
T	triangular screen configuration

CHAPTER I

INTRODUCTION

Control of the excessive energy of water downstream of the hydraulic structures is one of the main concerns of hydraulic engineers. To deal with the destructive effects of this excessive energy, flow control structures are used. These flow control structures should be selected properly to dissipate the required amount of energy from the flowing water in order to avoid erosion and scour so the life time of structures to be guarantied. This becomes important when the safety of the structure and the country's economy are considered, especially for developing countries. Stilling basins are the most commonly used control structures. In recent years, an alternative method has been introduced to dissipate the excessive energy of water downstream of small hydraulic structures, that is, the implementation of screens.

Screens or porous baffles have been used in the past for various purposes. The recent studies have shown them to be efficient tools also as an energy dissipator. In order to increase the efficiency, that is, the energy dissipation capability, different models of screens are tested in order to broaden the view on the performance of screens as an alternative method for energy dissipation.

The present study in a way is a continuation of the previous studies on the energy dissipation of different models of screens. This time, laboratory work and analysis have been performed for triangular screens.

Dimensional analysis shows that relative location of the screen, Froude number of the upstream flow, relative thickness of the screen are the major non-dimensional parameters.

For the present study, experiments are conducted according to the non-dimensional parameters specified in dimensional analysis for a range of Froude numbers from 7.5 to 25.5. Double screen arrangement with a porosity of 40% is used. Moreover, the gate opening is adjusted with various heights of 1 cm, 1.25 cm, 1.6 cm, 1.7 cm, 2 cm, 2.5 cm, 2.7 cm, 3.2 cm and 3.3 cm during the study.

In Chapter II, a brief summary of the previous works for different screen configuration as an energy dissipator are presented. In Chapter III, conceptual frame for the present study is introduced. In Chapter IV, the details of the experimental setup and procedure are given. The experimental results with discussions are described in Chapter V. Finally, conclusions of the analysis are drawn in Chapter VI.

CHAPTER II

LITERATURE REVIEW

The most recent studies on the topic of using screen-type energy dissipators downstream of small hydraulic structures are by Rajaratnam and Hurtig (2000), Çakır (2003) and Balkış (2004). The present study, in a way, is a continuation of the studies on the energy dissipation in order to broaden the view on the performance of screens by testing triangular screens' energy dissipative capability. Above mentioned recent studies are summarized below.

The laboratory experiments by Rajaratnam and Hurtig (2000) on the energy dissipation through screens or porous baffles showed that screens with a porosity of 40% could be effective energy dissipators. Two series of experiments were conducted in two different horizontal rectangular channels. They performed the main series of experiments in a horizontal rectangular channel 0.45 m wide, 0.43 m deep, and 6.3 m long. A headtank provided flow with a sharp–edged sluice gate. They controlled the tailwater depth by a tailgate located downstream end of the flume. A second series of experiments was performed in another rectangular channel, 0.305 m wide, 0.7 m deep and 6 m long with a sluice gate fitted with a streamlined bottom to produce a supercritical stream with a depth equal to the gate opening. The overall range of supercritical Froude number covered in both channels was from 4 to 13. The flow leaving the screen was also supercritical with reduced Froude number. The screen was placed perpendicularly across the flume 1.25 m away from the gate. Three types of screen arrangements, namely, double, single and triangular made of hard plastic with approximately square holes (of 5 mm sides) were used. The effect of screens resulted in free hydraulic jumps, forced hydraulic jumps, and in some cases submerged jumps. Results showed that energy dissipation by screens was

larger than that produced by the conventional hydraulic jump at the same Froude number.

Another investigation on the subject was executed by Çakır (2003). A horizontal rectangular channel with the dimensions of 7.5 m length, 29 cm width and 70 cm height was used. A pressurized tank with a sliding gate was used to simulate a small hydraulic structure. The porosity, thickness and location of the screens are the major parameters together with the supercritical upstream flow Froude number ranging from 4 to 18. Vertical screens made of Plexiglas with the porosities of 20%, 40%, 50%, and 60% were used. The location of the screens was arranged up to 100 times the upstream flow depth. The thickness of the screens was also arranged according to the upstream flow depth. This study also showed that screens could be used as effective energy dissipators below hydraulic structures.

A follow up investigation on the subject was performed by Balkış (2004). For this case another parameter, inclination of the screen was introduced. The experiments were executed in the same channel as Çakır's (2003). The thickness, location and inclination of the screens are the major parameters together with the supercritical upstream flow Froude number with a range from 5 to 24. The porosity of the screen used in the experiments was 40%. And the inclinations of the screen were tested at the angles of 60^0, 75^0 and 90^0. The location of the screens was arranged up to 100 times the upstream flow depth. The thickness of the screens was also arranged according to the upstream flow depth. This study showed that inclination of the screens did not have any further positive effect on the energy dissipation compared to vertically placed screens.

Findings of Çakır (2003) were presented by Bozkuş et al. (2004). The conclusions drawn were as follows;

- The porosity of 40% is the optimum porosity for screen-type energy dissipator,

- The system performance, $\Delta E_{GC} / E_{G,}$ increases with increasing Froude number,

where E_G is the total energy just downstream of the gate and ΔE_{GC} is the energy loss between just downstream of the gate and vena contracta point downstream of the screen

- As Froude number increases, system efficiency decreases

- Double screens dissipate more energy than single screens

- Screens were found to be more efficient as energy dissipator than traditional hydraulic jump stilling basins for downstream of small hydraulic structures.

CHAPTER III

CONCEPTUAL FRAME

In the present study, a gate beneath pressurized tank is used to simulate the flow conditions downstream of a small hydraulic structure. The main goal of the study, as stated previously, is to dissipate the excessive energy downstream of small hydraulic structures by using triangular screens as an alternative energy dissipator. No tailwater effect is considered in the present study. Water flows freely subsequent to the impingement on the screen. Therefore, flow remains supercritical even after passing by the screen.

3.1 THEORETICAL ASPECT

Based on the preliminary observations in the experiments two distinct forms of flow behavior upstream of the screens were detected.

The theoretical framework was constructed using those flow forms.

CASE 1:

Placing the screen on the channel may generate a full hydraulic jump having the length L far upstream of the screen, Figure 3.1. For this case, the detailed behavior of flow for upstream of the screens, between the screens and downstream of the screens is given in Figures 3.2 through 3.4.

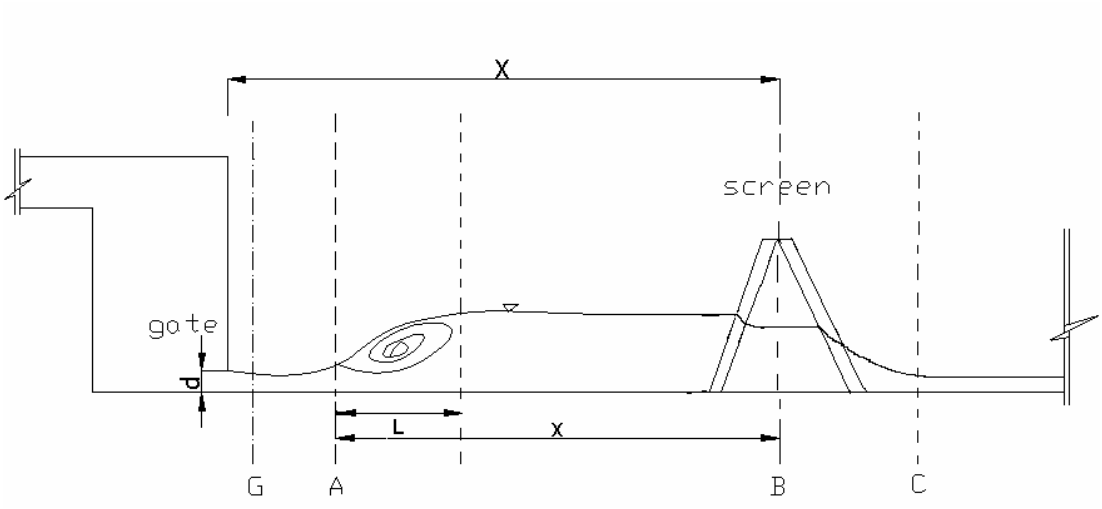

Figure 3.1 General Sketch of the flow for Case 1

Figure 3.2 A view of the upstream flow of Case 1

Figure 3.3 A view of Case 1 at the screen

Figure 3.4 A view of the downstream flow for Case 1

CASE 2:

The screen may lead to a pseudo hydraulic jump, just upstream of the screen, Figure 3.5. That is, a jump occurs at the screen and its length is not enough for the jump to be considered a complete hydraulic jump. Example views for this case are given in Figures 3.6 and 3.7. For this case, energy dissipation turns out to be much higher than the first case. That is, the effectiveness of the screens is much higher in the second case than in the first case. Therefore, the present study focuses mainly on the second case. However, the first case is also included for the completeness of the study.

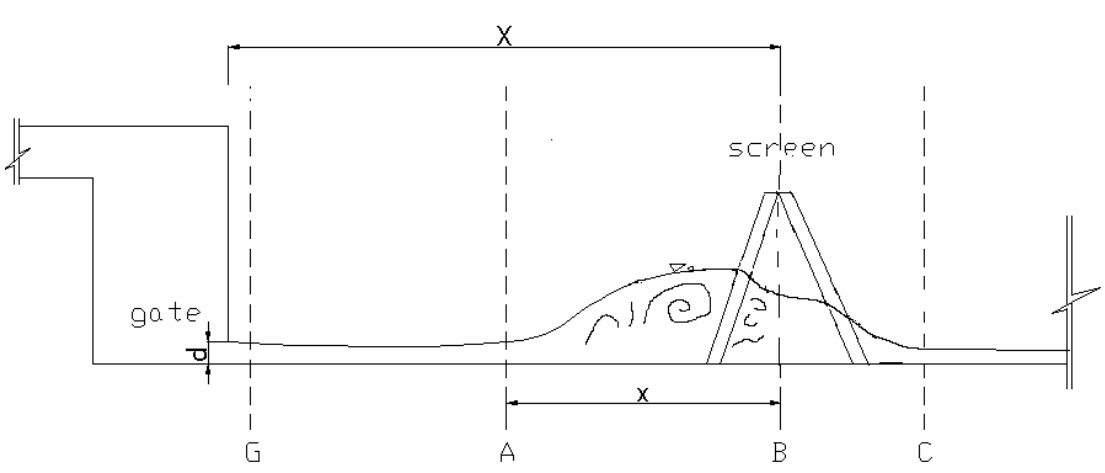

Figure 3.5 General Sketch of the flow for Case 2

Figure 3.6 A view of the upstream flow for Case 2

Figure 3.7 A view of the downstream flow for Case 2

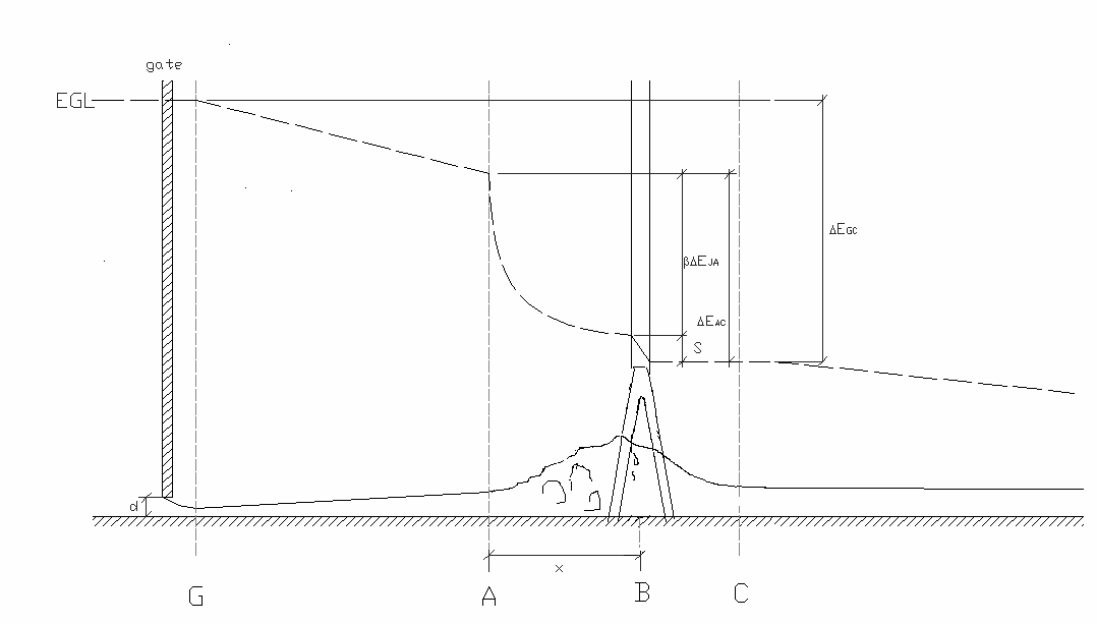

Figure 3.8 Energy loss definitions

The approach employed for the energy loss computations is the same as that of Çakır (2003).

The definition of all the variables involved in the analysis presented below is depicted in Figure 3.8.

The energy loss between section A and the screen is computed by using the below expressions.

$$\Delta E_{AB} = \beta \Delta E_{JA} \tag{3.1}$$

where β was defined by Çakır (2003) as

$$\beta = e^{(1-\frac{1}{\alpha})} \tag{3.2}$$

$$\alpha = \frac{x}{L} \tag{3.3}$$

For L >x, $0<\beta<1$ (3.4)

For L ≤ x, $\beta=1$ (3.5)

The length of a fully formed jump, L, is calculated after French (1986), as

$$L=9.75y_A(Fr_A-1)^{1.01} \tag{3.6}$$

where

$$Fr_A=\frac{V_A}{\sqrt{gy_A}} \tag{3.7}$$

in which y_A, Fr_A, V_A are the flow depth, Froude number and flow velocity respectively at section A and g is the gravitational acceleration. On the other hand, energy loss for a complete hydraulic jump can be expressed by

$$\Delta E_{JA}=(y_A+\frac{V_A^2}{2g})-(y_{A2}+\frac{V_{A2}^2}{2g}) \tag{3.8}$$

where ΔE_{JA} is designated as the energy loss due to a full jump if there were one occurred at section A, y_A is the flow depth at section A, V_A is the velocity at the section A, y_{A2} is the subcritical sequent depth of flow and V_{A2} is the velocity at the section where y_{A2} occurs.

The effectiveness of the screen is analyzed either by calculating the system loss, ΔE_{GC} or by calculating the energy loss through the screen, S. Furthermore, system efficiency η_{sys} and screen efficiency η_{scr} are defined based on those quantities.

The system loss, ΔE_{GC} is calculated, as

$$\Delta E_{GC}=(y_G+\frac{V_G^2}{2g})-(y_C+\frac{V_C^2}{2g}) \tag{3.9}$$

$$y_G=C_V \cdot d \tag{3.10}$$

with C_V=0.625 after Simon (1981)

The energy loss at the screen, S, is calculated, as

$$S=\Delta E_{AC}-\Delta E_{AB} \tag{3.11}$$

that is,

$$S=(y_A+\frac{V_A^2}{2g})-(y_C+\frac{V_C^2}{2g})-\beta\Delta E_{jA} \tag{3.12}$$

where y_C and V_C are the flow depth and velocity respectively at Section C.

Efficiency of the system is calculated as

$$\eta_{sys}=\frac{\Delta E_{GC}-\Delta E_{jG}}{\Delta E_{jG}} \tag{3.13}$$

where ΔE_{JG} is defined as energy loss due to a full jump that could be formed at section G.

Efficiency of the screen is calculated as

$$\eta_{scr}=\frac{S}{\Delta E_{jG}} \tag{3.14}$$

3.2 DIMENSIONAL ANALYSIS

The screen loss, S, as the dependent variable can be expressed as a function of the independent variables in the phenomena as follows:

$$S = f_1(Q, d, w, y_G, y_A, y_C, x, X, p, k, t, g, \rho, \mu, \theta) \tag{3.15}$$

in which

S: the screen loss or the energy head dissipated due to screen, [L],

Q: discharge, [L^3T^{-1}],

d: gate opening, [L],

w: width of the channel, [L],

y_G: water depth at Section G, [L],

y_A: water depth at Section A, [L],

y_C: water depth at Section C, [L],

x: the distance from the upstream end of the pseudo-jump to the screen, [L],

X: distance between the screen and the gate, [L],

p: porosity of the screen,

k: distance between the screens of the double screens, [L],

t: thickness of the screen, [L],

g: gravitational acceleration, [LT^{-2}],

ρ: density of water, [ML^{-3}],

μ: dynamic viscosity of water, [$ML^{-1}T^{-1}$)]

θ: inclination angle,

Recalling the fact that the slug length L and Fr_C, Froude number at section C, are functions of

$$L = f_2(g, w, Q, y_A) \tag{3.16}$$

$$Fr_C = f_3(g, w, Q, y_C) \tag{3.17}$$

Equation 3.15 can be rewritten by replacing y_A and y_C by L and Fr_C respectively.

$$S = f_4(Q, d, w, y_G, L, Fr_C, x, X, p, k, t, g, \rho, \mu, \theta) \tag{3.18}$$

After choosing y_G, g and ρ as repeating variables, the dimensional analysis is performed and following non-dimensional form is obtained:

$$\frac{S}{y_G} = f_5\left(\frac{w}{y_G}, Fr_G, \frac{L}{y_G}, Fr_C, \frac{x}{y_G}, \frac{X}{y_G}, p, \frac{k}{y_G}, \frac{t}{y_G}, \frac{d}{y_G}, Re, \theta\right) \tag{3.19}$$

where Re is the Reynolds number.

In addition, recalling the fact that E_G, energy at section G, having the length dimension is a function of

$$E_G = f_6(g, y_G, d, w, Q) \tag{3.20}$$

After choosing y_G, g as repeating variables, the dimensional analysis is performed and following non-dimensional form is obtained:

$$\frac{E_G}{y_G} = f_7\left(\frac{w}{y_G}, Fr_G, \frac{d}{y_G}\right) \tag{3.21}$$

As seen from equation 3.21, $\frac{E_G}{y_G}$ is a function of $\frac{w}{y_G}$. Therefore, equation 3.19 can be rewritten by replacing $\frac{w}{y_G}$ with $\frac{E_G}{y_G}$

$$\frac{S}{y_G} = f_8(\frac{E_G}{y_G}, Fr_G, \frac{L}{y_G}, Fr_C, \frac{x}{y_G}, \frac{X}{y_G}, p, \frac{k}{y_G}, \frac{t}{y_G}, \frac{d}{y_G}, Re, \theta) \tag{3.22}$$

The above equation can be put in a more convenient form such that

$$\frac{S}{E_G} = f_9(Fr_G, \frac{x}{L}, \frac{X}{d}, \frac{k}{d}, \frac{t}{d}, \left|\theta, p, Fr_C, \frac{E_G}{d}, \frac{x}{d}, C_V, Re\right|) \tag{3.23}$$

in which $\frac{x}{L}$ was defined as α in Equation 3.3.

As Çakır (2003) stated;

"The three of the last five parameters namely Fr_C, $\frac{E_G}{d}$, and $\frac{x}{d}$ are irrelevant to the scope of this study. C_V, which is defined as $\frac{y_G}{d}$ is a constant. As to the *Re*, the magnitude of Fr_G is relatively high in the range covered during the experiments therefore there is no dependence of the flow behavior on the Reynolds number."

In addition, the findings of Rajaratnam and Hurtig (2000) and Çakır (2003) showed that porosity of 40% is the most efficient porosity for screens as an energy dissipator. Therefore, the porosity is dropped out as a variable and 40% of porosity (optimum porosity) is chosen for the present study. Moreover, since Balkış' (2004) study showed that the inclination has no significant effect on energy dissipation, a convenient angle of 60 degree is chosen as the inclination angle. Furthermore, as Çakır's (2003) and Balkış' (2004) studies proved that double screens arrangement

dissipate more energy than single screens, only double screens were used. Thus, p, θ and k can be dropped out of the equation as variables.

Then, equation 3.23 can further be reduced into the following form

$$\frac{S}{E_G} = f_{10}(Fr_G, \alpha, \frac{X}{d}, \frac{t}{d}) \tag{3.24}$$

That is, the present experimental study is carried out by taking into account the following dimensionless parameters: $Fr_G, \alpha, \frac{X}{d}, \frac{t}{d}$.

CHAPTER IV

LABORATORY WORK

In this chapter, the details of the experimental setup and procedure are described in accordance with the conceptual frame.

4.1 EXPERIMENTAL SETUP

The experiments are conducted on a horizontal rectangular channel of 7.5 m long, 29 cm wide and 70 cm deep, details of which are given in Figure 4.1. A constant head tank is used to supply water. A 206 mm inside diameter pipe connected to that tank is utilized to carry water to the pressurized tank having a gate at its bottom. In addition, a valve is placed on the pipe in order to adjust the discharge during the study. For the discharge measurements, an orifice meter is installed on the pipe. Moreover, for flow depth measurements, a mobile point gage is operated. The value of 40% is chosen for the porosity of the screens since Çakır's study proved that 40% is the most efficient porosity of the screens as an energy dissipator. Since Balkış (2004) study showed that there is no significant effect of inclination on the system's energy dissipation and also it is practical and easily constructed, in this study isosceles triangular screens are used. A detailed schematic view of the channel and the setup is shown in Figure 4.1.

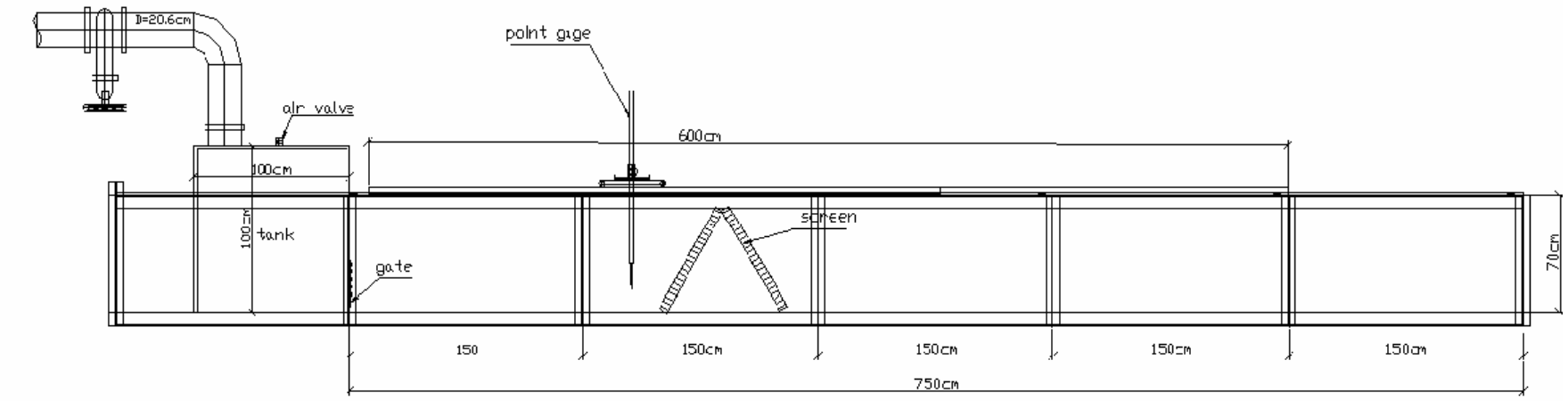

Figure 4.1 Side view of the experimental setup

4.1.1 GATE

The gate located at the bottom of the pressurized tank ensures the upstream supercritical flow conditions necessitated for the study. Froude number range covered during the study is from 7.5 to 25.5. The gate opening is adjusted with various heights of 1 cm, 1.25 cm, 1.6 cm, 1.7 cm, 2 cm, 2.5 cm, 2.7 cm, 3.2 cm and 3.3 cm during the study in order to secure the range wide enough to study effects of *t/d* and *X/d* parameters specified in the dimensional analysis. For calculation of the upstream energy, the point downstream of the gate is employed assuming that there is no energy loss between the exit of the gate (i.e. point G of Figure 3.8) and the point at which the measurements are taken.

4.1.2 SCREENS

The material used for screens is Plexiglas, which is chosen for its easy handling property. The thickness of the screens is 1 cm and they have a porosity of 40%, which is achieved by drilling 1 cm diameter holes arranged with a uniform triangular mesh. During the study, experiments with only double screen arrangement (two screens set so that 2 cm gap between them is formed) are conducted since Balkış (2004) and Çakır(2003) works proved that double screen arrangement dissipates the energy more than single screen arrangement does. For the stability purpose, screens are fixed at the top edges and bottom of the channel by means of screws. In addition, the required inclination was obtained by a simple mechanism, which was manufactured and installed onto the screens. In the present work, by changing the height of gate opening and the location of the screen, the effects of the relative screen position*, X/d,* and the relative screen thickness, *t/d* are examined. The screen configuration is given in Figure 4.2.

4.1.3 ORIFICE METER

An orifice meter whose design is made according to the Institution of Turkish Standards (TSE) specifications is constructed on the pipe serving as a link between the constant head tank and the pressurized tank. A 30 degree inclined

mercury manometer, by the help of which discharge measurements were made, is connected to the orifice meter. The details of TSE requirements are given in Appendix A. A detailed drawing and correction coefficient chart for the orifice meter are also given in Appendix A.

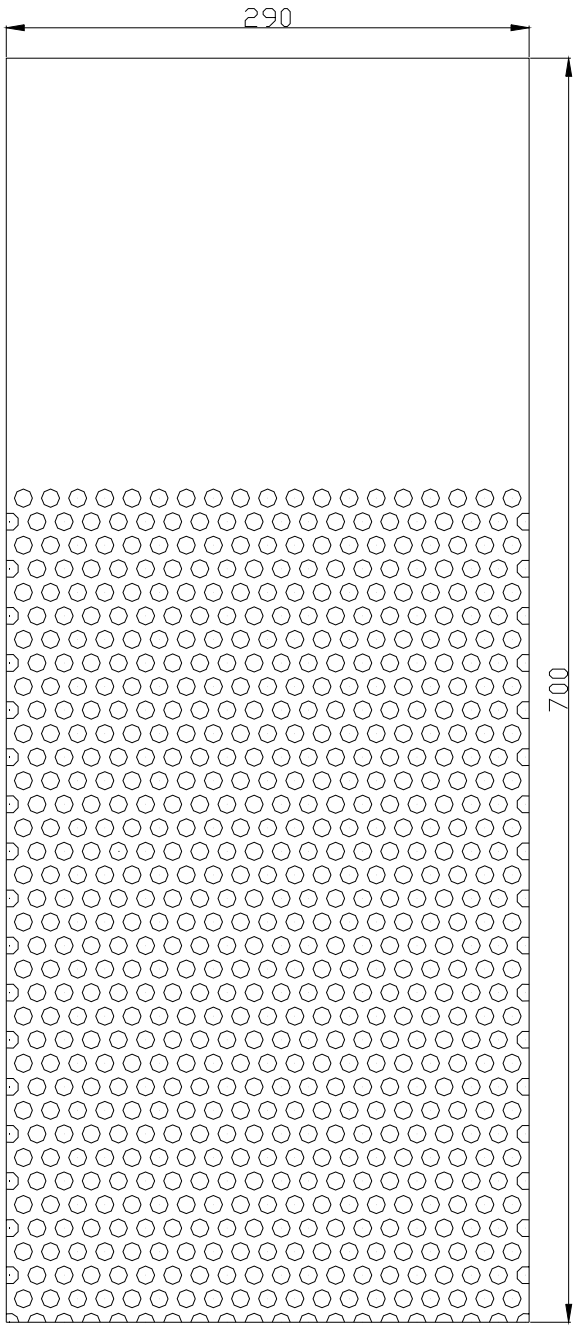

Figure 4.2 Screen with a porosity of 40%

4.2 EXPERIMENTAL PROCEDURE

Table 4.1 shows all of the experimental runs that were performed for the present study to investigate the effects of *X/d* and *t/d* values on the energy dissipation. These particular tests were selected according to all *X/d* and *t/d* combinations that could be achieved in the experimental setup. In Table 4.2, all adjusted values for the height of gate opening and the X distances where the screens were placed in the channel are presented.

Table 4.1a The scope of the experiments (all are in cm)

X	**200**	**250**			
X/d	**200**	**125**	**147**	**200**	**250**
t/d	**4D**	**2D**	**2.35D**	**3.2D**	**4D**

Table 4.1b The scope of the experiments (all are in cm)

X	**400**						**500**					
X/d	**125**	**148**	**200**	**250**	**320**	**400**	**151.5**	**200**	**250**	**312**	**400**	**500**
t/d	**1.25D**	**1.48D**	**2D**	**2.5D**	**3.2D**	**4D**	**1.21D**	**1.6D**	**2D**	**2.5D**	**3.2D**	**4D**

Table 4.2 X values and gate openings (all are in cm)

X	**d=1**	**d=1.25**	**d=1.6, d=1.7**	**d=2**	**d=2.5, d=2.7**	**d=3.2, d=3.3**
200	+					
250	+	+	+	+		
400	+	+	+	+	+	+
500	+	+	+	+	+	+

For each specified set of experiments, the location of the screen is arranged so that desirable *X/d* values are obtained. For a given location of the screen, the height of the gate opening is changed providing proper experiment set and consistent *t/d* values. After the location of the screen and gate opening are fixed, discharge is regulated by means of the valve situated on the supply pipe between the pressure tank and the orifice meter. For each set of experiment, several discharge values are adjusted between possible maximum and minimum discharge values. The maximum discharge value is determined according to the top level of porous section of the screen above which water should not rise. The minimum discharge is the discharge at which the water start to choke the gate. For each discharge value, using the mercury manometer of the orifice meter, differential pressure head readings are taken. Then, the discharge values are calculated by using equation A.2 given in Appendix A using the mercury manometer readings. In addition, for each discharge value, depth measurements are taken on pre-determined sections, namely at G, A and C, by means of a mobile point gage at three points along the width of the channel. The average of these readings is used in the calculations in order to be more accurate. The points A, G and C are determined based on the observation of water surface behavior. Section A is the upstream section of the real or pseudo jump. Point C is the vena contracta point at the downstream section of the screen. As mentioned before, point G is located just downstream of the gate. Namely, for each set of experiment, manometer readings and depth measurements at section A, G and C are taken and all necessary calculations are performed. For the next position of the height of the gate opening, all depth measurements at A, C, and G; manometer readings and all calculations are repeated. Finally, the screen is moved at the next scheduled location. Then, the same procedure is performed at the new location.

CHAPTER V

RESULTS AND DISCUSSIONS

5.1 INTRODUCTION

The results of the experimental study are discussed in this Chapter. The original data are given in Appendix C. The reference key for the presentation of the experimental results of the present study is given below in Table 5.1, in which D implies two screens of 1 cm thick each put together with a 2 cm space between them. The number preceding D is the ratio of total width of two screens with the space between them to the gate opening height.

Table 5.1 Reference key

Reference	θ (degree)	t/d	X/d	Fr_G
90-1D-100-11.15	90	1 (double)	100	11.15
60T-4D-200-20.53	60T (triangular screen)	4 (double)	200	20.53

5.2 PERFORMANCE OF THE SYSTEM

As indicated before the total energy loss between just downstream of the gate (i.e. point G of Figure 3.8) and just downstream of the screen (i.e. point C of Figure 3.8) is denoted as ΔE_{GC}. This energy loss includes the friction losses, losses due to a pseudo or real jump and the screen loss. The relative energy loss defined as $\Delta E_{GC}/E_G$ is used to analyze the system performance. The effects of relative screen thickness, *t/d*; and relative screen position, *X/d* on the system performance are presented in the following figures from 5.1 through 5.9.

5.2.1 PERFORMANCE OF THE SYSTEM AT LARGE

The main goal of the present study is to determine the effects of triangular screens on the energy dissipation. Figures 5.1 through 5.8 are selected to show the variation of $\Delta E_{GC}/E_G$ with Froude number at the downstream of the gate, $Fr_{G,}$. On these figures, the relative energy loss that would occur if there were a conventional hydraulic jump at section G is also drawn as a dotted line.

From the figures, one may discern that

i. All of the tests performed on the triangular screen showed that energy dissipation is always more than that of a classical full jump that would have been forced to occur at the gate.

ii. The relative energy loss, $\Delta E_{GC}/E_G$ increases with increasing Froude number, Fr_G.

iii. There is no apparent dependence observed on the relative screen thickness, *t/d* and on the relative screen position, *X/d.*

In Figure 5.9, best fit curve for the entire data of the present study is shown emphasizing that all of the data exhibit the same trend. The equation of the best fit curve is of the following form obtained with a root mean square (rms) value of 0.021 and a correlation coefficient (r) of 0.998 indicating a good approximation of the data.

$$\frac{\Delta E_{GC}}{E_G} = 0.92 + 0.0019 Fr_G^{\,2} - \frac{9.36}{Fr_G^{\,2}} \qquad (5.1)$$

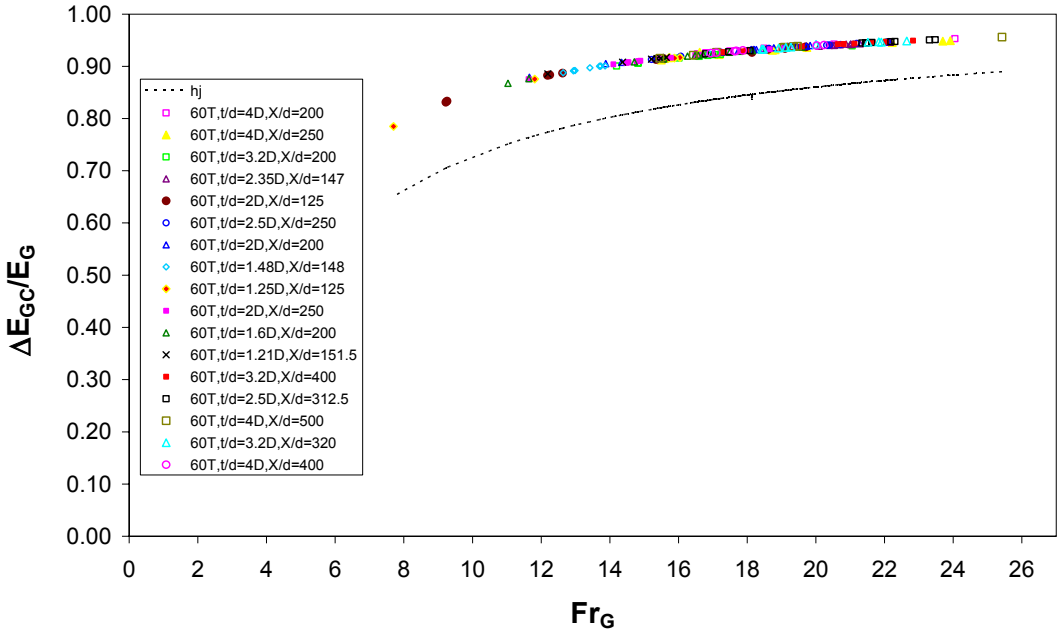

Figure 5.1 $\Delta E_{GC}/E_G$ vs. Fr_G for all of the present data

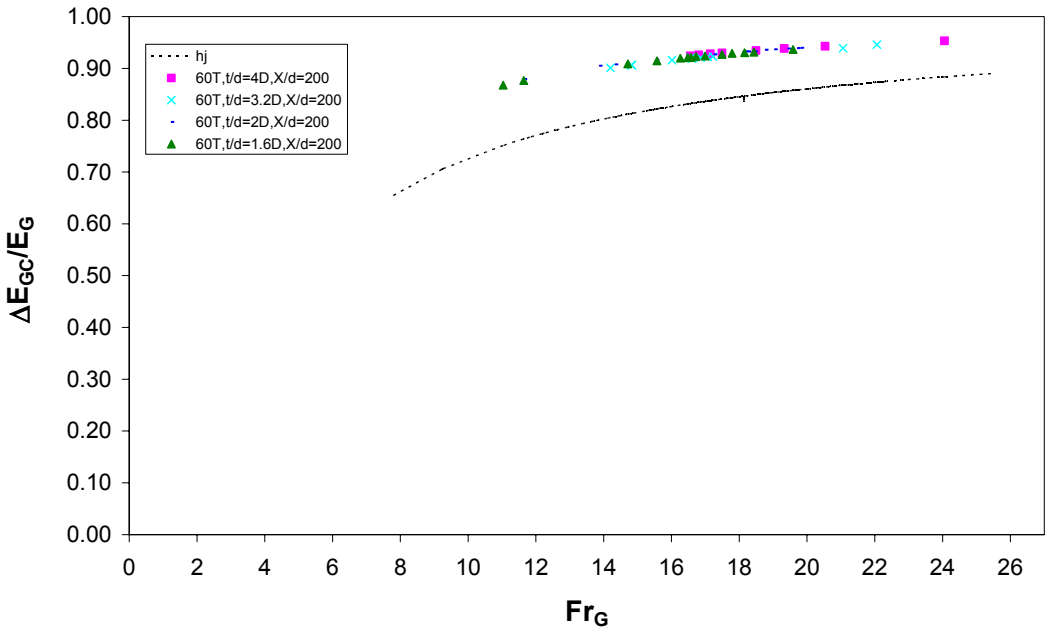

Figure 5.2 $\Delta E_{GC}/E_G$ vs. Fr_G at the relative screen distance of *X/d*=200

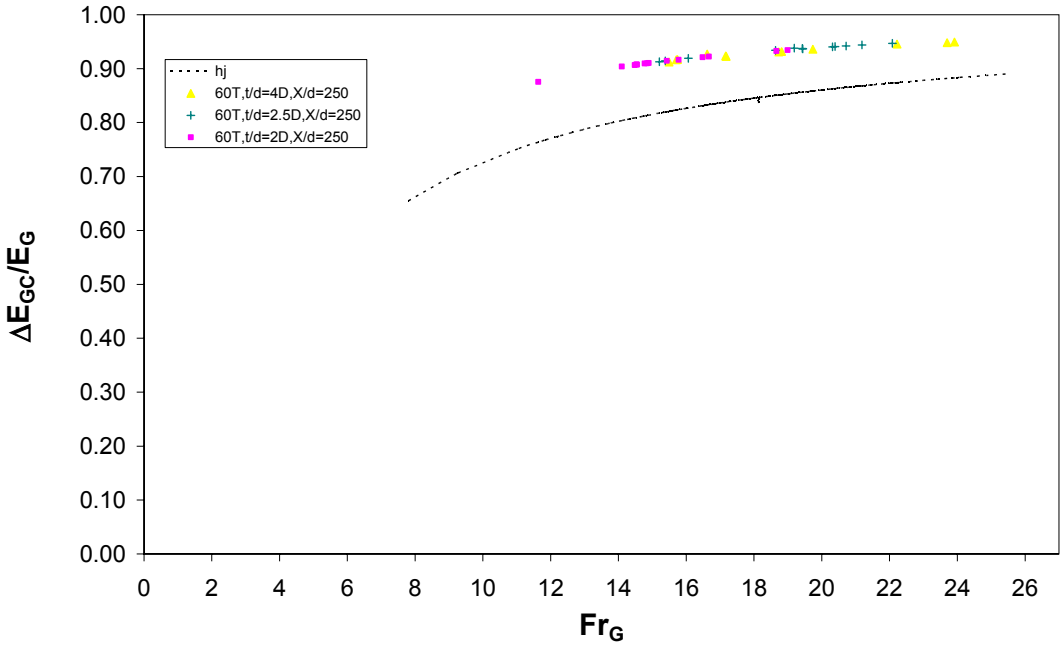

Figure 5.3 $\Delta E_{GC}/E_G$ vs. Fr_G at the relative screen distance of *X/d*=250

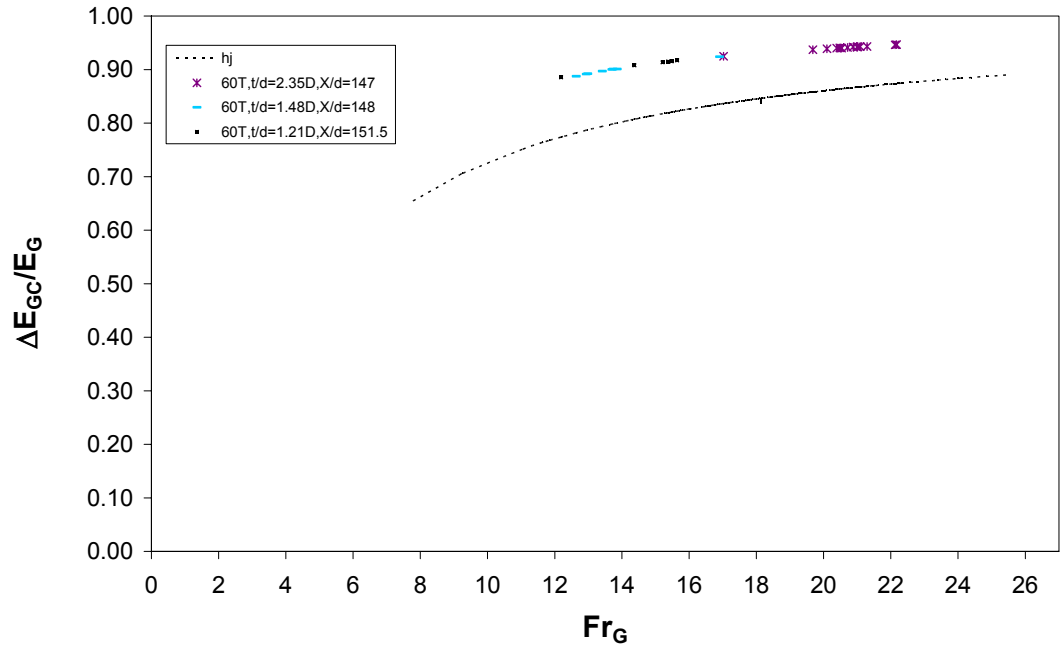

Figure 5.4 $\Delta E_{GC}/E_G$ vs. Fr_G at the relative screen distance of X/d=148

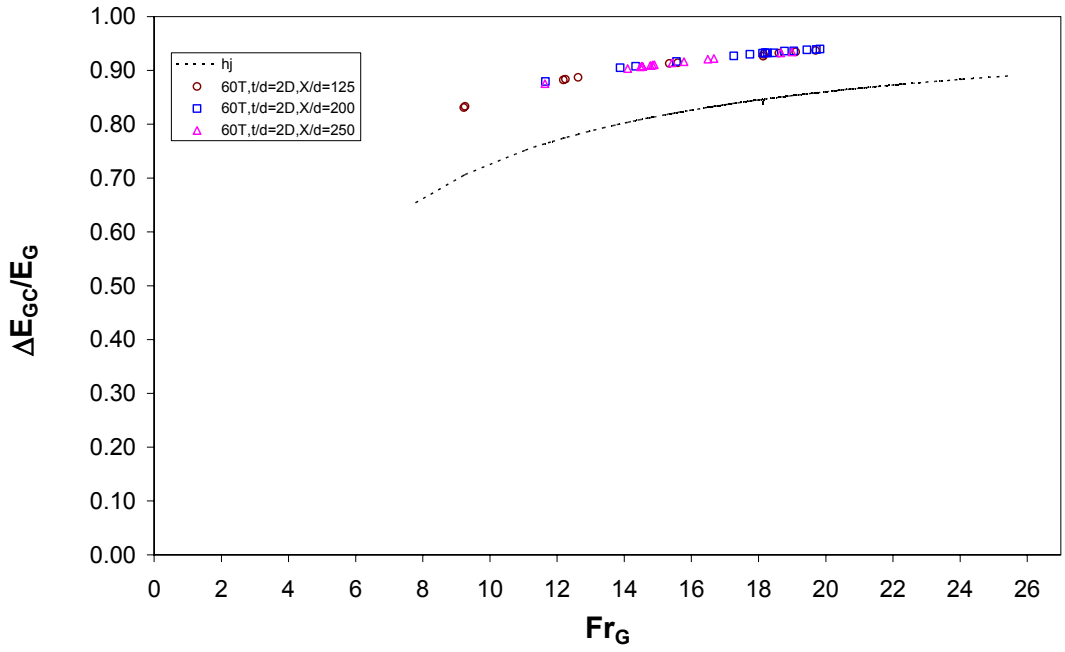

Figure 5.5 $\Delta E_{GC}/E_G$ vs. Fr_G at the relative screen thickness of t/d=2D

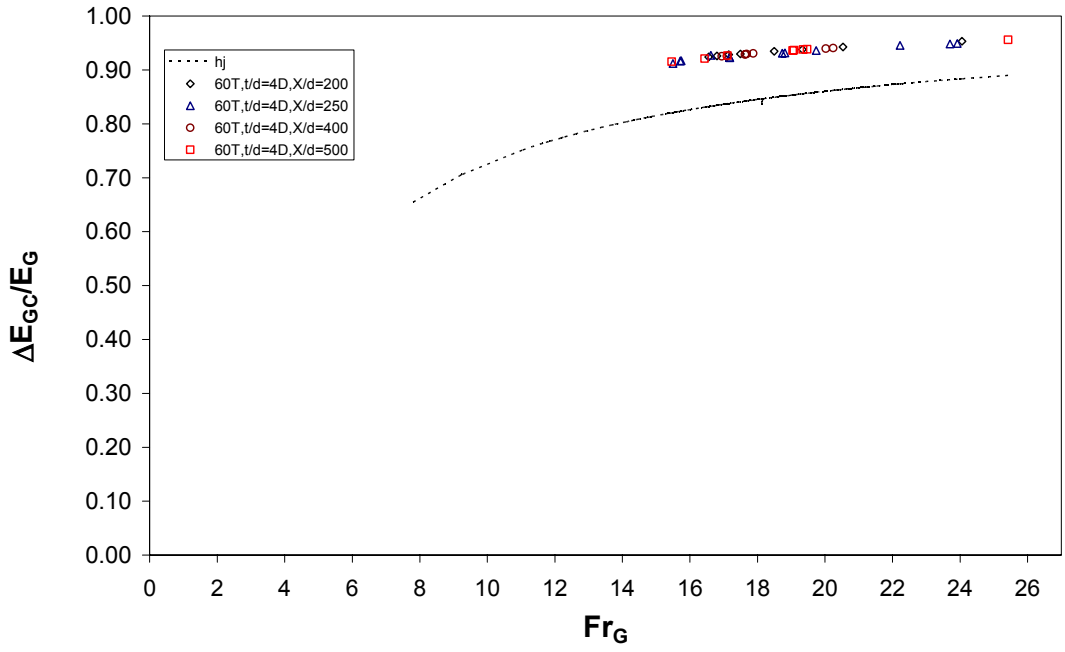

Figure 5.6 $\Delta E_{GC}/E_G$ vs. Fr_G at the relative screen thickness of t/d=4D

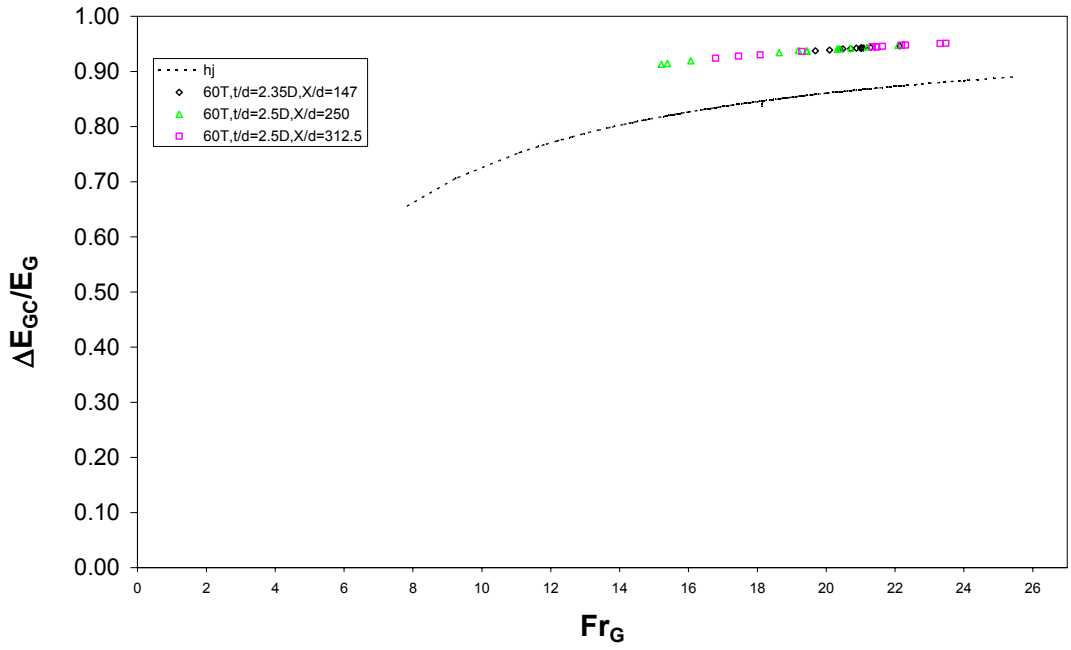

Figure 5.7 $\Delta E_{GC}/E_G$ vs. Fr_G at the relative screen thickness of t/d=2.5D

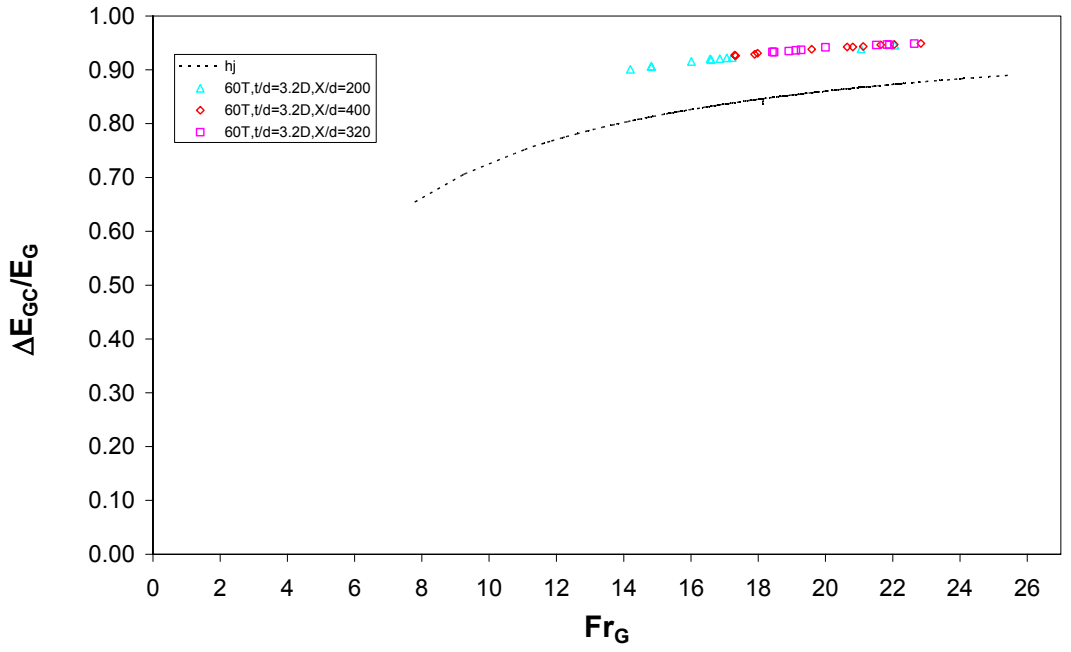

Figure 5.8 $\Delta E_{GC}/E_G$ vs. Fr_G at the relative screen thickness of t/d=3.2D

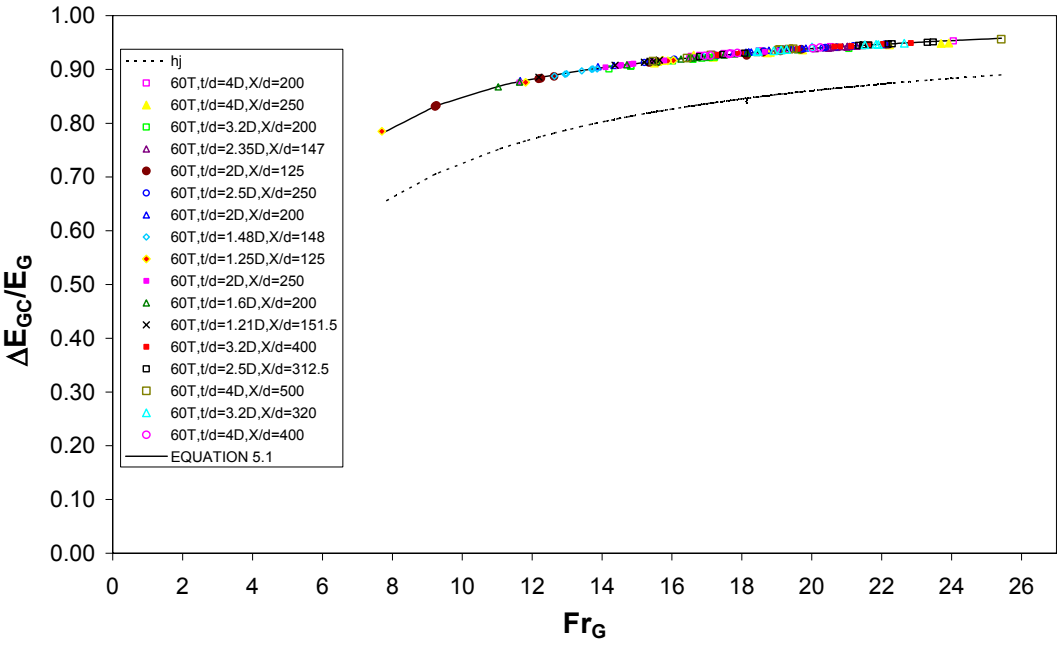

Figure 5.9 $\Delta E_{GC}/E_G$ vs. Fr_G for the entire present data and its best fit curve

5.2.2 COMPARISON OF THE PRESENT DATA WITH THAT OF BALKIŞ, ÇAKIR, AND RAJARATNAM AND HURTIG

Balkış' findings demonstrated that various screens of different inclination angles like 60^0, 75^0 and 90^0 have no significant additional gain on the energy dissipation over vertically placed screens, as depicted in Figure 5.10. Furthermore, both Balkış and Çakır's studies showed that double screens dissipate energy more than single screens. Since the configuration of the triangular screen set-up with 60-degree inclination is practical and easy, in the present study, double screens with 60-degree inclination angle are used. Considering the fact that there is no appreciable differences for *t/d*= 1D, 2D and 1.33D cases on the energy dissipation, as demonstrated in Figure 5.11, and the effects of inclination of the screens are insignificant, all available previous data, data of Rajaratnam and Hurtig (2000), Çakır (2003) and Balkış (2004) are put into Equation 5.1, as depicted in Figure 5.12 in order to show the agreement between the present study and previous work . The rms value of the data of all the previous study turns out to be equal to 0.133 and the

correlation coefficient of all the previous data with that of the present work is r= 0.987. This finding manifests the agreement between the present data and the previous studies performed by Rajaratnam and Hurtig (2000), Çakır (2003) and Balkış (2004). There is a high correlation between all of the previous data and the best fit obtained from the present work, that is, Equation 5.1. Namely, the general trend of the entire data including present work exhibit similar behavior. Since inclination of double screen configurations with the same pore geometry have no significant additional gain on the energy dissipation all double screen data including that of the present study are fitted as a best fit curve to show the amount of energy dissipation in general sense, as shown in Figure 5.13 with the following form

$$\frac{\Delta E_{GC}}{E_G} = 0.898 + 0.003 Fr_G^{\,2} - \frac{7.996}{Fr_G^{\,2}} \tag{5.2}$$

The r-values of the entire data, the data of the previous work alone, the present data alone are 0.993, 0.993, 0.995 respectively, conforming the significant agreement among the findings. The data from the previously conducted screen studies in our laboratory by Çakır (2003) and Balkış (2004) will be called previous METU data and they together with the present study data will be called the entire METU data thereafter.

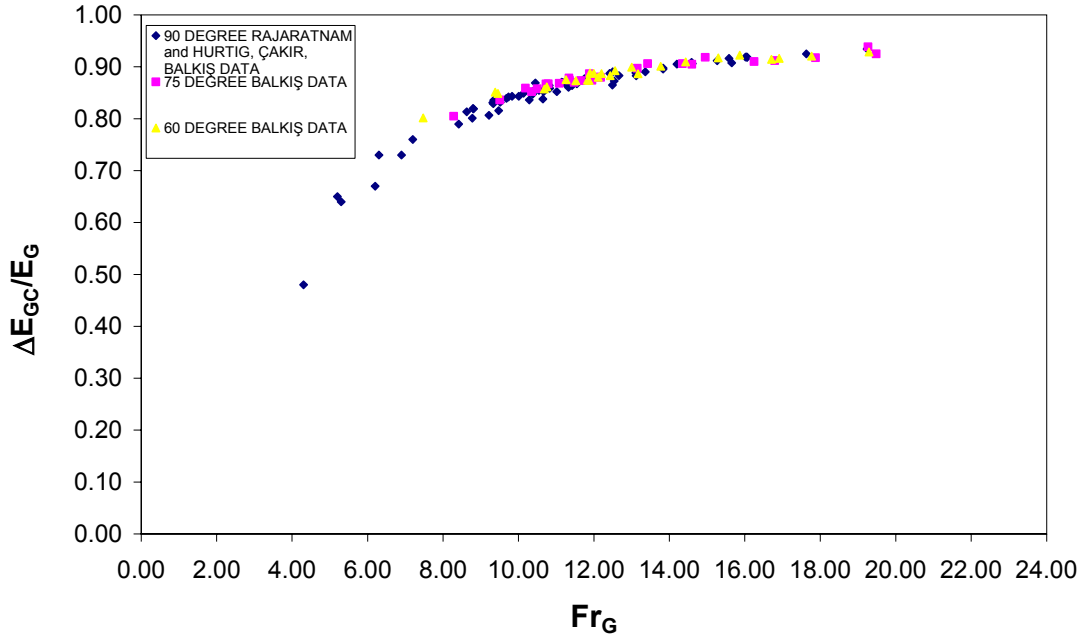

Figure 5.10 All previous data with double screen of $\theta = 90^0$, $\theta = 75^0$, $\theta = 60^0$

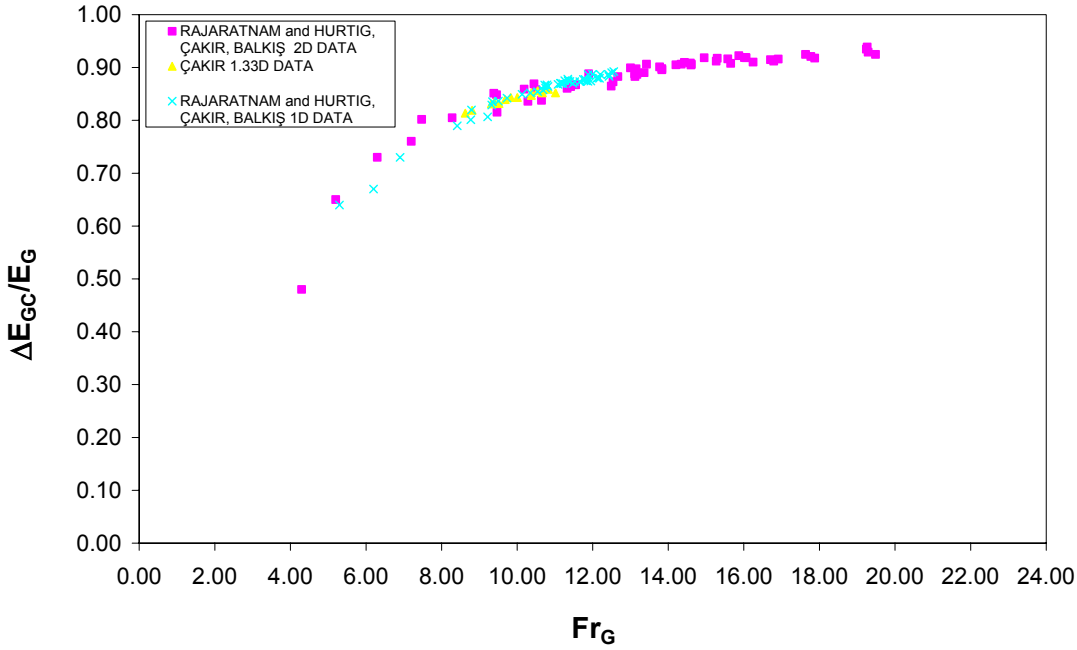

Figure 5.11 All previous data with double screen of 1D, 2D, 1.33D data

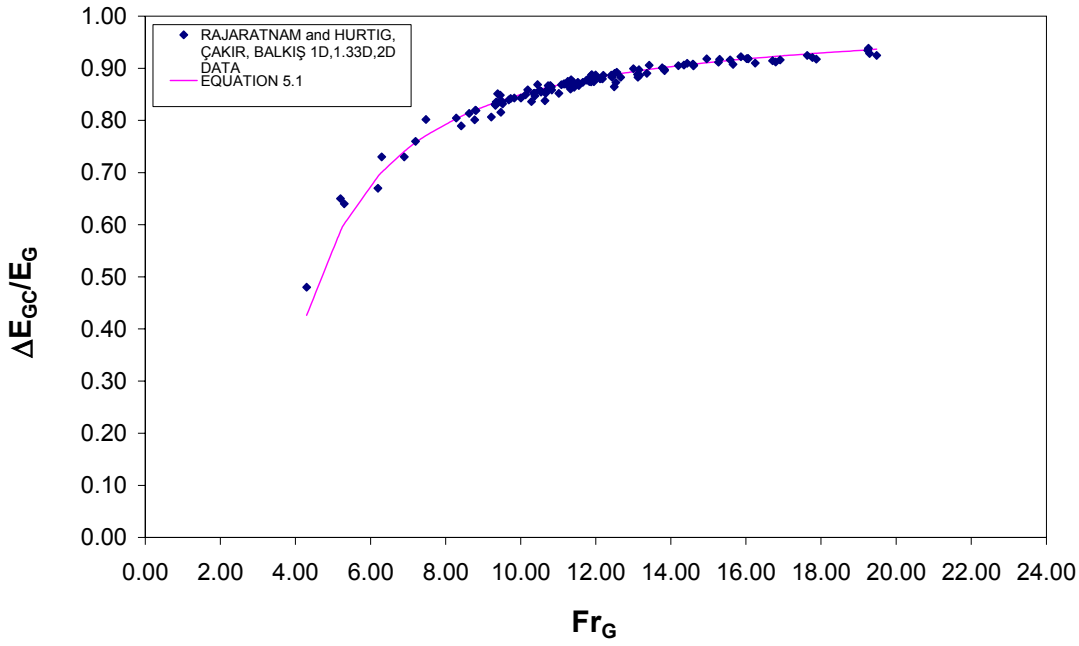

Figure 5.12 Data of previous studies and its curve based on Equation 5.1

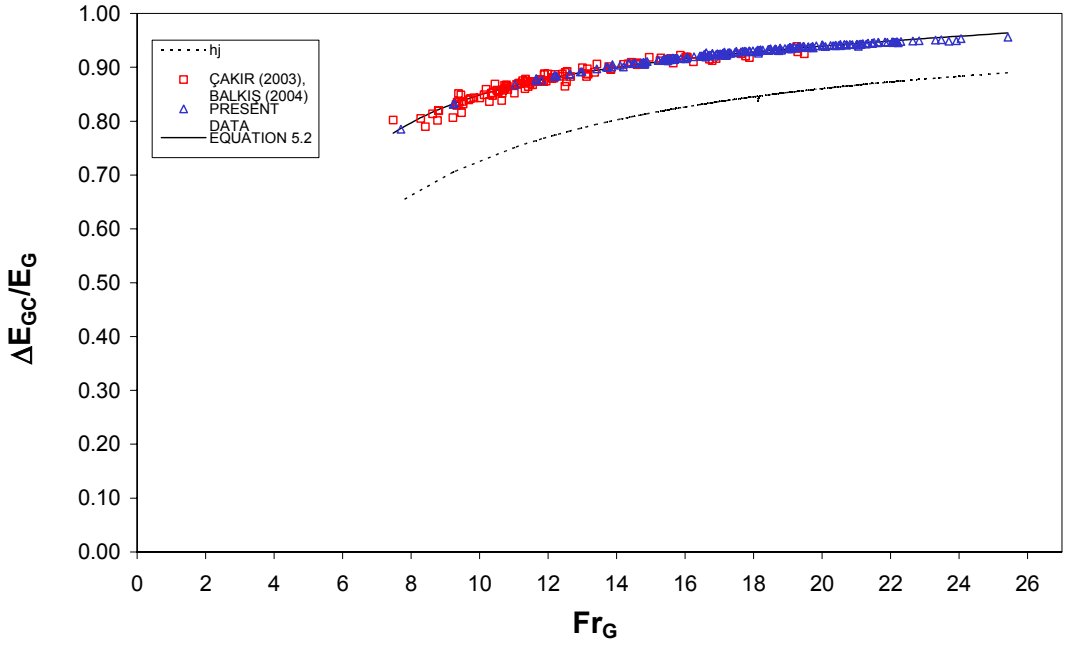

Figure 5.13 Entire METU data and its curve based on Equation 5.2

Having demonstrated the significant agreement among the data of all works including the present one as exhibited on the small rms values and large correlation coefficients, the best fit curve of Equation 5.2 had been simplified for practical reasons as given below, also shown in Figure 5.14,

$$\frac{\Delta E_{GC}}{E_G} = 0.9 + 0.003 Fr_G - \frac{8}{Fr_G^{\,2}} \tag{5.3}$$

The corresponding rms value and correlation coefficient of all the data including the present data are 0.110 and 0.993, respectively.

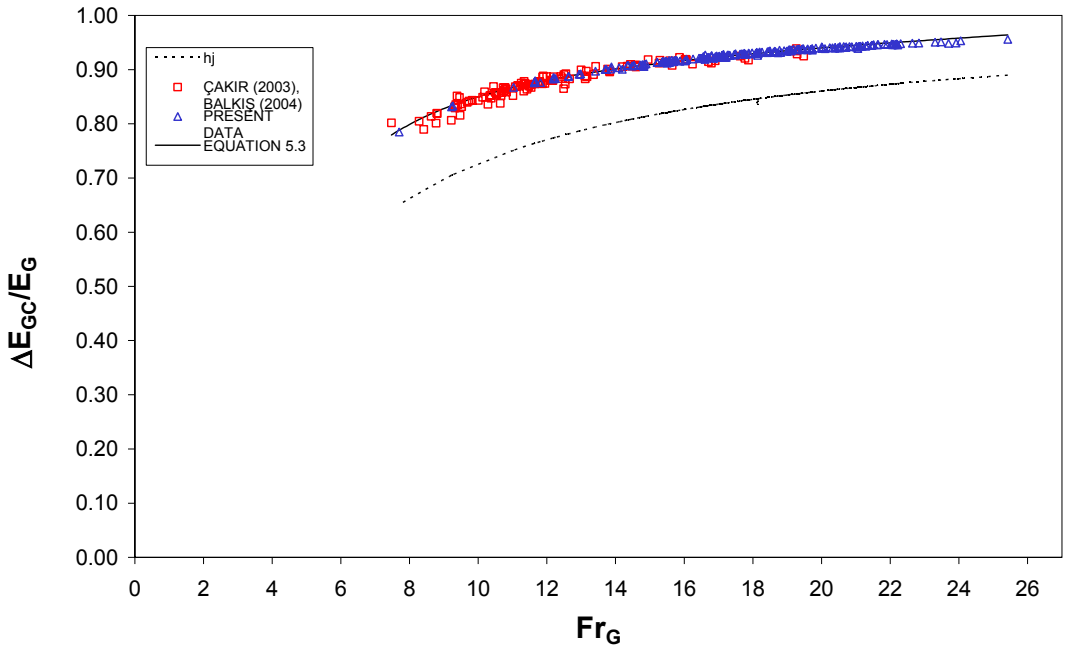

Figure 5.14 Entire METU data and its curve based on Equation 5.3

5.3 PERFORMANCE OF THE SCREEN

As indicated before the energy loss at the screen is denoted as *S*. The relative energy loss S/E_G is formulated to represent the screen performance.

5.3.1 PERFORMANCE OF THE SCREENS AT LARGE

The variations of the screen performance for the triangular screen as observed for different configurations used in this study are presented in Appendix D.

In Figure 5.15, the best fit curve to all data of the present study excluding one set of data (t/d= 2.35D, X/d= 147) which exhibits an unexplainable deviation from the rest is shown. The equation of the best fit curve is

$$\frac{S}{E_G} = \frac{1}{(3.489 + 0.497 Fr_G)} \tag{5.4}$$

The corresponding rms value and correlation coefficient are 0.187 and 0.634, respectively.

From the figure, one may discern that there is no significant dependence of the screen performance, S/E_G, on the relative screen position, X/d and on the relative screen thickness, t/d.

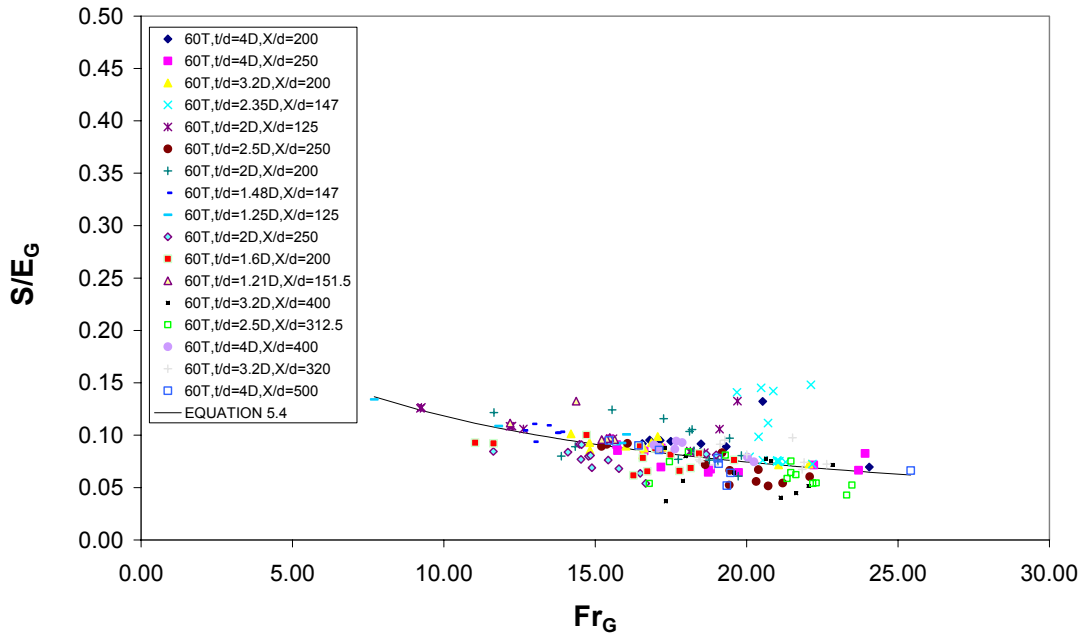

Figure 5.15 S/E_G vs. Fr_G for the present data and Equation 5.4 curve

5.3.2 COMPARISON OF THE PRESENT DATA WITH THAT OF BALKIŞ & ÇAKIR

In Figure 5.16, the screen performance of the present study and previous work by (Çakır (2003), Balkış (2004)) are classified according to the value of the relative distance, *X/d*. The examination of the data reveals two distinct types of dependence of S/E_G on Fr_G. For the cases where screen was located at a relative position with X/d≥ 99, both for the present and previous data, S/E_G decreases while for X/d<99 it increases. These two distinct behaviors may be attributed to the form adopted for the loss within the pseudo-jump; that is the β expression. This disparity is not observed on the system performance since the total loss, that is the loss through the jump and the screen combined is considered. Based on this observation one may conclude that as the Froude number increases the contribution of the loss through the screen increases if X/d<99, and decreases if X/d≥ 99.

All of the data for X/d≥ 99 with double screen configuration including the present data except one set from the present data (t/d= 2.35D, X/d= 147) and the Balkış data of t/*d*= 2D, X/d= 100, both of which abnormally deviate from the rest of the data are shown in Figure 5.17. On the same figure, the best fit curve for the screen performance is of the following form obtained with an rms value of 0.253 and an r value of 0.562.

$$\frac{S}{E_G} = \frac{1}{(4.835 + 0.423 Fr_G)} \tag{5.5}$$

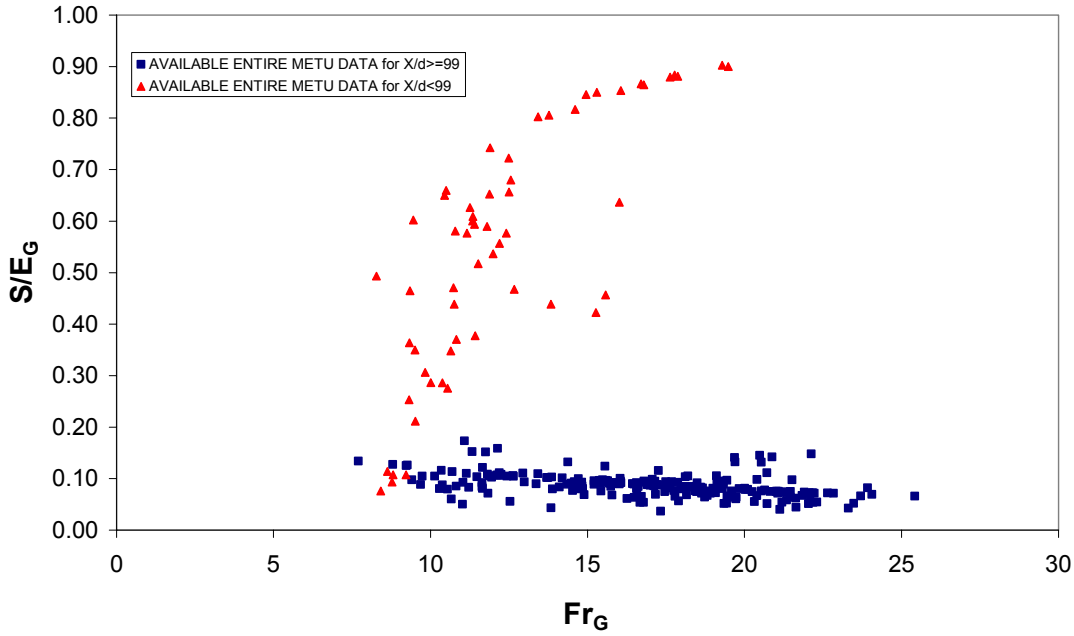

Figure 5.16 Effect of X/d<99 and X/d≥ 99 on the screen performance, S/E_G

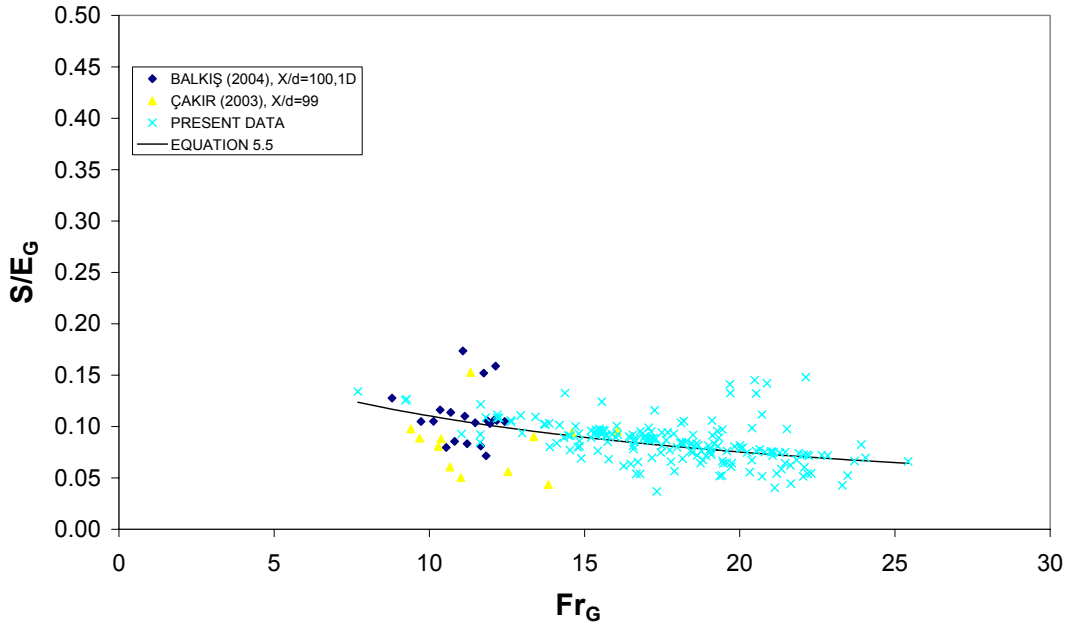

Figure 5.17 S/E_G vs. Fr_G for the entire METU data and its best fit curve

5.4 SYSTEM EFFICIENCIES

The system efficiency is defined as the ratio of the difference between the system loss, ΔE_{GC} and the energy loss that would occur if there were a jump at section G, ΔE_{JG} to ΔE_{JG};

$$\eta_{sys} = \frac{\Delta E_{GC} - \Delta E_{jG}}{\Delta E_{jG}} \tag{5.6}$$

In Figure 5.18, the entire set of the present data and its best fit curve are shown. The equation of the best fit curve is of the following form with the rms value of 0.024 and the correlation coefficient r= 0.996.

$$\eta_{sys} = \frac{1}{(1.098 + 0.49 Fr_G)} \tag{5.7}$$

From the figure, one may discern that the system efficiency decreases with increasing Fr_G regardless of the relative screen positions and the relative screen thicknesses. However, the system efficiency is as high as approximately 20% at relatively low Froude number and also at least approximately 10% more efficient than full hydraulic jump throughout the Froude number range employed in the present study.

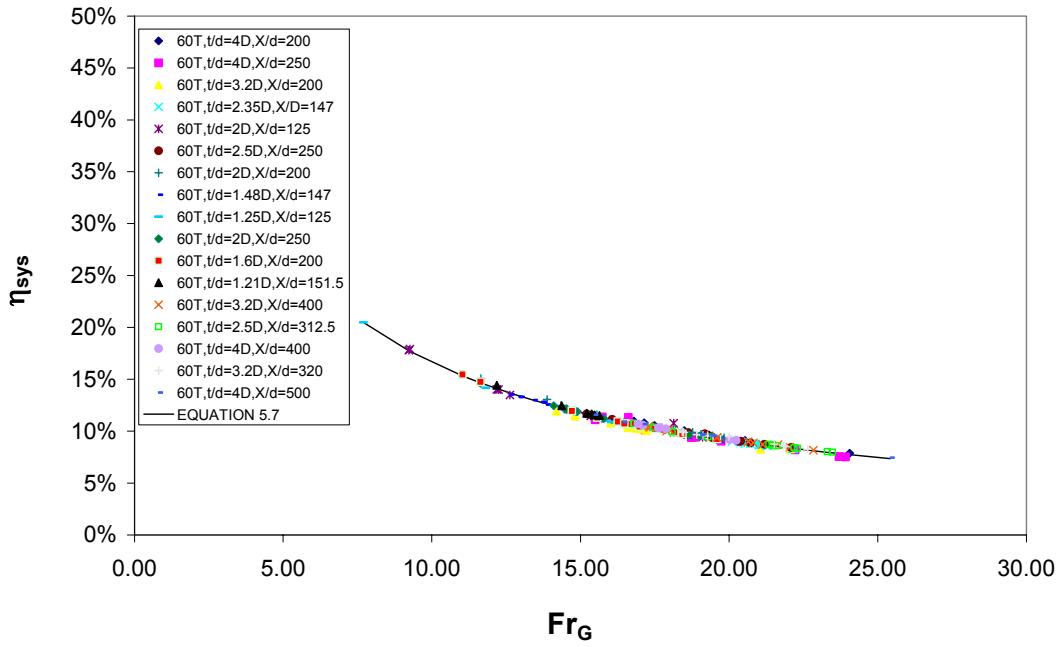

Figure 5.18 η_{sys} vs. Fr_G for the present data and its best fit curve

5.4.1 COMPARISON OF THE PRESENT DATA WITH THAT OF BALKIŞ & ÇAKIR

To show the agreement between present data and previous works by (Çakır (2003) and Balkış (2004)), all of the previous data are put into Equation 5.7, as shown in Figure 5.19. The rms value turns out to be equal to 0.115 and the

correlation coefficient r= 0.923. There is a high correlation between all of the previous data and the best fit obtained from the present work, that is, the general

trend of the entire data including the present work exhibit similar behavior. Therefore, entire METU data are fitted in a best fit curve to show the system efficiency in general sense, as depicted in Figure 5.20, yielding the following equation with the rms value of 0.116 and the r value of 0.972.

$$\eta_{sys} = \frac{1}{(1.187 + 0.49 Fr_G)} \tag{5.8}$$

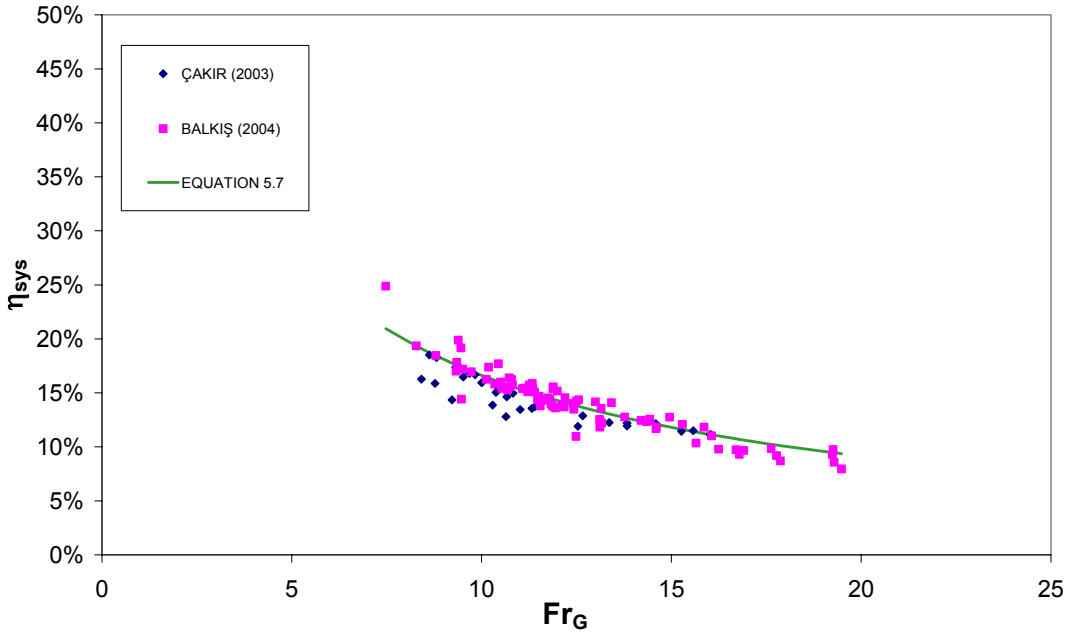

Figure 5.19 Previously studied METU data and its curve based on Equation 5.7

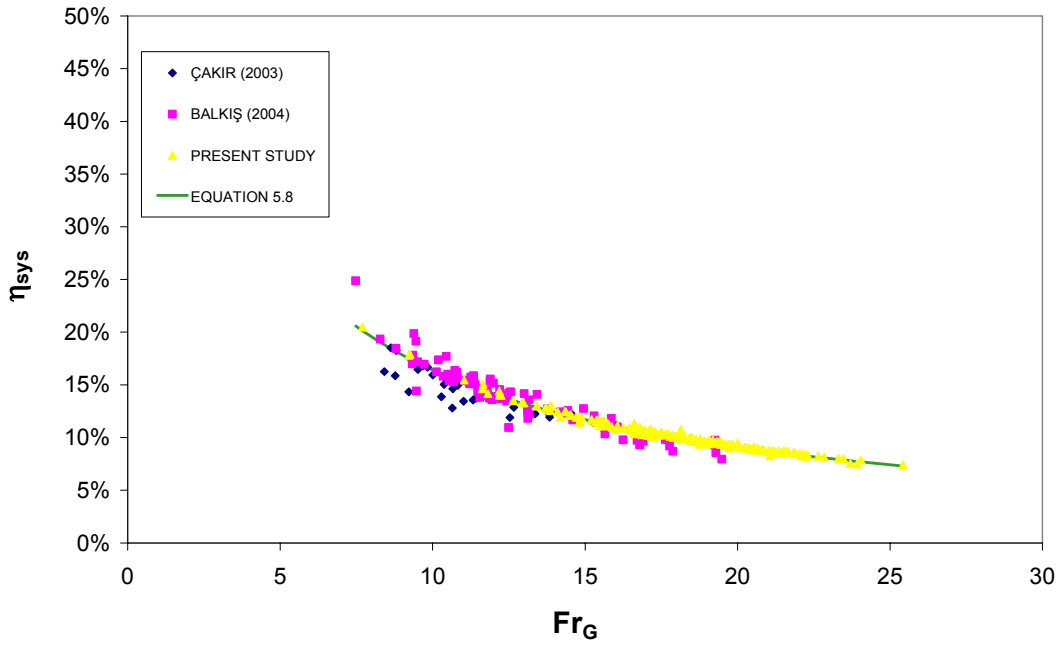

Figure 5.20 η_{sys} vs. Fr_G for the entire METU data and its best fit curve

5.5 SCREEN EFFICIENCIES

Screen efficiency is defined as the ratio of the energy loss at the screen over the loss of a hypothetical jump considered occurring at section G

$$\eta_{scr} = \frac{S}{\Delta E_{jG}} \tag{5.9}$$

In Figure 5.23, entire set of the present data and its best fit curve excluding one set data (t/d= 2.35D, X/d= 147) are shown. The equation of the best fit curve is of the form with the rms value of 0.222 and correlation coefficient of r= 0.751.

$$\frac{S}{\Delta E_{jG}} = \frac{1}{(0.748 + 0.542 Fr_G)} \tag{5.10}$$

From the figure, one may discern that there is no significant dependence of the screen efficiency, $\eta_{scr,}$ on the relative screen position, X/d and on the relative screen thickness, t/d.

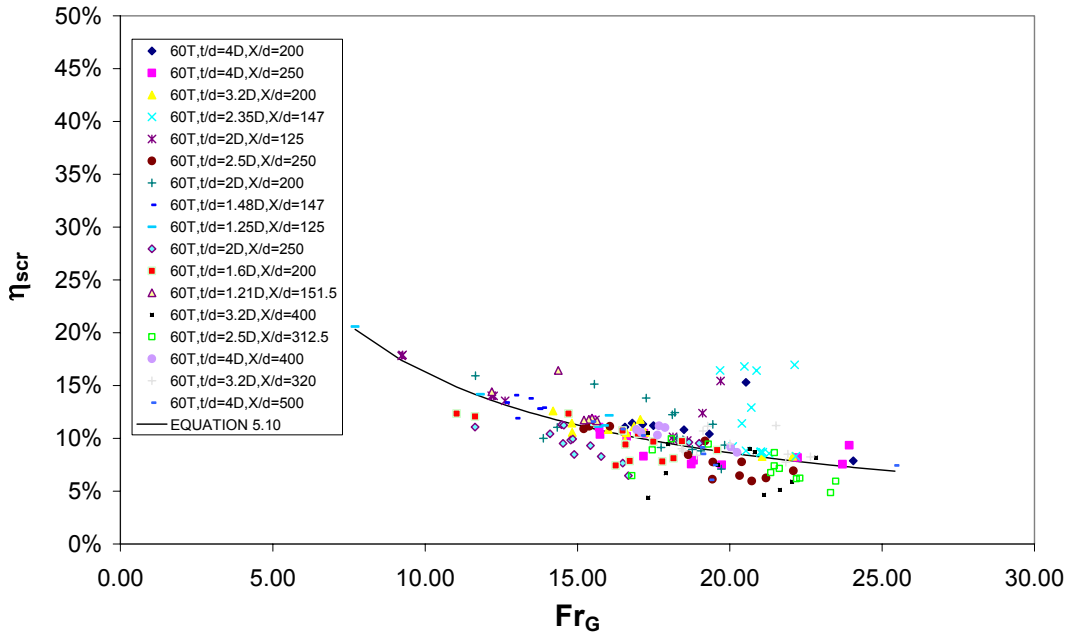

Figure 5.21 η_{scr} vs. Fr_G for the present data and Equation 5.10 curve

5.5.1 COMPARISON OF THE PRESENT DATA WITH THAT OF BALKIŞ & ÇAKIR

In Figure 5.24 the screen performance of the present study and previous work by (Çakır (2003) and Balkış (2004)) are classified according to the value of the relative distance X/d. The same behavior as S/E_G is also visible for this case since β expression is used to demonstrate also the screen efficiency. That is, there are also

two distinct types of dependence of screen efficiency on Fr_G. For the cases where screen was located at a position with $X/d \geq 99$, both for the present and previous data, screen efficiency decreases while for $X/d < 99$ it increases. Thus, as Froude number

increases the contribution of the loss through the screen increases if *X/d*<99 and decreases if X/d≥ 99.

All of the data for X/d≥ 99 with double screen configuration including present data except one set (t/d= 2.35D, X/d= 147) and the Balkış data of t/*d*= 2D, X/d= 100 which differently deviates from the rest of the data are shown in Figure 5.25. On the same figure, the best fit curve of the form is depicted with the rms value of 0.315 and correlation coefficient of r= 0.691.

$$\frac{S}{\Delta E_{jG}} = \frac{1}{(1.782 + 0.485 Fr_G)} \tag{5.11}$$

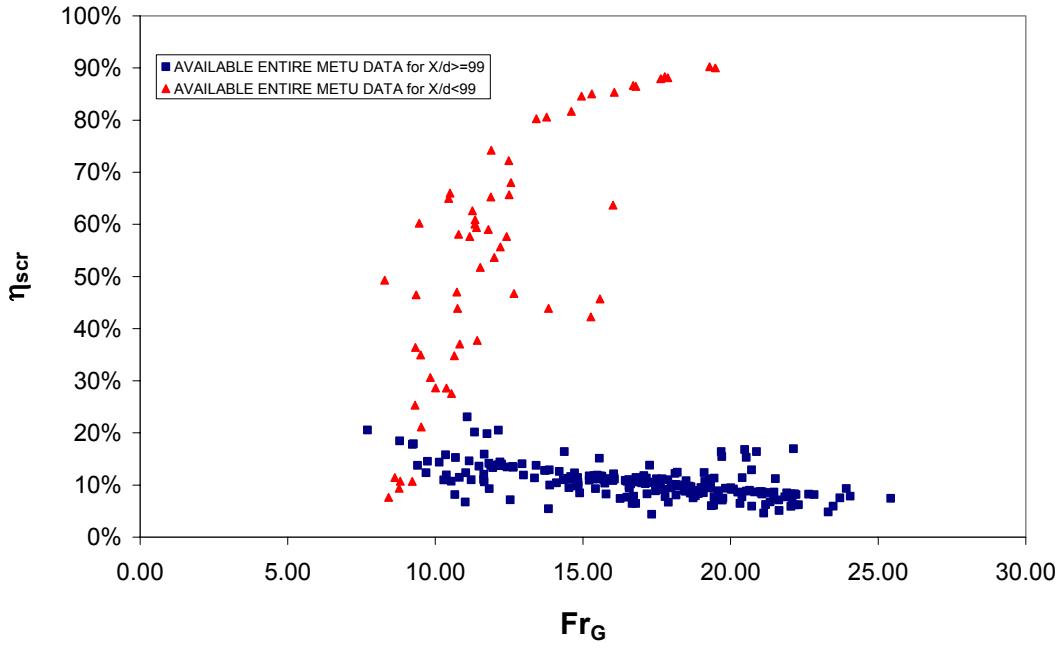

Figure 5.22 Effect of X/d< 99 and X/d≥ 99 on the screen efficiency, $S/\Delta E_{JG}$

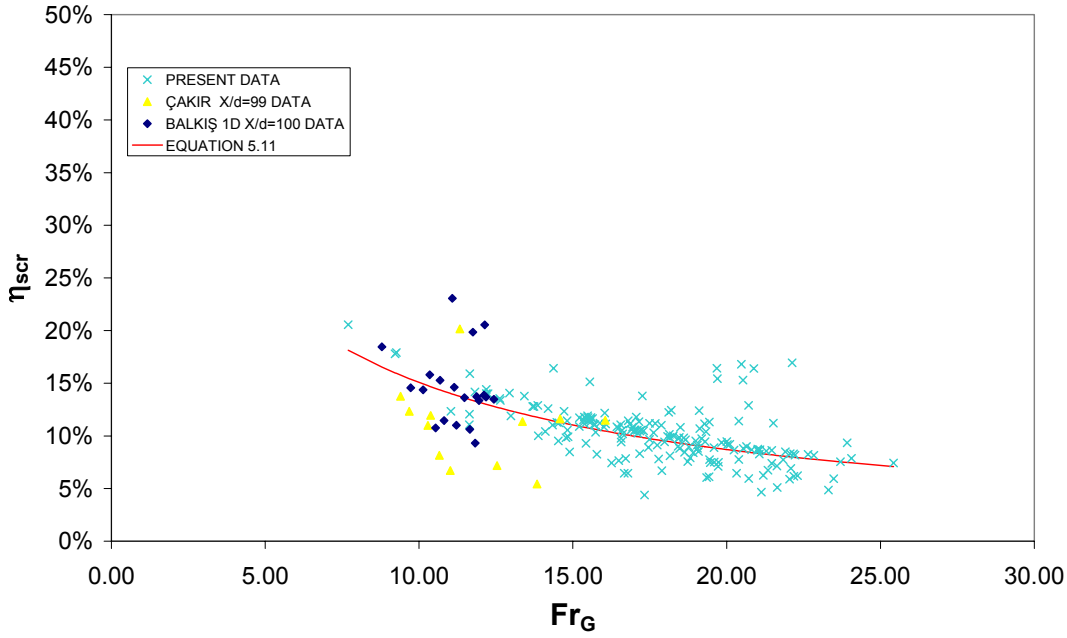

Figure 5.23 $S/\Delta E_{JG}$ vs. Fr_G for the entire METU data and its best fit curve

CHAPTER VI

CONCLUSIONS AND RECOMMENDATIONS

In the present thesis work, the efficiency of the triangular screens on the energy dissipation is analyzed experimentally. As indicated in the previous chapters, double screens with 60-degree inclination angle and with a porosity of 40% are utilized for the experiments. Froude number range covered during the study is from 7.5 to 25.5. The gate opening is adjusted with the heights of 1 cm, 1.25 cm, 1.6 cm, 1.7 cm, 2 cm, 2.5 cm, 2.7 cm, 3.2 cm and 3.3 cm in accordance with *t/d* and *X/d* relation specified in the dimensional analysis.

From the analysis of the experimental data, the following outcomes are gathered;

1. All of the tests performed on the triangular screen showed that energy dissipation is always more than that of a classical full jump for the same Froude number as shown in Figure 5.1,

2. There is a general trend that the system performance increase (shown in Figure 5.1) while the system efficiency decreases with increasing Fr_G (shown in Figure 5.18),

3. For $X/d \geq$ 99, screen performance and screen efficiency decrease with increasing Fr_G, as seen in Figures 5.16 and 5.24, respectively,

4. For X/d< 99, screen performance and screen efficiency increases with increasing $Fr_{G,}$ as seen in Figures 5.16 and 5.24, respectively,

5. The relative screen position, X/d has no significant effect on the system performance and system efficiency.

6. In the range studied, the relative screen thickness, t/d has no significant effect on the system performance, screen performance, screen efficiency and system efficiency.

7. All of the screen configurations studied at METU indicated that no configuration has any substantial superiority over the rest for the effectiveness of the screens in energy dissipation. Therefore, it is recommended that the vertical screen be used in practice since it is cheaper and easier to build it.

Present study can be further developed by considering the followings;

- Multiple screens
- Thicker screens
- Effect of tailwater
- Different functions for β parameter

Before putting into practice the screen-type energy dissipator, real life factors such as vibration or debris accumulation behind the screen should be investigated extensively.

REFERENCES

Balkış, Görkem, (2004). "Experimental Investigation of Energy Dissipation through Inclined Screens". MSc Thesis Department of Civil Engineering Middle East Technical University, Ankara, Turkey

Bozkuş, Z., Çakır, P., Ger, M. and Özeren, Y.(2004) "Energy Dissipation Through Screens ", Proceedings of ASCE World Water & Environmental Resources Congress 2004 ,Salt Lake City, Utah, U.S.A.

Çakır, Pınar, (2003). "Experimental Investigation of Energy Dissipation through screens". MSc Thesis Department of Civil Engineering Middle East Technical University, Ankara, Turkey

French, R. H. (1986). "Open Channel Hydraulics." McGraw-Hill Book Company, Singapore.

Munson, B.R., Young, D. F. and Okiishi, T. H. (1994). "Fundamentals of Fluid Mechanics." John Wiley and Sons, Inc., Toronto, Canada.

Rajaratnam, N., Hurtig, K. I. (2000). "Screen-Type Energy Dissipator for Hydraulic Structures." Journal of Hydraulic Engineering, Vol. 126, No. 4, 310-312

Simon, A. L. (1981). "Practical Hydraulics." John Wiley and Sons, Inc., Toronto, Canada.

APPENDIX A

ORIFICE METER DETAILS

An orifice meter whose design is made according to the Institution of Turkish Standards (TSE) specifications (Figure A.1) is constructed on the pipe serving as a link between the constant head tank and the pressurized tank. A 30 degree inclined mercury manometer, by the help of which discharge measurements were made, is connected to the orifice meter.

The working basis of the orifice is measuring the pressure drop between the taps by the help of the 30-degree inclined manometer. The reduction in pressure is obtained by reducing the cross section of the flowing stream in passing through the orifice that causes an increase in velocity and therefore, a decrease in pressure.

To determine the flow rate, a correlation between the increase in velocity head and the decrease in pressure head is obtained by means of energy equation (Munson, Young, and Okiishi (1994)).

Assuming the flow is horizontal, steady, inviscid and incompressible between points (1) and (2), then Energy equation becomes

$$\frac{p_1}{\gamma}+\frac{V_1^{\,2}}{2g}=\frac{p_2}{\gamma}+\frac{V_2^{\,2}}{2g}+h_L \qquad \text{(A.1)}$$

Ideally hydraulic losses, $h_L = 0$. However, non-ideal case occurs for two reasons. Firstly, the vena contracta area, A_2, is less than the area of the hole, A_0, by

an unknown amount. Thus, $A_2 = C_c A_0$, where C_c is the contraction coefficient (C_c<1). Secondly, a head loss occurs due to the swirling flow and turbulent motion near the orifice plate that cannot be calculated theoretically. Therefore, to account for those losses an orifice discharge coefficient, C_0, is utilized. As a result, the equation by which the discharge is calculated becomes:

$$Q = C_0 Q_{ideal} = C_0 A_0 \sqrt{\frac{2(p_1 - p_2)}{\rho(1-\phi^4)}} \tag{A.2}$$

where $\phi = 0.5$ is defined as $\phi = \frac{D_0}{D_1}$ with D_0 being the orifice meter throat diameter and D_1 is the pipe inside diameter on which the orifice meter is located, and $A_0 = \frac{\pi D_0^{\,2}}{4}$ is the area of the hole in the orifice plate. The coefficient, C_0 is a function of $\phi = \frac{D_0}{D_1}$ and the Reynolds number $Re = \frac{\rho V_1 D_1}{\mu}$ with $V_1 = \frac{Q}{A_1}$. The value of C_0 depends on the specific construction of the orifice meter.

For the determination of the value of C_0, the distinct values specified by TSE are used by adapting a proper trend curve for the discharge calculations (Figure A.2).

The detailed drawing of the orifice-meter is given in Figure A.1.

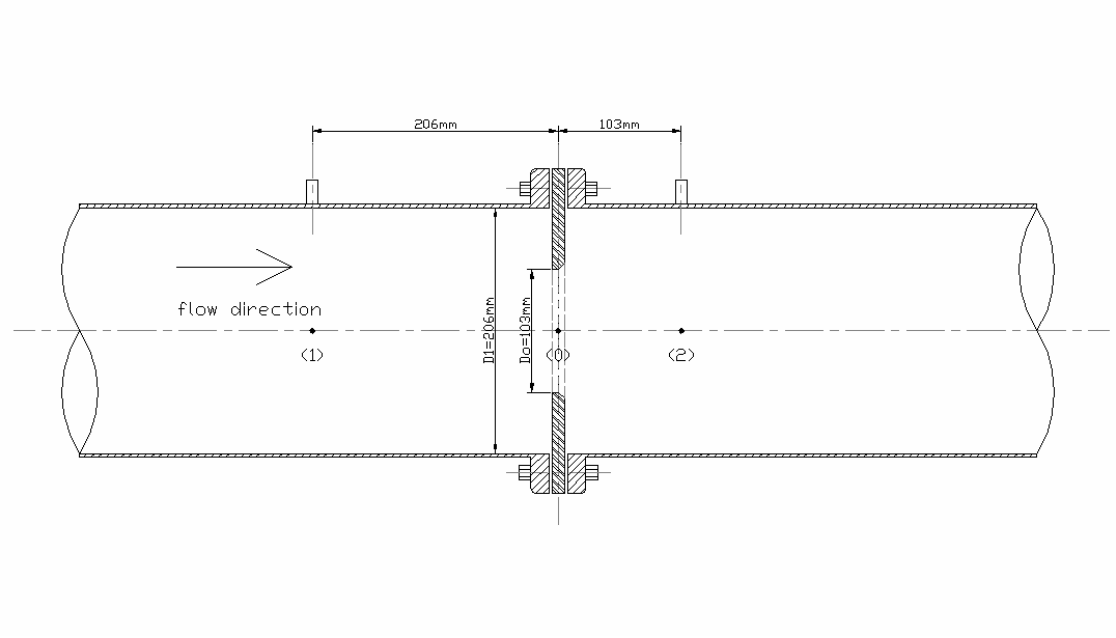

Figure A.1 Details of the orifice-meter

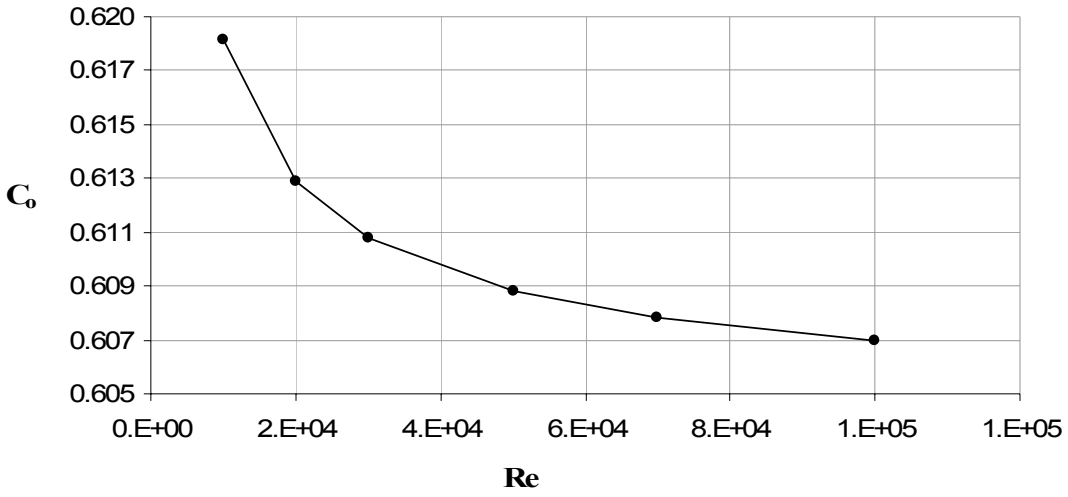

Figure A.2 Variation of C_0 with respect to Reynolds number

APPENDIX B

UNCERTAINTY ANALYSIS OF EXPERIMENTAL DATA

Since no measurements are perfect, a mechanism is necessitated to determine the rate of the errors made during measurements. As a common agreement in engineering, uncertainty analysis is the appropriate concept to express the errors. Therefore, uncertainty analysis was performed for Q, E_{GC} and S values by using the following basic definitions;

$$\delta R=\left\{\sum_{1}^{n}\left(\left(\partial R/\partial x_i\right)\delta x_i\right)^2\right\}^{\frac{1}{2}} \tag{B.1}$$

$$\delta R=\left\{\sum_{1}^{n}\left[R\left(x_i+\delta x_i\right)-R\left(x_i\right)\right]^2\right\}^{\frac{1}{2}} \tag{B.2}$$

where R denotes the result computed from the n measurands $x_1,\ldots,x_i,\ldots,x_n$. δR is the overall uncertainty interval of R and δx_i is the precision error associated with x_i.

B.1 UNCERTAINTY ANALYSIS FOR Q

Equation A.2 used for the discharge calculation can be rewritten as follows;

$$Q = C_0 Q_{ideal} = \frac{C_0 A_0}{(1-\phi^4)^{\frac{1}{2}}}\sqrt{2g\Delta h} \tag{B.3}$$

In the present study, discharge, Q is computed from one measurand, that is, Δh. Then, Equation B.2 becomes

$$\delta Q = Q(\Delta h + \delta\Delta h) - Q(\Delta h) \tag{B.4}$$

$$\delta Q = \frac{C_0 A_0}{(1-\phi^4)^{\frac{1}{2}}}\sqrt{2g(\Delta h + \delta\Delta h)} - \frac{C_0 A_0}{(1-\phi^4)^{\frac{1}{2}}}\sqrt{2g(\Delta h)} \tag{B.5}$$

where δΔh is the precision error associated with Δh. Since the minimum segment of the instrument used for Δh measurements is $\pm 0.001m$, δΔh can be taken as $0.002m$

Overall uncertainty values for the discharge, δQ_j can be normalized by the corresponding discharge values, Q_j as depicted in Figure B.1. (where j is the number of the measurement for Q values taken for the present study.)

From the figure, one may discern that the relative uncertainty decreases as the Reynolds number increases.

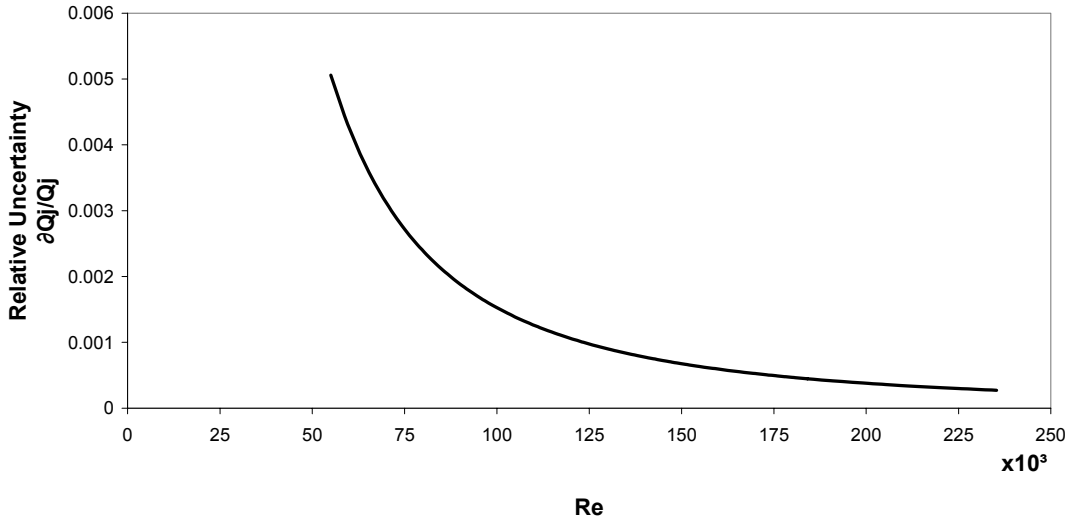

Figure B.1 Relative Uncertainty for Q_j values vs. Re

B.2 UNCERTAINTY ANALYSIS FOR ΔE_{GC}

ΔE_{GC} is calculated as follows;

$$\Delta E_{GC}=(y_G+\frac{V_G^2}{2g})-(y_C+\frac{V_C^2}{2g}) \tag{B.6}$$

In present study, ΔE_{GC} is computed from three measurands; Δh, y_C and y_G. Then, Equation B.2 becomes

$$\delta\Delta E_{GC}=\left\{\sum_{1}^{3}\left[\Delta E_{GC}\left(x_i+\delta x_i\right)-\Delta E_{GC}\left(x_i\right)\right]^2\right\}^{\frac{1}{2}} \tag{B.7}$$

Then, Equation B.7 can be also written as follows;

$$\delta\Delta E_{GC}=\left\{\left(\Delta E_{GC}(\Delta h+\delta\Delta h)-\Delta E_{GC}(\Delta h)\right)^2+\left(\Delta E_{GC}(y_C+\delta y_C)-\Delta E_{GC}(y_C)\right)^2+\left(\Delta E_{GC}(y_G+\delta y_G)-\Delta E_{GC}(y_G)\right)^2\right\}^{\frac{1}{2}} \tag{B.8}$$

where $\delta\Delta h$, δy_C, δy_G are the precision errors associated with Δh, y_C, y_G, respectively. Since the minimum segment of the instrument used for Δh, y_C, y_G measurements are $\pm 0.001m$, $\pm 0.0001m$ and $\pm 0.0001m$, respectively, random errors for $\delta\Delta h$, δy_C, δy_G can be taken as $0.002m$, $0.0002m$ and $0.0002m$, respectively.

Overall uncertainty values of $\delta\Delta E_{GC}$ can be normalized by the corresponding ΔE_{GC} values as depicted in Figure B.2.

From the figure, one may discern that the relative uncertainty interval of ΔE_{GC} is in the range of 0.015 - 0.065. That is due to the reading error during the measurement. These values are at the same level with the rms values.

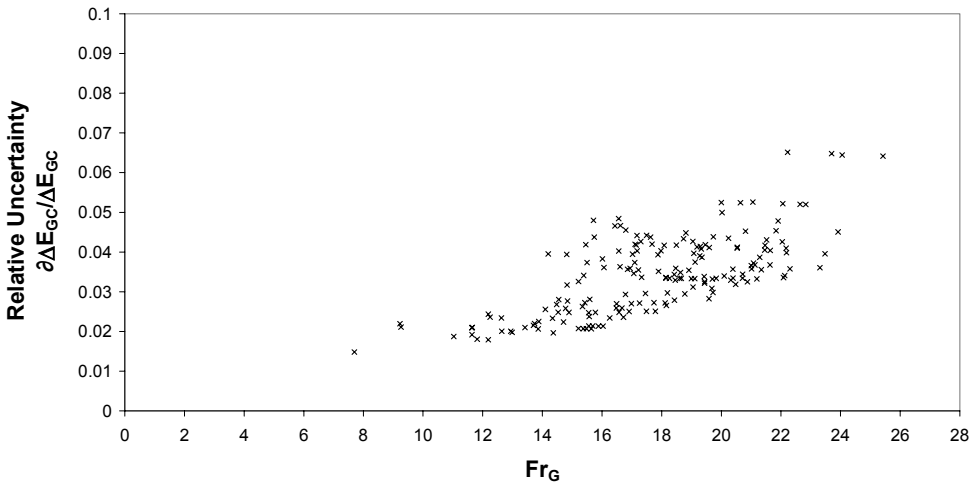

Figure B.2 $\delta\Delta E_{GC}/\Delta E_{GC}$ vs. Fr_G for the present data

B.3 UNCERTAINTY ANALYSIS FOR S

S is calculated as follows;

$$S = (y_A + \frac{V_A^2}{2g}) - (y_C + \frac{V_C^2}{2g}) - \beta \Delta E_{jA} \tag{B.9}$$

In the present study, S is computed from four measurands; x, Δh, y_A and y_C. (β is computed from one measurand; x, V_A is computed from two measurands; Δh and y_A, and V_C is computed from two measurands Δh and y_C.) Then, Equation B.2 becomes

$$\delta S = \left\{ \sum_1^4 \left[S(x_i + \delta x_i) - S(x_i) \right]^2 \right\}^{\frac{1}{2}} \tag{B.10}$$

where x_1=x and $\delta x_1 = \delta x$ (the precision error associated with x and equal to $\pm 0.002m$), x_2=Δh and $\delta x_2 = \delta \Delta h$ (the precision error associated with Δh and equal to $\pm 0.002m$), $x_3 = y_A$ and $\delta x_3 = \delta y_A$ (the precision error associated with y_A and equal to $\pm 0.0002m$), $x_4 = y_C$ and $\delta x_4 = \delta y_C$ (the precision error associated with y_C and equal to $\pm 0.0002m$).

Overall uncertainty values of δS can be normalized by the corresponding S values as depicted in Figure B.3.

From the figure, one may discern that the relative uncertainty interval of S is in the range of 0.009 - 0.033. That is due to the reading error during the measurement. These values are at the same level with the rms values.

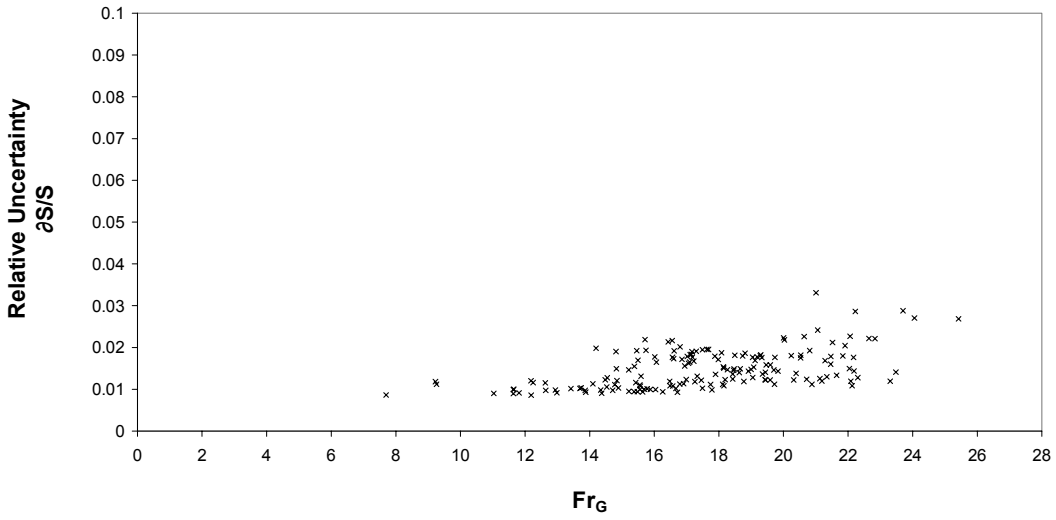

Figure B.3 δS/S vs. Fr_G for the present data

APPENDIX C

EXPERIMENTAL DATA

The measurements taken are given in Table C.1.

Table C.1 Experimental Data

Reference	Q(m^3/s)	y_C (cm)	y_A (cm)	S/E_G	$\Delta E_{GC}/E_G$
40-4d-199-20.53-60T	0.0187	5.75	1.00	0.132	0.943
40-4d-199-19.32-60T	0.0179	5.62	1.01	0.089	0.938
40-4d-199-18.49-60T	0.0166	5.37	0.99	0.092	0.935
40-4d-199-17.14-60T	0.0156	5.22	1.00	0.095	0.928
40-4d-199-17.49-60T	0.0146	4.91	0.94	0.094	0.930
40-4d-199-16.79-60T	0.0135	4.70	0.92	0.095	0.926
40-4d-199-16.55-60T	0.0121	4.34	0.87	0.092	0.924
40-4d-199-24.05-60T	0.0108	3.94	0.63	0.070	0.953
40-4d-249-23.91-60T	0.0187	5.12	0.98	0.082	0.949
40-4d-249-15.49-60T	0.0171	4.99	1.32	0.096	0.912
40-4d-249-19.73-60T	0.0164	4.85	1.24	0.064	0.936
40-4d-249-17.18-60T	0.0166	4.85	1.23	0.088	0.923
40-4d-249-18.73-60T	0.0160	4.72	1.24	0.064	0.931
40-4d-249-18.81-60T	0.0152	4.61	1.16	0.067	0.932
40-4d-249-17.16-60T	0.0144	4.47	1.16	0.070	0.923
40-4d-249-15.74-60T	0.0136	4.51	1.06	0.085	0.917
40-4d-249-16.61-60T	0.0128	4.82	1.00	0.085	0.927
40-4d-249-15.71-60T	0.0118	4.10	0.91	0.091	0.917
40-4d-249-23.69-60T	0.0106	3.51	0.63	0.067	0.948
40-4d-249-22.22-60T	0.0100	3.50	0.63	0.071	0.946
40-3.2d-199-14.82-60T	0.0212	5.69	1.49	0.086	0.906

Table C.1 Experimental Data (continued)

Reference	Q(m^3/s)	y_C (cm)	y_A (cm)	S/E_G	$\Delta E_{GC}/E_G$
40-3.2d-199-17.06-60T	0.0208	5.66	1.21	0.099	0.922
40-3.2d-199-17.22-60T	0.0202	5.51	1.17	0.088	0.923
40-3.2d-199-16.85-60T	0.0197	5.43	1.12	0.093	0.921
40-3.2d-199-16.6-60T	0.0189	5.26	1.15	0.088	0.919
40-3.2d-199-16.01-60T	0.0169	4.95	1.17	0.090	0.916
40-3.2d-199-16.56-60T	0.0161	4.87	1.20	0.081	0.920
40-3.2d-199-14.81-60T	0.0152	4.60	1.09	0.093	0.907
40-3.2d-199-14.19-60T	0.0147	4.47	1.03	0.101	0.901
40-3.2d-199-22.06-60T	0.0138	4.43	0.78	0.073	0.946
40-3.2d-199-21.05-60T	0.0132	4.00	0.78	0.072	0.939
40-2.35d-146-19.68-60T	0.0279	7.14	1.35	0.141	0.937
40-2.35d-146-20.48-60T	0.0276	7.07	1.30	0.145	0.941
40-2.35d-146-20.87-60T	0.0271	7.05	1.27	0.142	0.942
40-2.35d-146-22.12-60T	0.0266	6.87	1.21	0.148	0.946
40-2.35d-146-20.71-60T	0.0259	6.76	1.24	0.112	0.941
40-2.35d-146-20.39-60T	0.0255	6.70	1.24	0.098	0.940
40-2.35d-146-20.09-60T	0.0246	6.51	1.22	0.079	0.939
40-2.35d-146-21.01-60T	0.0236	6.45	1.15	0.076	0.943
40-2.35d-146-21-60T	0.0228	6.15	1.13	0.075	0.942
40-2.35d-146-21.08-60T	0.0223	6.14	1.11	0.075	0.943
40-2.35d-146-21.28-60T	0.0212	5.88	1.06	0.074	0.943
40-2.35d-146-22.17-60T	0.0201	5.73	1.00	0.073	0.946
40-2.35d-146-20.53-60T	0.0187	5.37	1.00	0.076	0.940
40-2.35d-146-17.02-60T	0.0169	5.20	1.06	0.088	0.925
40-2d-124-12.62-60T	0.0294	7.33	1.87	0.106	0.887
40-2d-124-15.34-60T	0.0288	7.29	1.62	0.094	0.913
40-2d-124-12.24-60T	0.0283	7.26	1.86	0.109	0.884
40-2d-124-9.26-60T	0.0275	7.13	2.20	0.127	0.833
40-2d-124-12.18-60T	0.0270	6.99	1.81	0.109	0.883
40-2d-124-15.59-60T	0.0265	6.83	1.52	0.097	0.914
40-2d-124-9.22-60T	0.0258	6.77	2.12	0.126	0.831
40-2d-124-19.7-60T	0.0250	6.62	1.25	0.132	0.937
40-2d-124-19.1-60T	0.0243	6.44	1.25	0.106	0.934

Table C.1 Experimental Data (continued)

Reference	Q(m^3/s)	y_C (cm)	y_A (cm)	S/E_G	$\Delta E_{GC}/E_G$
40-2d-124-18.6-60T	0.0236	6.35	1.25	0.083	0.932
40-2d-124-18.14-60T	0.0230	6.23	1.25	0.083	0.930
40-2d-124-18.13-60T	0.0223	6.04	1.25	0.085	0.926
40-2.5d-249-22.08-60T	0.0271	7.17	1.75	0.060	0.947
40-2.5d-249-21.19-60T	0.0266	7.06	1.79	0.054	0.944
40-2.5d-249-20.31-60T	0.0260	6.86	1.78	0.056	0.940
40-2.5d-249-19.44-60T	0.0255	6.76	1.84	0.066	0.937
40-2.5d-249-20.71-60T	0.0247	6.65	1.82	0.052	0.942
40-2.5d-249-19.42-60T	0.0240	6.61	1.88	0.052	0.937
40-2.5d-249-20.39-60T	0.0230	6.38	1.46	0.067	0.941
40-2.5d-249-18.63-60T	0.0221	6.32	1.42	0.072	0.934
40-2.5d-249-15.21-60T	0.0206	5.93	1.40	0.089	0.913
40-2.5d-249-15.38-60T	0.0195	5.71	1.29	0.091	0.914
40-2.5d-249-16.06-60T	0.0185	5.53	1.17	0.092	0.919
40-2.5d-249-19.18-60T	0.0174	5.59	1.00	0.083	0.938
40-2d-199-13.87-60T	0.0334	8.65	2.48	0.080	0.905
40-2d-199-14.34-60T	0.0326	8.27	2.32	0.089	0.908
40-2d-199-11.65-60T	0.0323	8.28	2.19	0.122	0.879
40-2d-199-15.55-60T	0.0319	8.12	1.77	0.124	0.917
40-2d-199-18.11-60T	0.0314	8.09	1.73	0.104	0.932
40-2d-199-17.74-60T	0.0308	7.94	1.78	0.077	0.930
40-2d-199-17.25-60T	0.0303	7.76	1.62	0.116	0.927
40-2d-199-19.72-60T	0.0295	7.65	1.86	0.061	0.939
40-2d-199-18.77-60T	0.0287	7.70	1.62	0.076	0.936
40-2d-199-18.19-60T	0.0276	7.44	1.56	0.105	0.933
40-2d-199-19.05-60T	0.0266	7.21	1.48	0.075	0.936
40-2d-199-19.43-60T	0.0259	7.11	1.26	0.097	0.938
40-2d-199-19.83-60T	0.0249	6.91	1.24	0.080	0.940
40-2d-199-18.45-60T	0.0239	6.56	1.27	0.084	0.933
40-2d-199-18.26-60T	0.0232	6.52	1.25	0.085	0.932
40-1.48d-147-12.98-60T	0.0387	8.93	2.50	0.094	0.892
40-1.48d-147-13.86-60T	0.0383	8.86	2.15	0.103	0.901
40-1.48d-147-12.93-60T	0.0379	8.77	2.14	0.111	0.891
40-1.48d-147-12.63-60T	0.0372	8.62	2.28	0.105	0.888

Table C.1 Experimental Data (continued)

Reference	Q(m^3/s)	y_C (cm)	y_A (cm)	S/E_G	$\Delta E_{GC}/E_G$
40-1.48d-147-13.41-60T	0.0364	8.63	2.00	0.109	0.897
40-1.48d-147-13.69-60T	0.0355	8.53	2.01	0.102	0.900
40-1.48d-147-13.73-60T	0.0345	8.40	1.97	0.102	0.901
40-1.48d-147-16.9-60T	0.0337	8.16	1.69	0.088	0.924
40-1.25d-124-7.69-60T	0.0419	9.23	3.30	0.134	0.785
40-1.25d-124-11.81-60T	0.0415	9.13	2.46	0.109	0.876
40-1.25d-124-16.03-60T	0.0412	9.08	2.00	0.101	0.917
40-1.25d-124-15.88-60T	0.0408	9.05	2.00	0.093	0.916
40-1.25d-124-15.68-60T	0.0403	8.96	2.00	0.091	0.914
40-1.25d-124-15.55-60T	0.0400	9.01	2.00	0.093	0.914
40-2d-249-11.63-60T	0.0327	7.98	2.71	0.084	0.876
40-2d-249-15.78-60T	0.0322	7.89	2.51	0.068	0.916
40-2d-249-16.67-60T	0.0316	7.79	2.58	0.054	0.922
40-2d-249-14.89-60T	0.0307	7.74	2.39	0.069	0.911
40-2d-249-14.52-60T	0.0300	7.66	2.24	0.077	0.908
40-2d-249-16.48-60T	0.0295	7.43	2.23	0.064	0.921
40-2d-249-14.77-60T	0.0287	7.37	2.06	0.080	0.909
40-2d-249-14.1-60T	0.0281	7.27	2.01	0.084	0.904
40-2d-249-15.42-60T	0.0274	7.14	1.92	0.076	0.914
40-2d-249-14.48-60T	0.0267	6.98	1.72	0.091	0.907
40-2d-249-14.84-60T	0.0259	6.88	1.84	0.081	0.910
40-2d-249-14.54-60T	0.0250	6.71	1.64	0.091	0.907
40-2d-249-18.99-60T	0.0241	6.49	1.25	0.081	0.934
40-2d-249-18.66-60T	0.0237	6.36	1.25	0.082	0.933
40-1.6d-199-11.64-60T	0.0372	8.79	2.94	0.092	0.877
40-1.6d-199-11.03-60T	0.0370	8.76	2.90	0.093	0.868
40-1.6d-199-16.71-60T	0.0366	8.61	2.72	0.066	0.923
40-1.6d-199-16.26-60T	0.0361	8.51	2.66	0.062	0.920
40-1.6d-199-14.71-60T	0.0356	8.45	2.31	0.100	0.909
40-1.6d-199-17.78-60T	0.0351	8.38	2.29	0.066	0.929
40-1.6d-199-17.49-60T	0.0346	8.25	2.11	0.081	0.927
40-1.6d-199-15.57-60T	0.0341	8.13	1.91	0.095	0.915
40-1.6d-199-16.57-60T	0.0336	8.03	1.94	0.078	0.921
40-1.6d-199-18.15-60T	0.0328	7.94	1.93	0.069	0.930

Table C.1 Experimental Data (continued)

Reference	Q(m^3/s)	y_C (cm)	y_A (cm)	S/E_G	$\Delta E_{GC}/E_G$
40-1.6d-199-19.58-60T	0.0318	7.74	1.53	0.076	0.937
40-1.6d-199-16.47-60T	0.0313	7.67	1.64	0.089	0.921
40-1.6d-199-18.42-60T	0.0309	7.58	1.50	0.083	0.931
40-1.6d-199-16.98-60T	0.0301	7.46	1.56	0.087	0.924
40-1.21d-151-12.19-60T	0.0426	9.89	2.46	0.112	0.886
40-1.21d-151-14.37-60T	0.0424	9.84	2.19	0.133	0.908
40-1.21d-151-15.64-60T	0.0421	9.74	2.06	0.096	0.917
40-1.21d-151-15.47-60T	0.0416	9.58	2.06	0.098	0.916
40-1.21d-151-15.37-60T	0.0414	9.59	2.06	0.097	0.915
40-1.21d-151-15.21-60T	0.0409	9.46	2.06	0.096	0.914
40-3.2d-398-21.12-60T	0.0227	6.29	2.14	0.040	0.943
40-3.2d-398-17.32-60T	0.0219	6.13	2.56	0.037	0.926
40-3.2d-398-17.89-60T	0.0211	5.91	1.82	0.057	0.929
40-3.2d-398-21.64-60T	0.0201	6.03	1.76	0.044	0.947
40-3.2d-398-22.04-60T	0.0188	5.65	1.42	0.052	0.947
40-3.2d-398-19.59-60T	0.0179	5.46	1.29	0.064	0.938
40-3.2d-398-17.97-60T	0.0171	5.31	1.13	0.080	0.931
40-3.2d-398-20.81-60T	0.0163	5.10	0.93	0.075	0.943
40-3.2d-398-17.29-60T	0.0152	4.91	0.98	0.088	0.927
40-3.2d-398-22.83-60T	0.0143	4.65	0.78	0.072	0.949
40-3.2d-398-20.64-60T	0.0129	4.43	0.78	0.078	0.943
40-2.5d-311-17.45-60T	0.0268	7.11	1.69	0.075	0.928
40-2.5d-311-16.78-60T	0.0263	7.02	2.29	0.054	0.924
40-2.5d-311-23.3-60T	0.0255	6.85	1.92	0.043	0.951
40-2.5d-311-22.3-60T	0.0249	6.76	1.61	0.054	0.948
40-2.5d-311-21.34-60T	0.0241	6.68	1.57	0.059	0.945
40-2.5d-311-21.63-60T	0.0232	6.46	1.41	0.062	0.946
40-2.5d-311-23.47-60T	0.0223	6.27	1.42	0.052	0.951
40-2.5d-311-22.18-60T	0.0210	6.04	1.42	0.054	0.947
40-2.5d-311-21.46-60T	0.0199	5.75	1.19	0.064	0.945
40-2.5d-311-21.46-60T	0.0190	5.65	0.98	0.075	0.945
40-2.5d-311-19.29-60T	0.0175	5.30	1.00	0.081	0.936
40-2.5d-311-18.08-60T	0.0164	5.03	1.00	0.084	0.930
40-4d-498-19.34-60T	0.0195	5.90	1.72	0.052	0.938

Table C.1 Experimental Data (continued)

Reference	Q(m^3/s)	y_C (cm)	y_A (cm)	S/E_G	$\Delta E_{GC}/E_G$
40-4d-498-19.07-60T	0.0185	5.67	1.34	0.073	0.937
40-4d-498-19.46-60T	0.0173	5.46	1.29	0.064	0.938
40-4d-498-19.04-60T	0.0165	5.18	1.09	0.078	0.936
40-4d-498-17.11-60T	0.0155	5.03	1.04	0.086	0.927
40-4d-498-15.45-60T	0.0143	4.70	1.01	0.095	0.915
40-4d-498-16.43-60T	0.0128	4.30	0.90	0.090	0.921
40-4d-498-25.42-60T	0.0114	4.01	0.63	0.066	0.956
40-3.2d-318-18.42-60T	0.0224	6.37	1.49	0.076	0.933
40-3.2d-318-18.91-60T	0.0218	6.20	1.39	0.072	0.935
40-3.2d-318-18.47-60T	0.0210	6.05	1.31	0.075	0.933
40-3.2d-318-19.12-60T	0.0202	5.92	1.05	0.091	0.936
40-3.2d-318-19.27-60T	0.0191	5.74	0.95	0.095	0.937
40-3.2d-318-21.51-60T	0.0181	5.65	0.74	0.098	0.946
40-3.2d-318-21.83-60T	0.0169	5.34	1.01	0.067	0.947
40-3.2d-318-21.9-60T	0.0157	4.97	0.85	0.074	0.946
40-3.2d-318-22.64-60T	0.0142	4.65	0.78	0.072	0.949
40-3.2d-318-20-60T	0.0125	4.59	0.78	0.081	0.942
40-4d-398-16.94-60T	0.0195	5.79	1.25	0.091	0.925
40-4d-398-17.09-60T	0.0185	5.56	1.16	0.088	0.926
40-4d-398-17.87-60T	0.0177	5.47	1.00	0.093	0.931
40-4d-398-20.24-60T	0.0169	5.25	1.03	0.075	0.941
40-4d-398-17.68-60T	0.0159	5.09	0.91	0.094	0.930
40-4d-398-17.62-60T	0.0149	4.82	0.95	0.087	0.929
40-4d-398-20.02-60T	0.0136	4.51	0.82	0.079	0.940

APPENDIX D

GRAPHICAL REPRESENTATIONS

D.1 GRAPHICS FOR THE SYSTEM PERFORMANCE

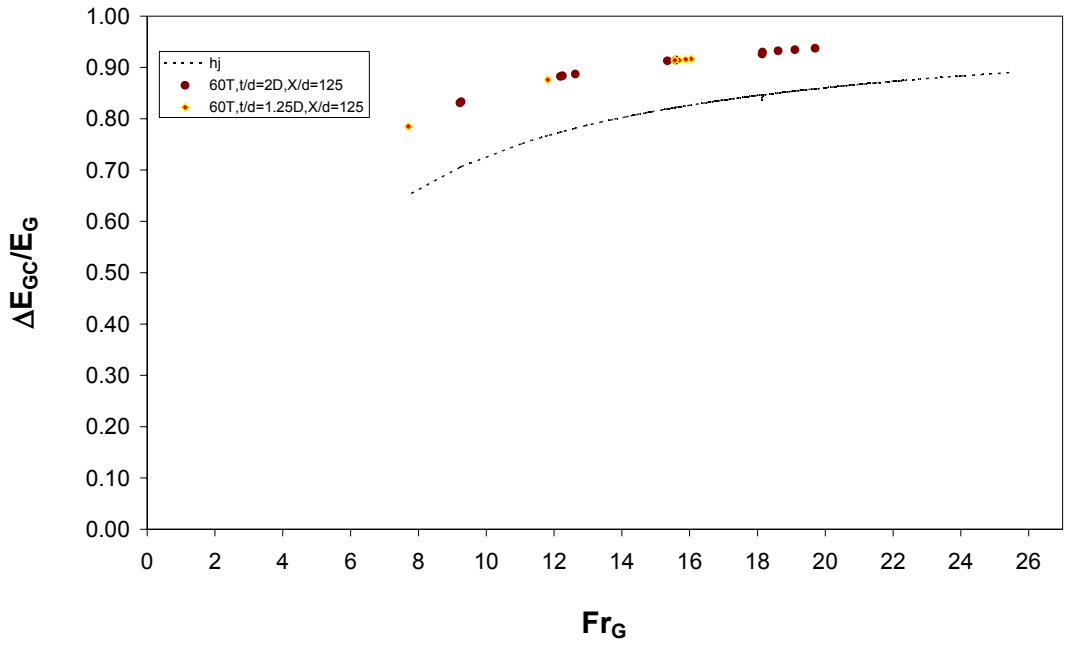

Figure D.1 $\Delta E_{GC}/E_G$ vs. Fr_G at the relative screen distance of X/d=125

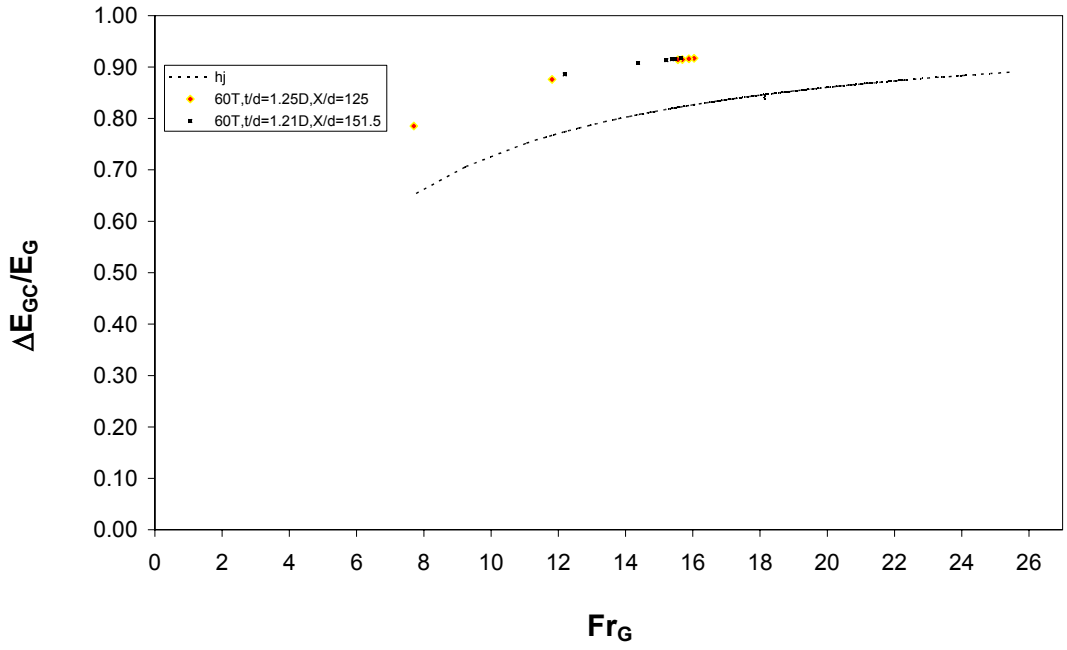

Figure D.2 $\Delta E_{GC}/E_G$ vs. Fr_G at the relative screen thickness of X/d=1.25D

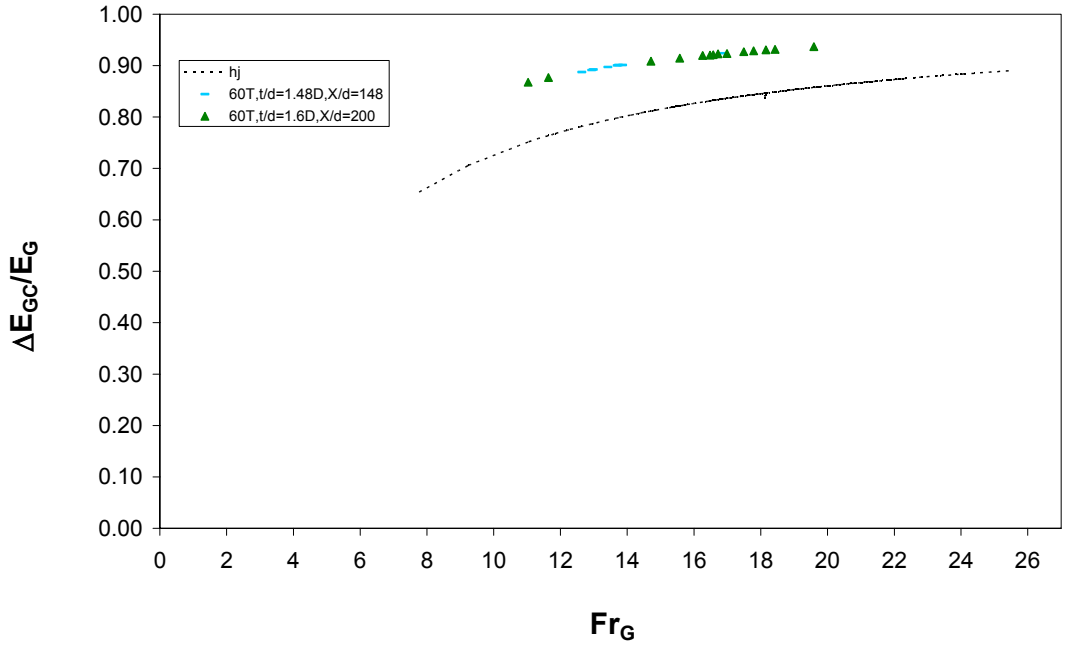

Figure D.3 $\Delta E_{GC}/E_G$ vs. Fr_G at the relative screen thickness of X/d=1.48D

D.2 GRAPHICS FOR THE SCREEN PERFORMANCE

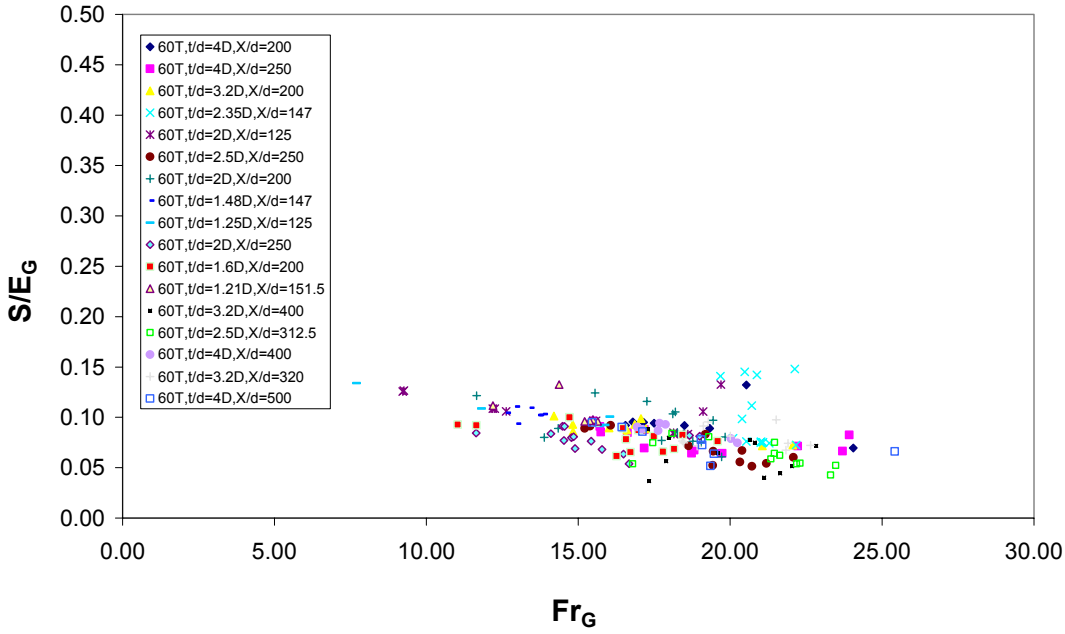

Figure D.4 S/E_G vs. Fr_G for all of the present study

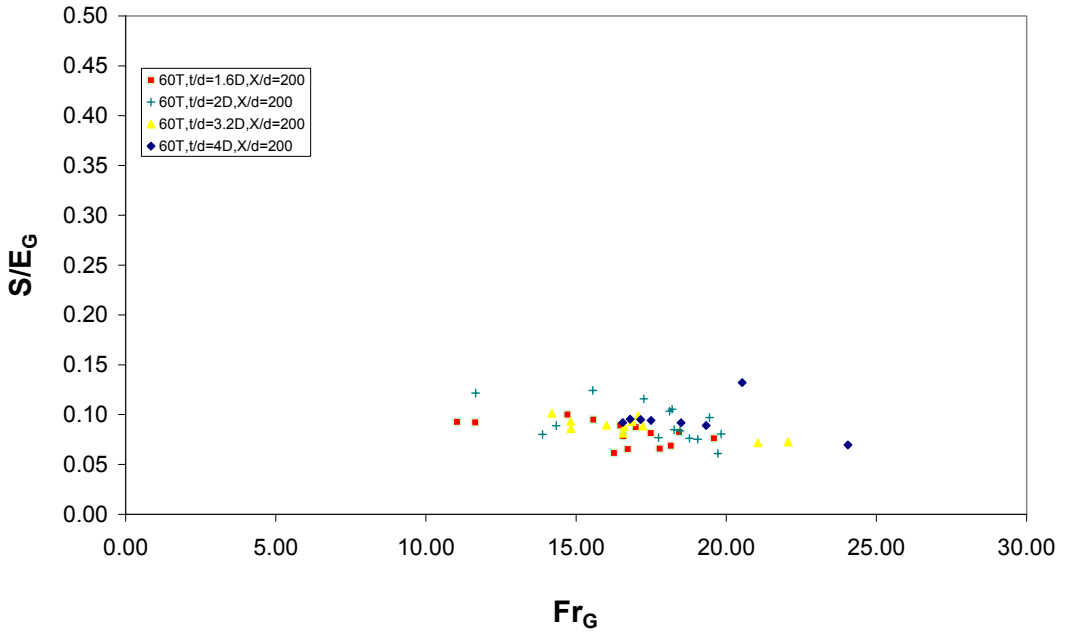

Figure D.5 S/E_G vs. Fr_G at X/d=200

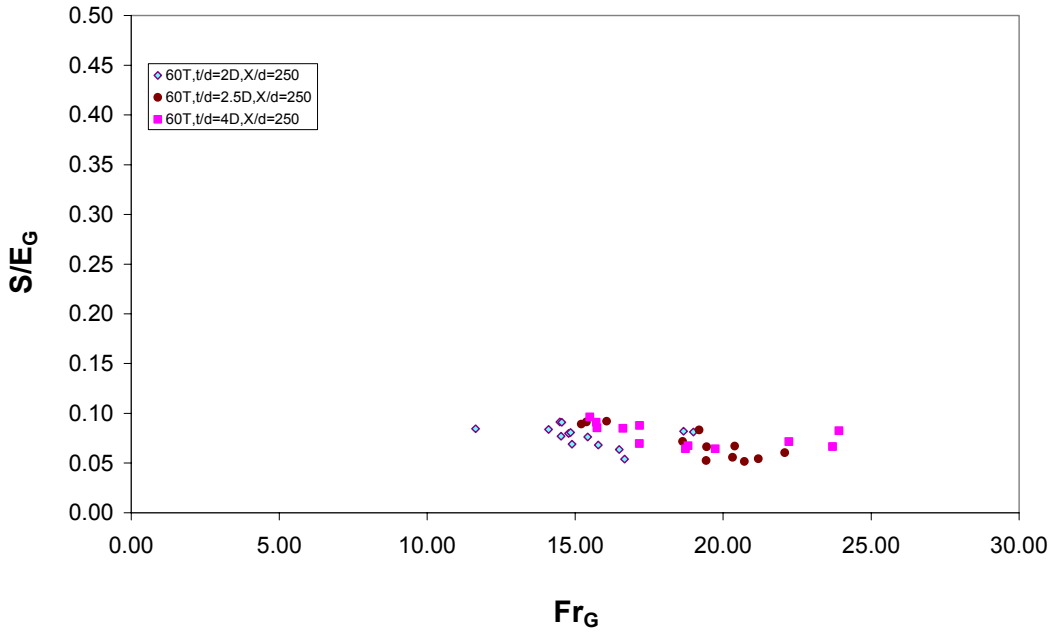

Figure D.6 S/E_G vs. Fr_G at X/d=250

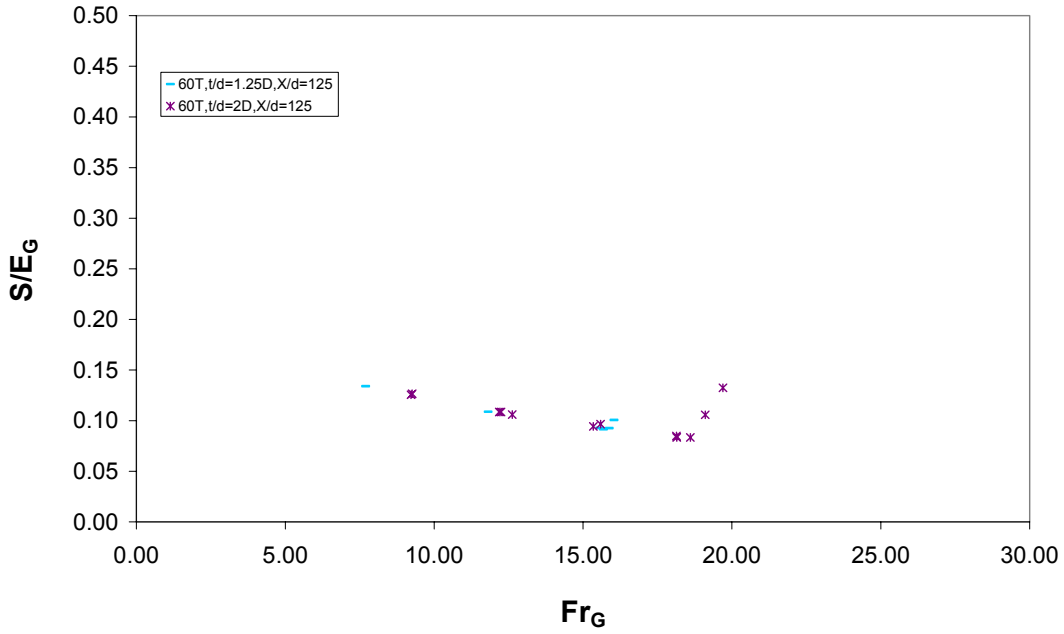

Figure D.7 S/E_G vs. Fr_G at X/d=125

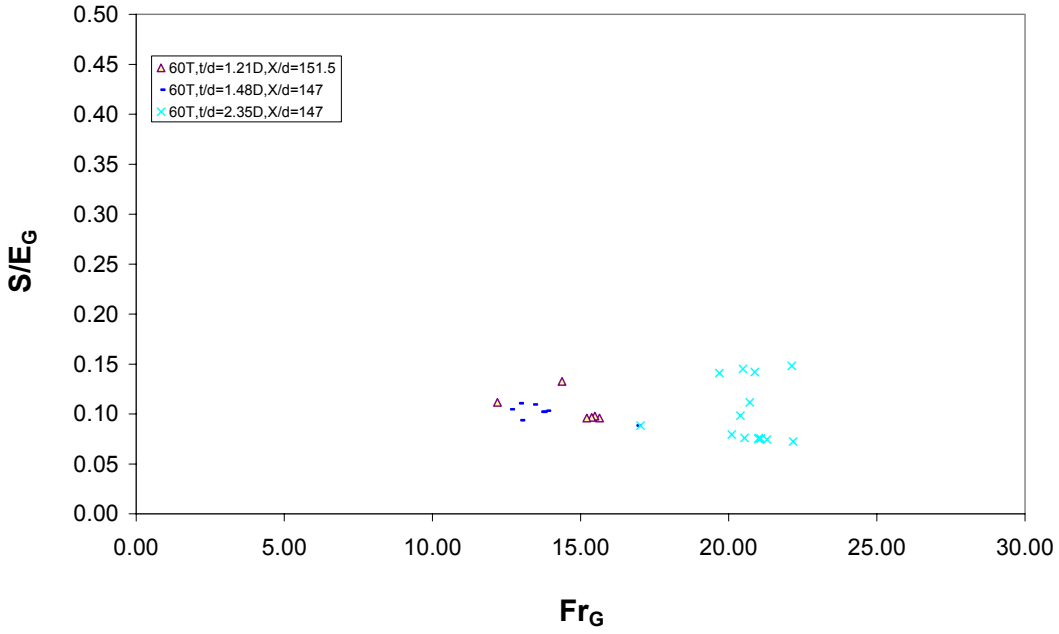

Figure D.8 S/E_G vs. Fr_G at X/d=148

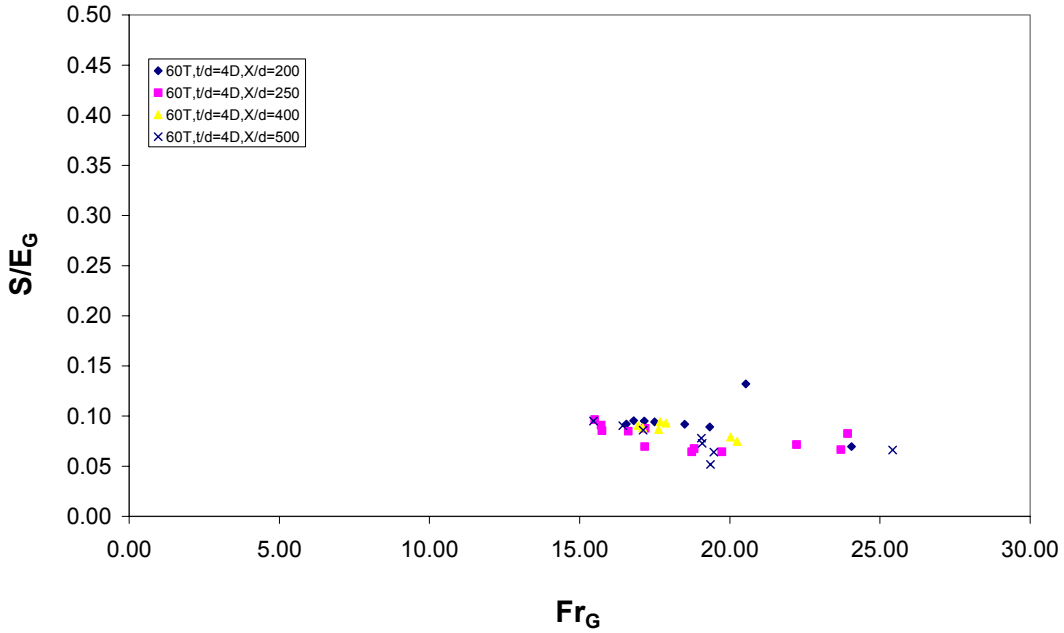

Figure D.9 S/E_G vs. Fr_G at t/d=4D

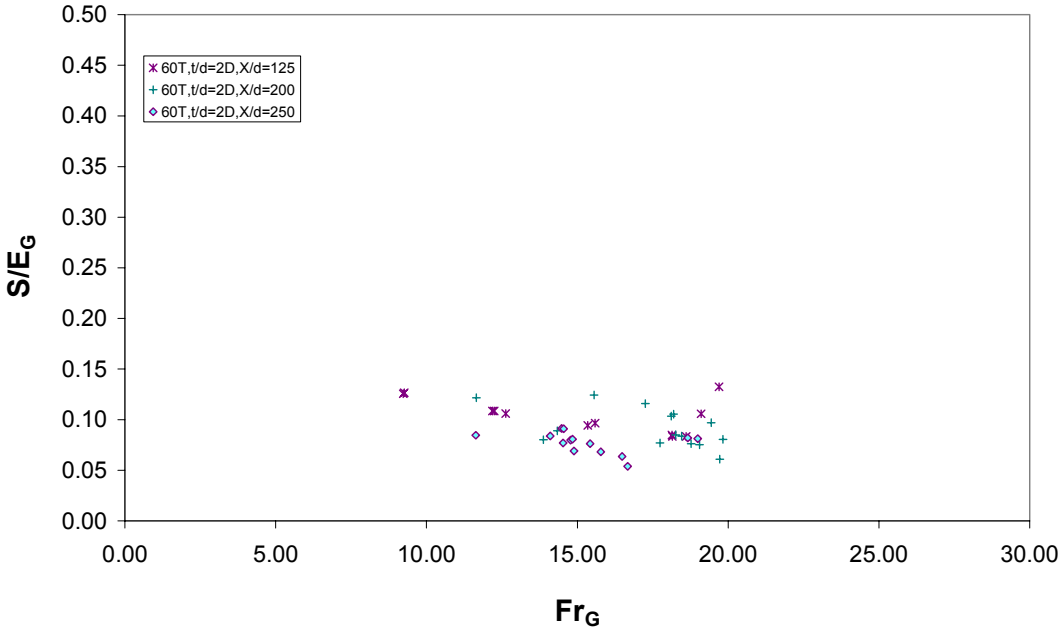

Figure D.10 S/E_G vs. Fr_G at t/d=2D

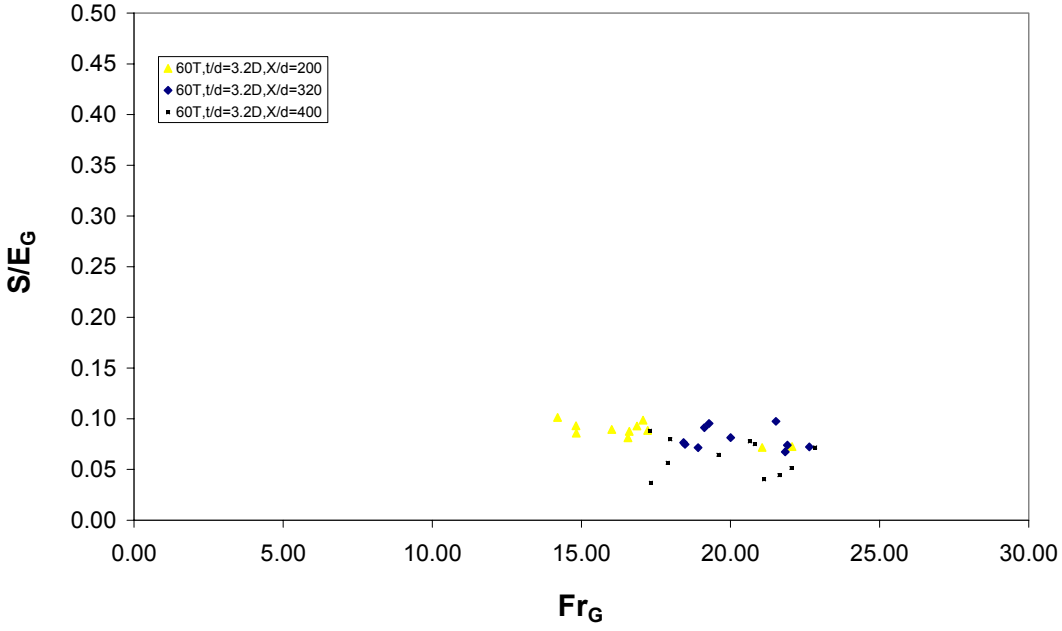

Figure D.11 S/E_G vs. Fr_G at t/d=3.2D

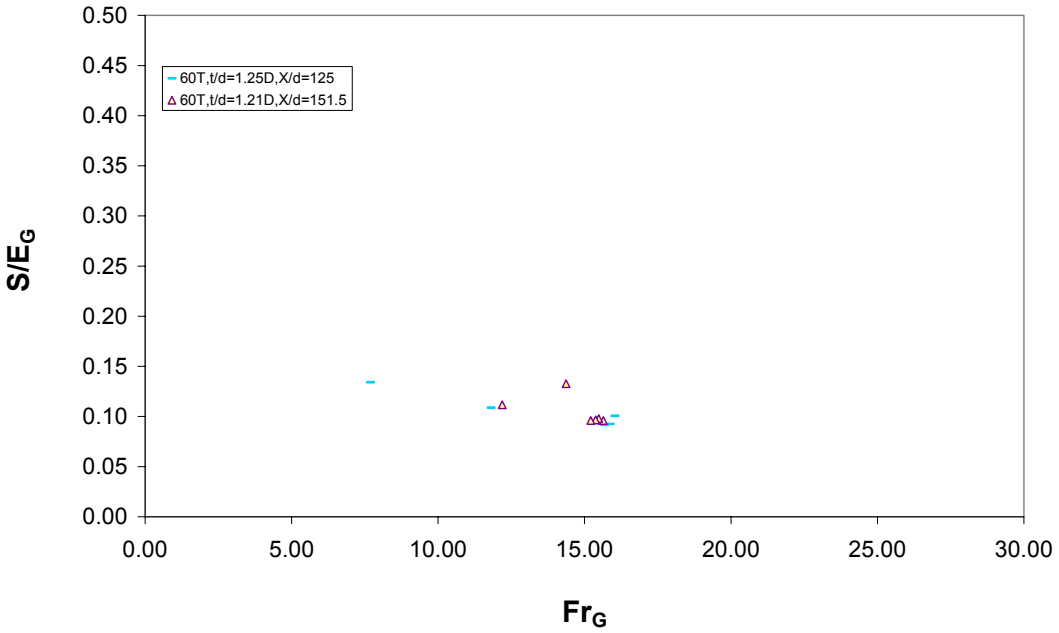

Figure D.12 S/E_G vs. Fr_G at t/d=1.25D

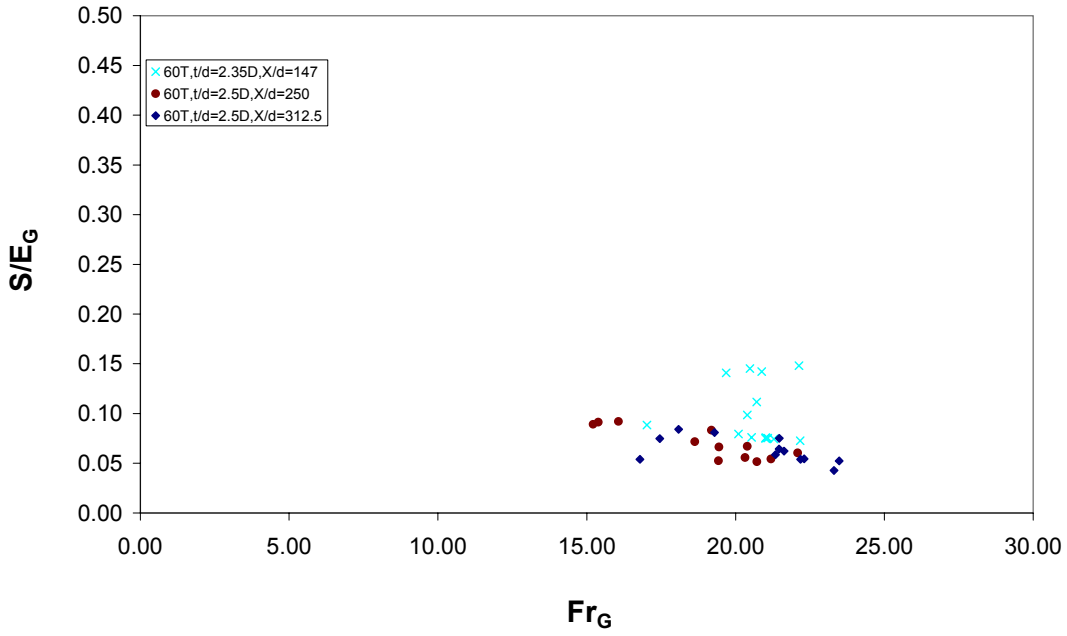

Figure D.13 S/E_G vs. Fr_G at t/d=2.5D

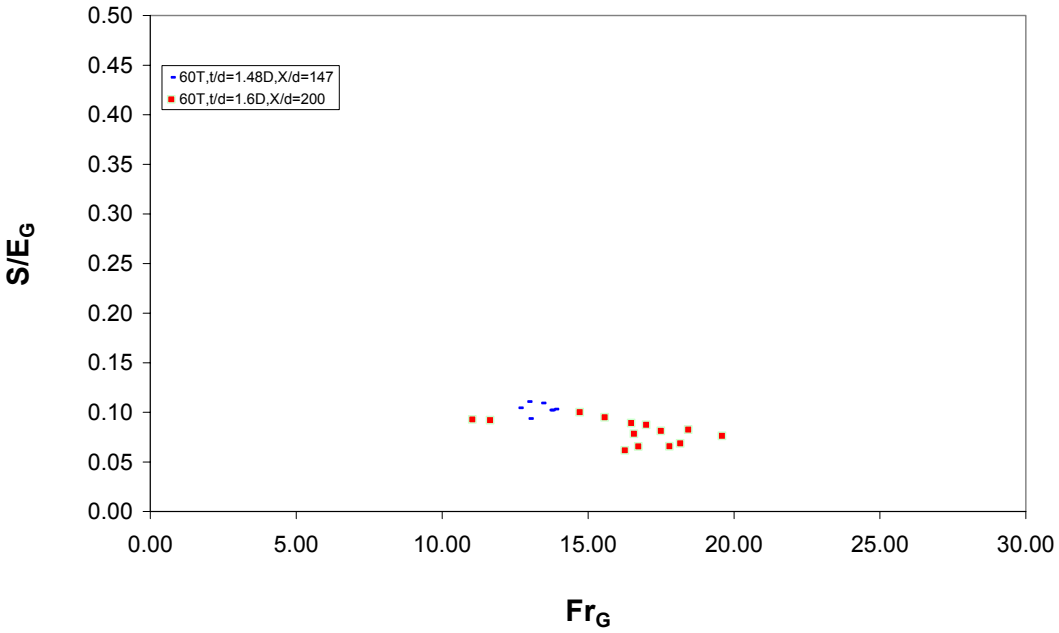

Figure D.14 S/E_G vs. Fr_G at t/d=1.48D

D.3 GRAPHICS FOR THE SYSTEM EFFICIENCY

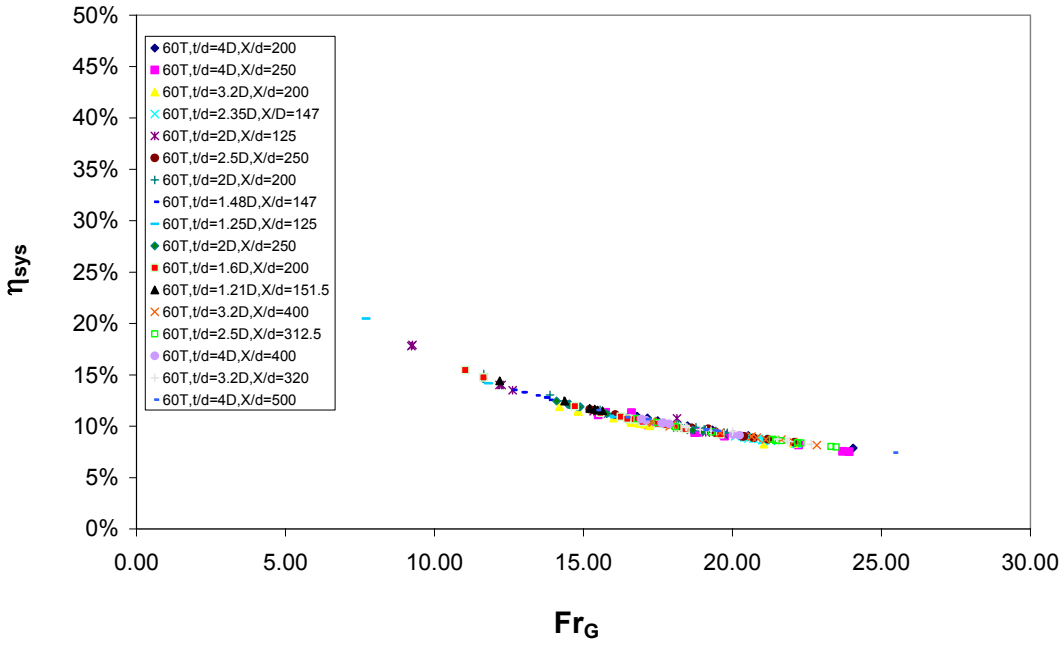

Figure D.15 η_{sys} vs. Fr_G for all of the present study data

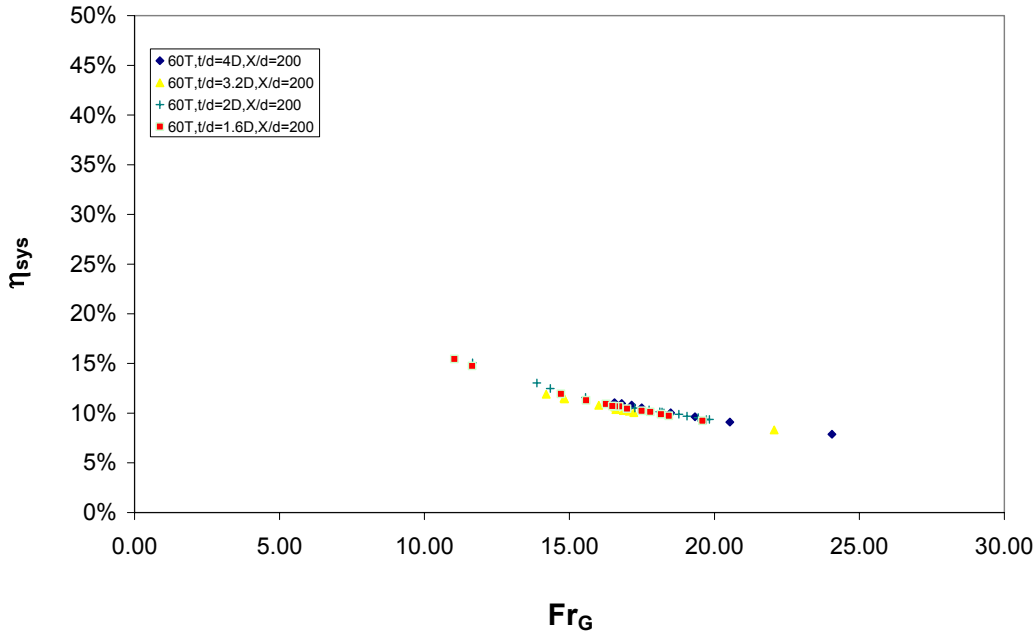

Figure D.16 η_{sys} vs. Fr_G at X/d=200

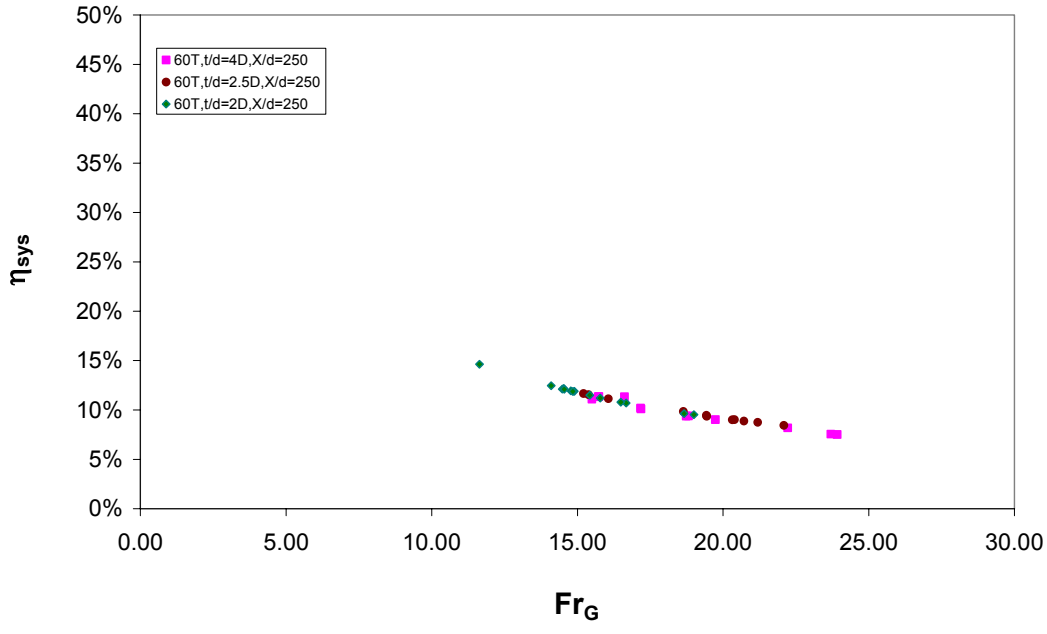

Figure D.17 η_{sys} vs. Fr_G at X/d=250

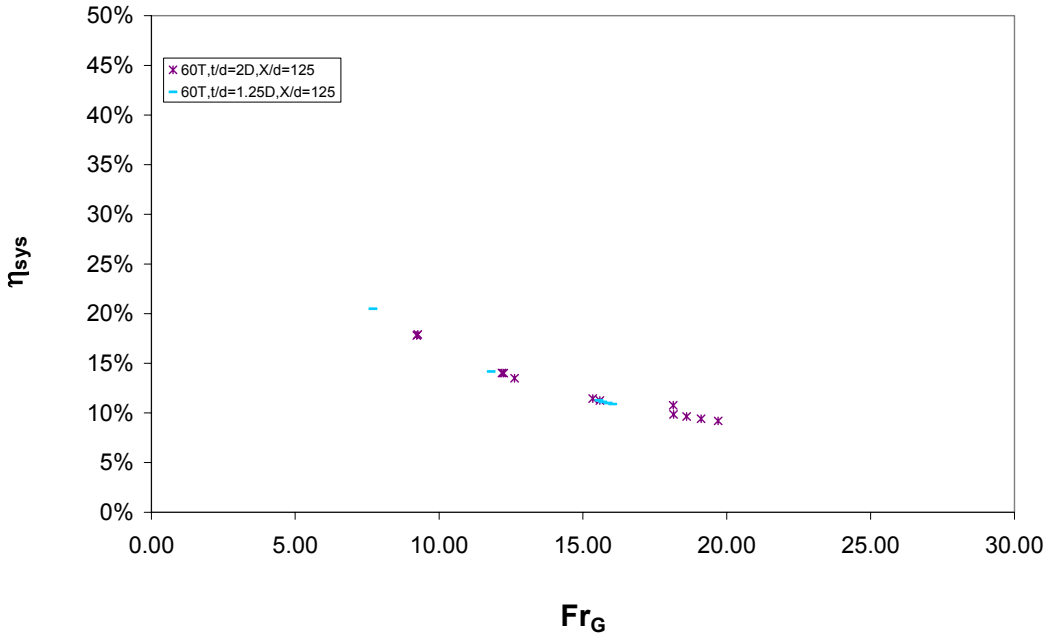

Figure D.18 η_{sys} vs. Fr_G at X/d=125

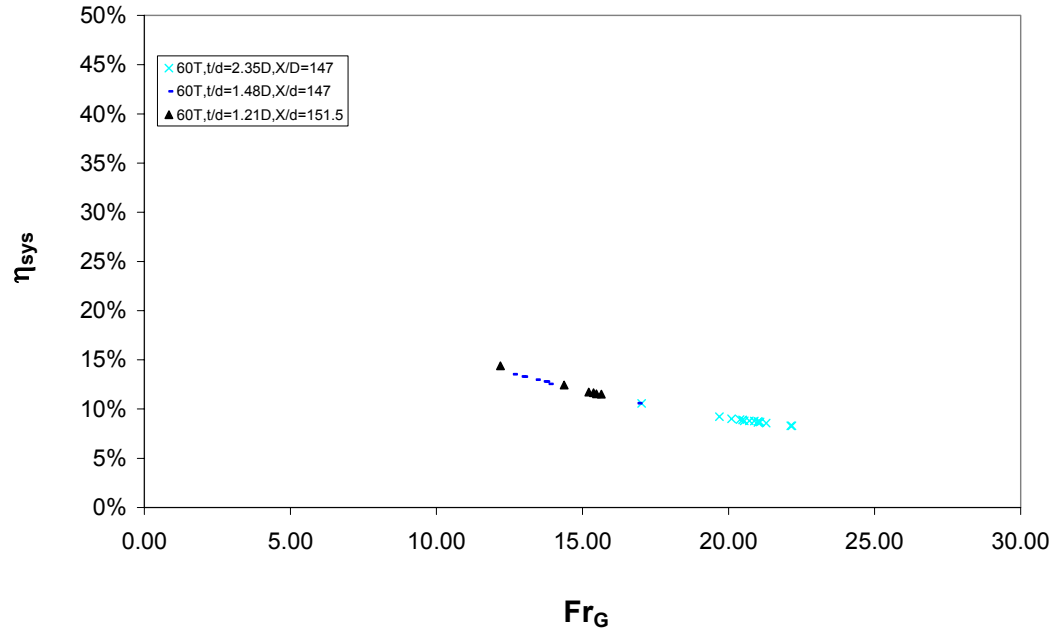

Figure D.19 η_{sys} vs. Fr_G at X/d=148

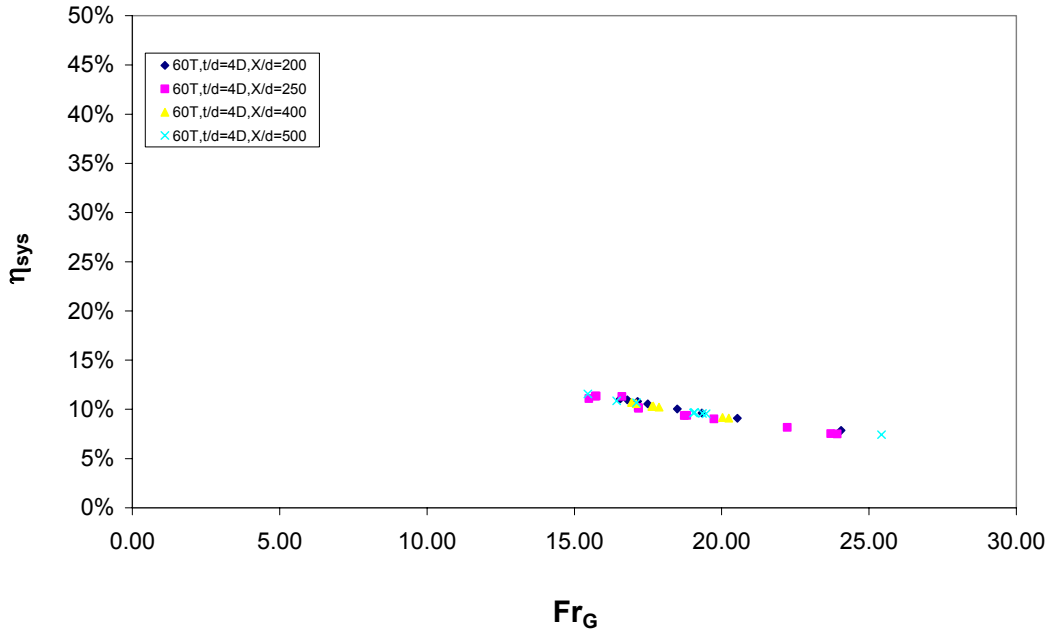

Figure D.20 η_{sys} vs. Fr_G at t/d=4D

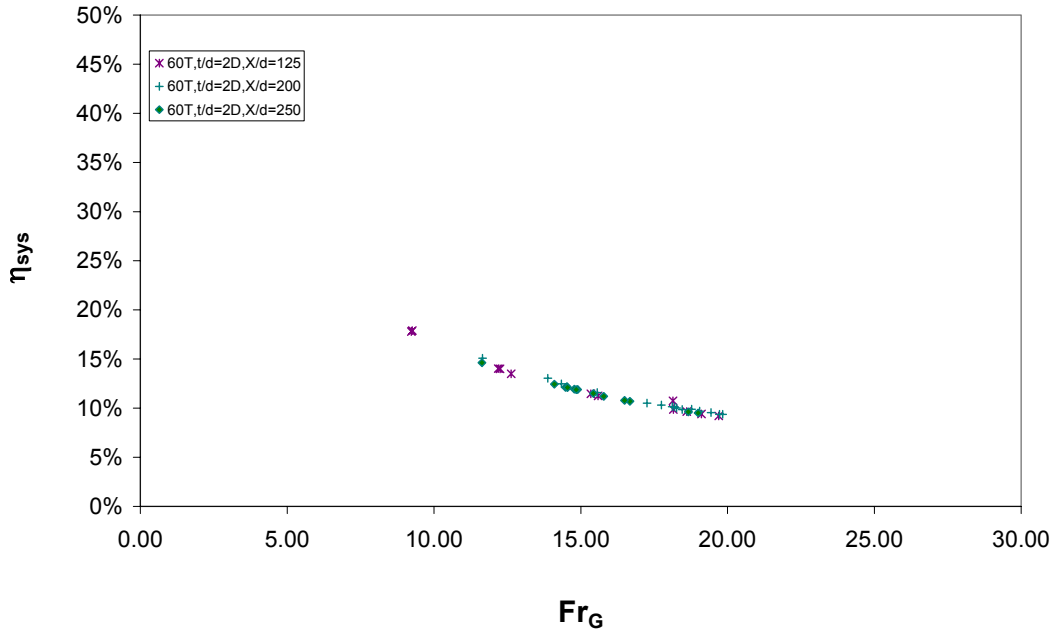

Figure D.21 η_{sys} vs. Fr_G at t/d=2D

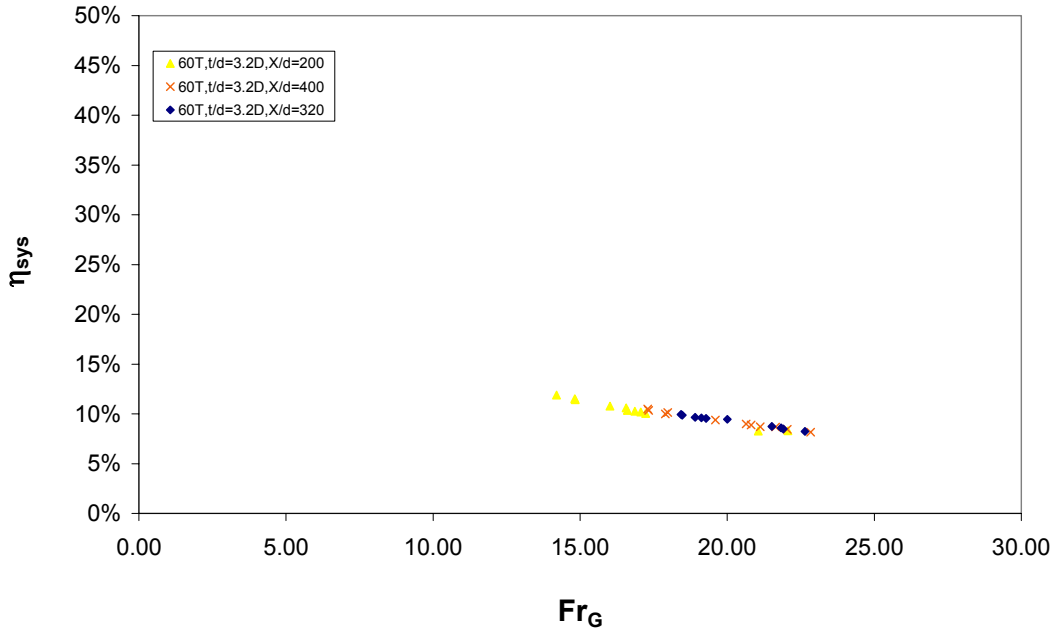

Figure D.22 η_{sys} vs. Fr_G at t/d=3.2D

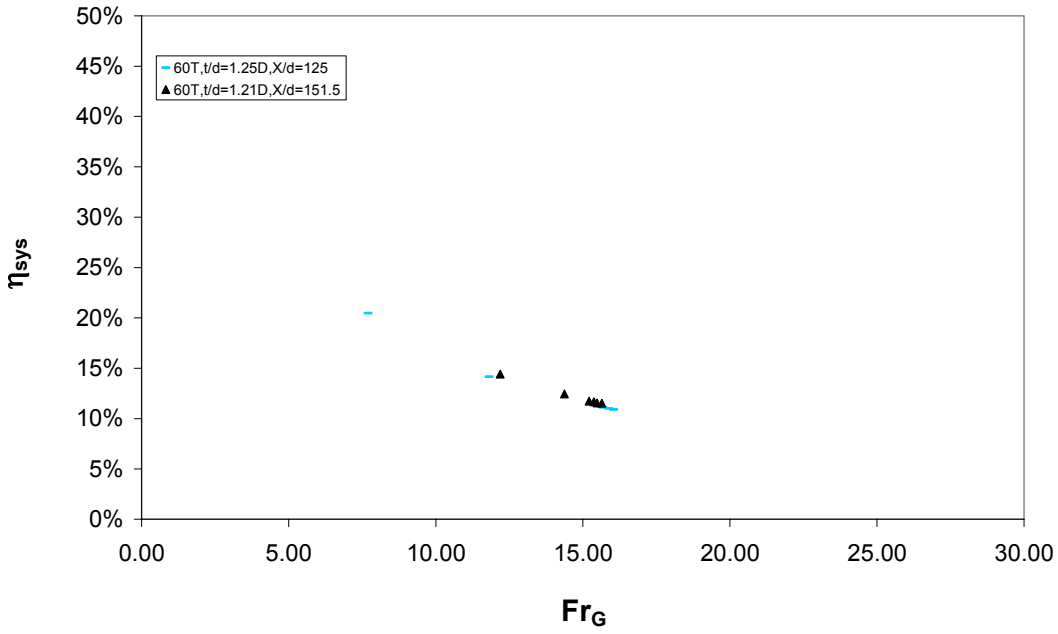

Figure D.23 η_{sys} vs. Fr_G at t/d=1.25D

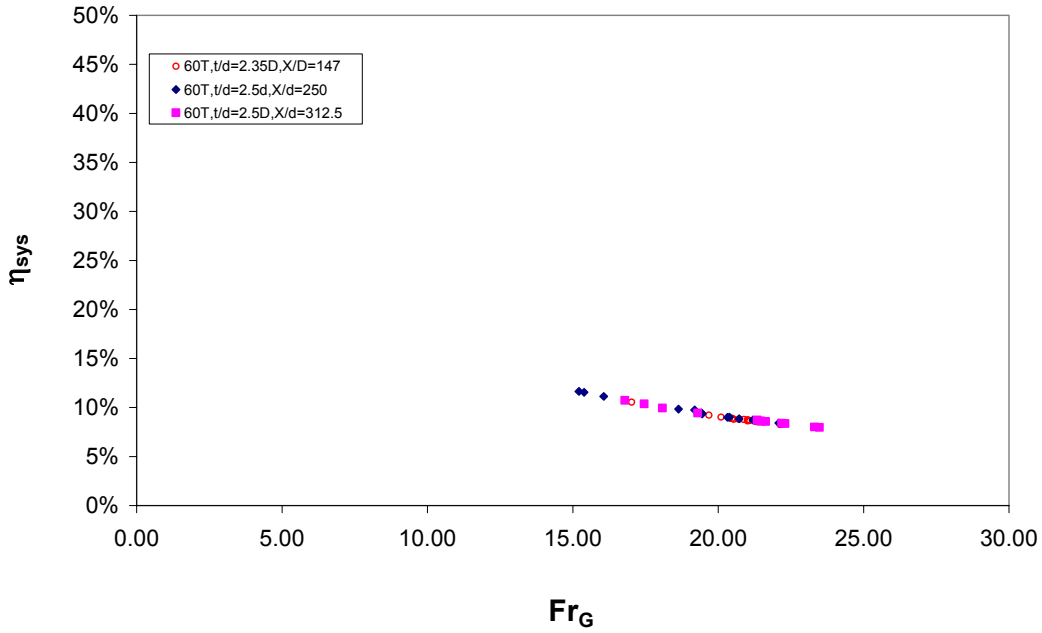

Figure D.24 η_{sys} vs. Fr_G at t/d=2.5D

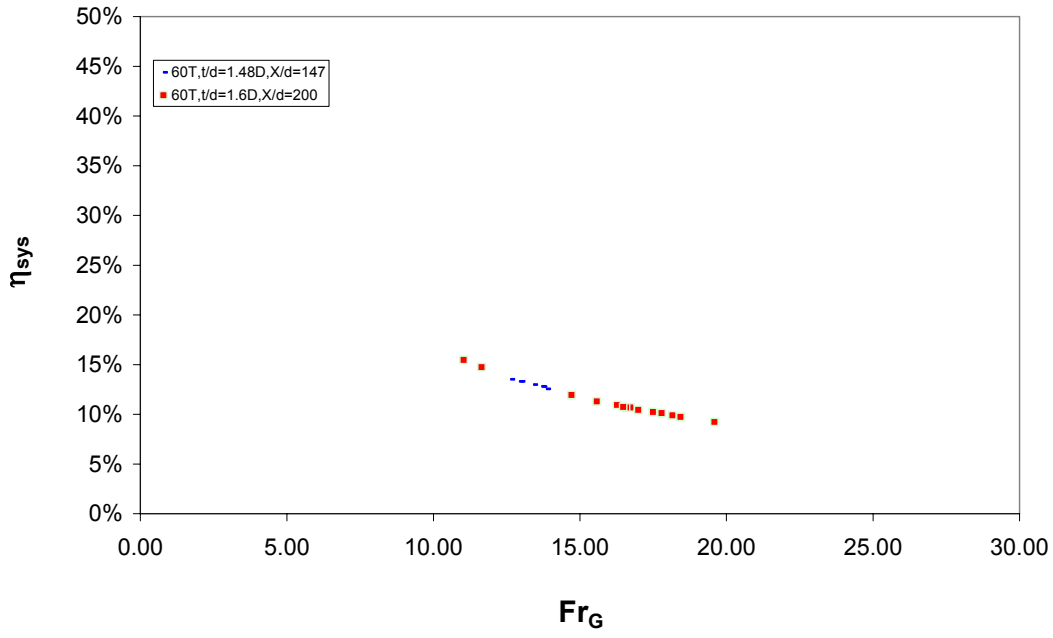

Figure D.25 η_{sys} vs. Fr_G at t/d=1.48D

D.3 GRAPHICS FOR THE SCREEN EFFICIENCY

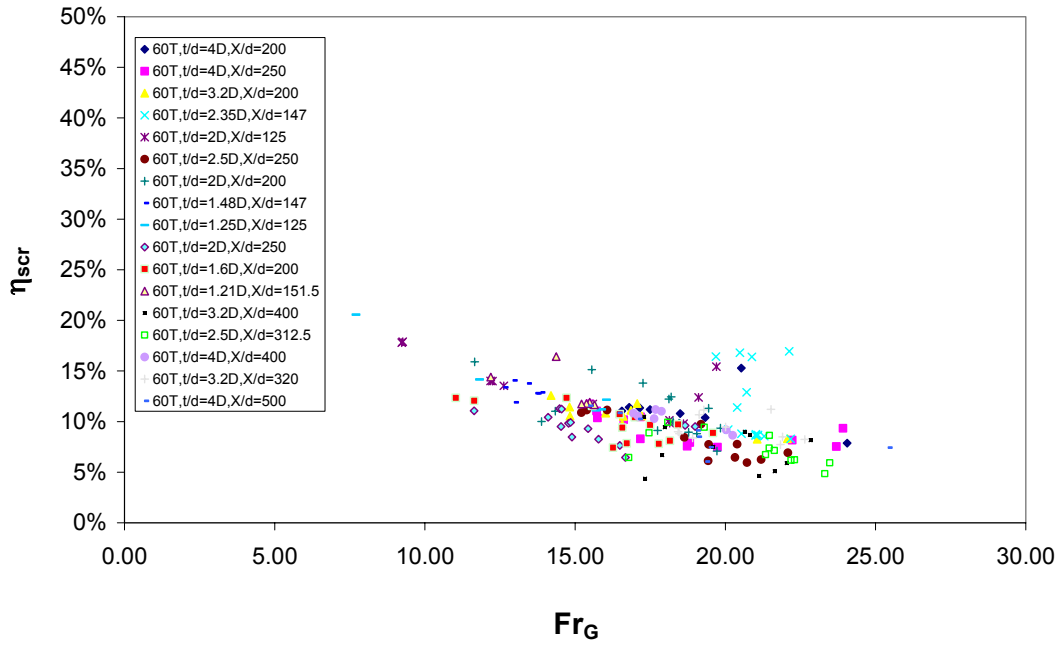

Figure D.26 η_{scr} vs. Fr_G for all of the present study data

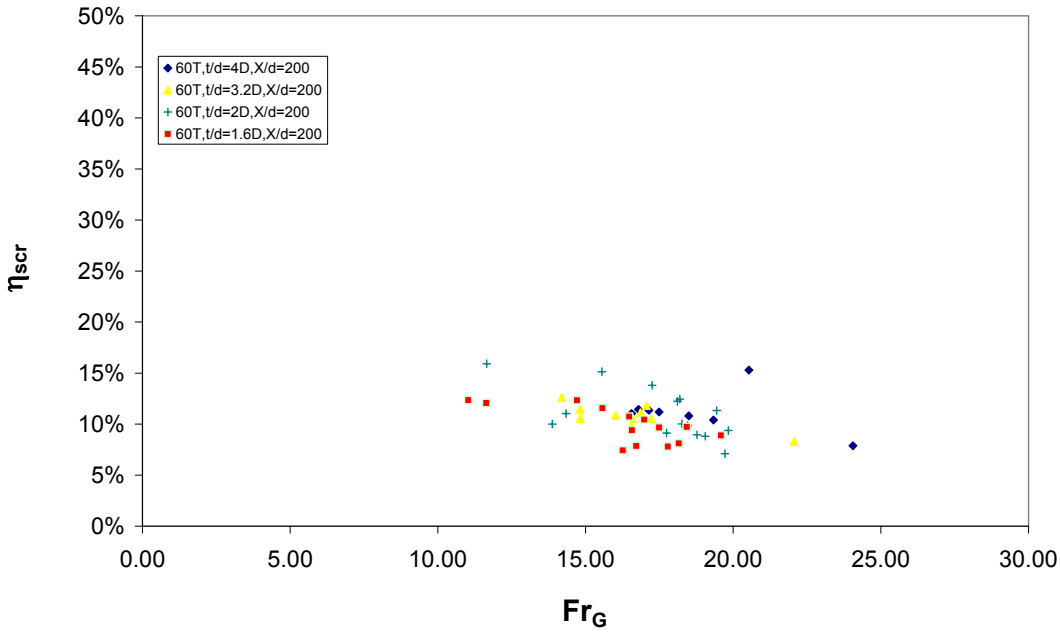

Figure D.27 η_{scr} vs. Fr_G at X/d=200

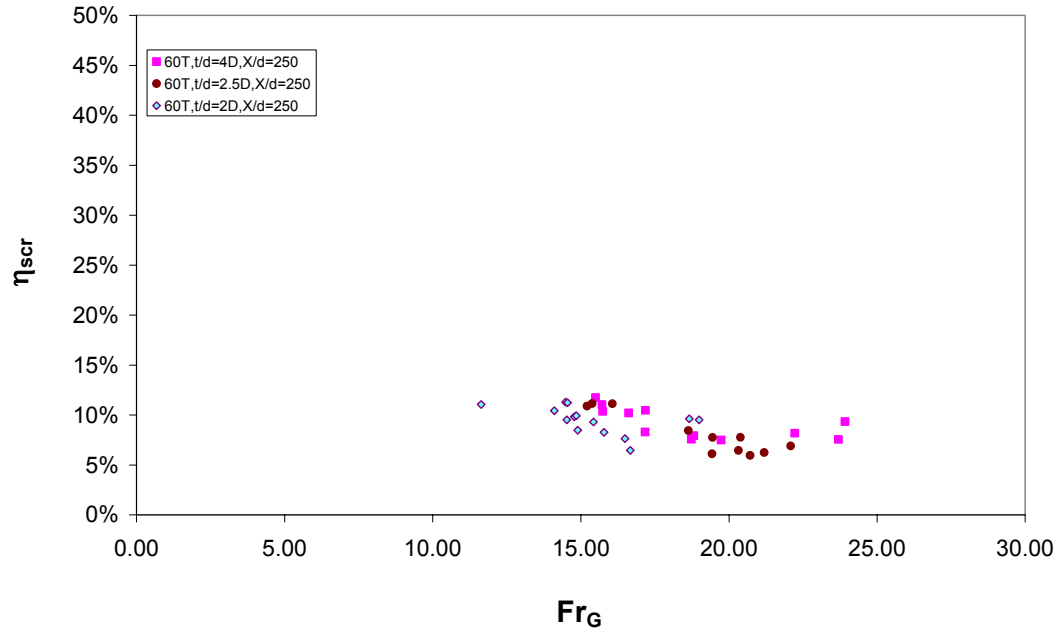

Figure D.28 η_{scr} vs. Fr_G at X/d=250

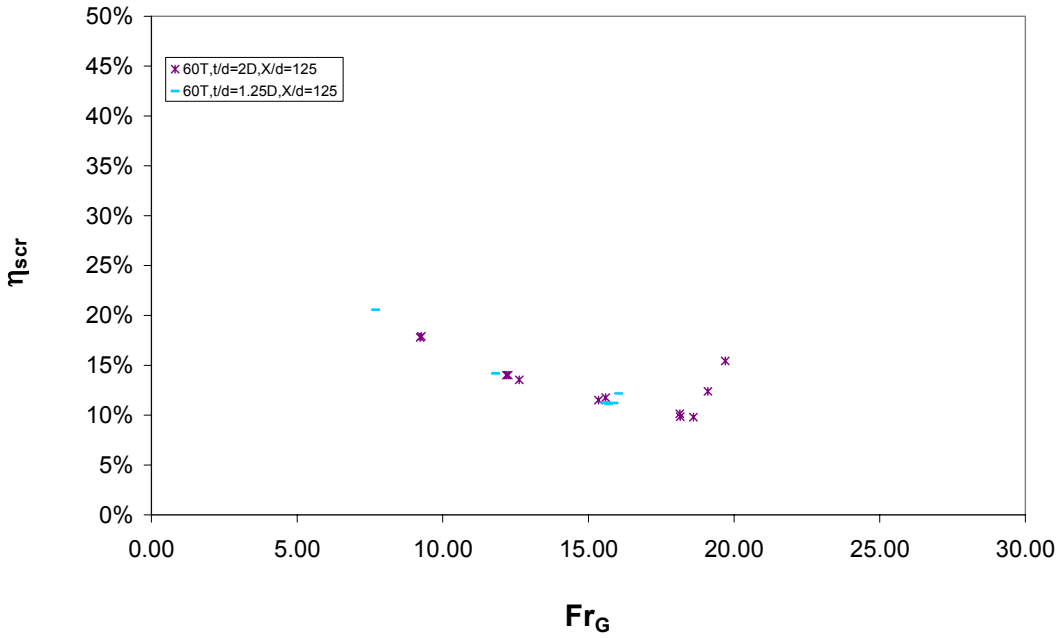

Figure D.29 η_{scr} vs. Fr_G at X/d=125

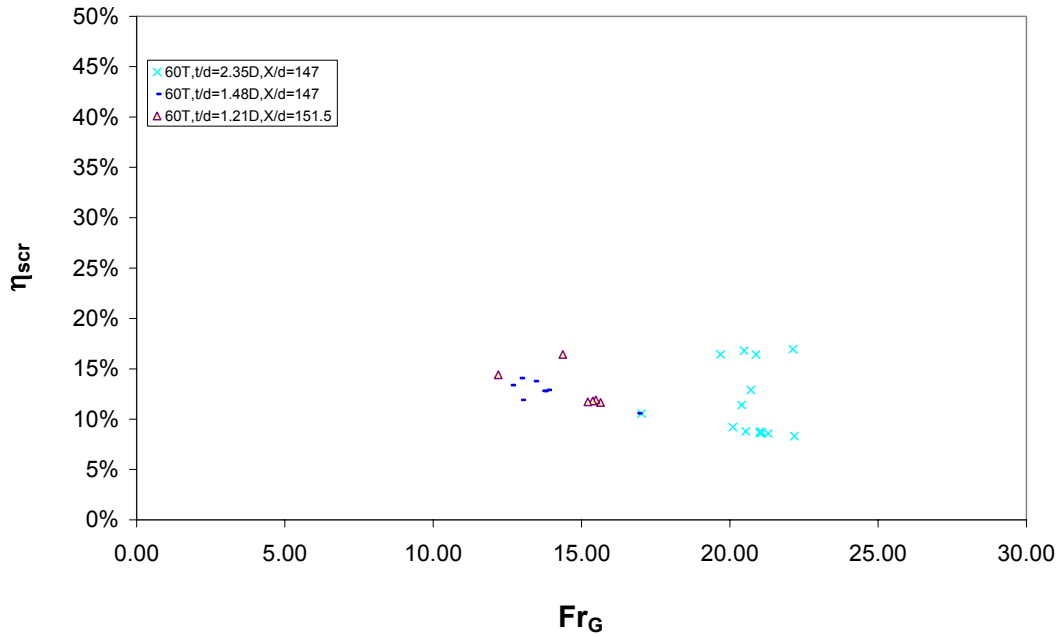

Figure D.30 η_{scr} vs. Fr_G at X/d=148

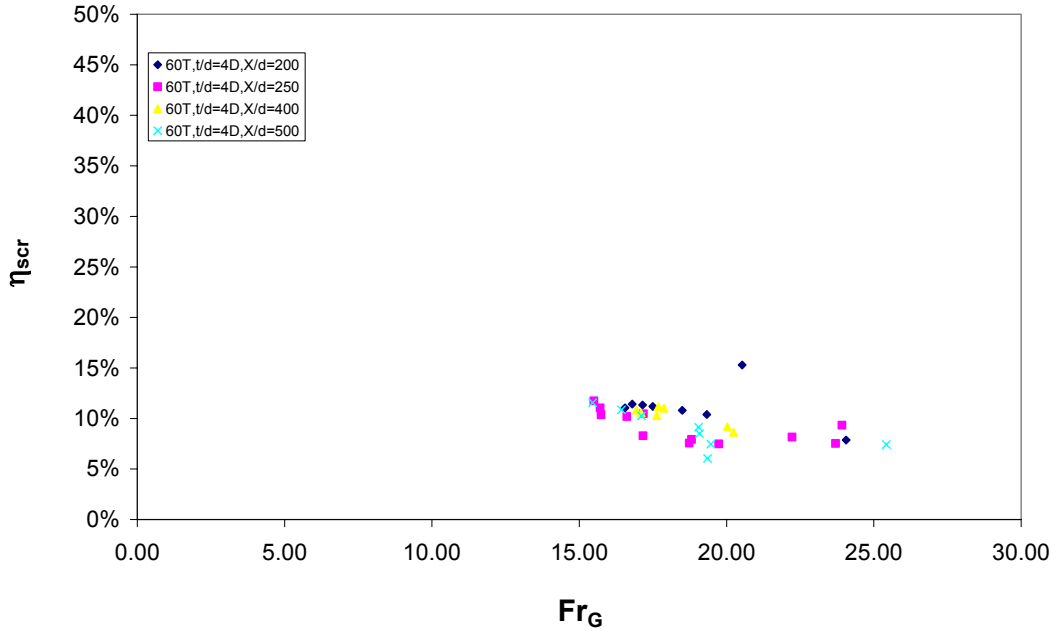

Figure D.31 η_{scr} vs. Fr_G at t/d=4D

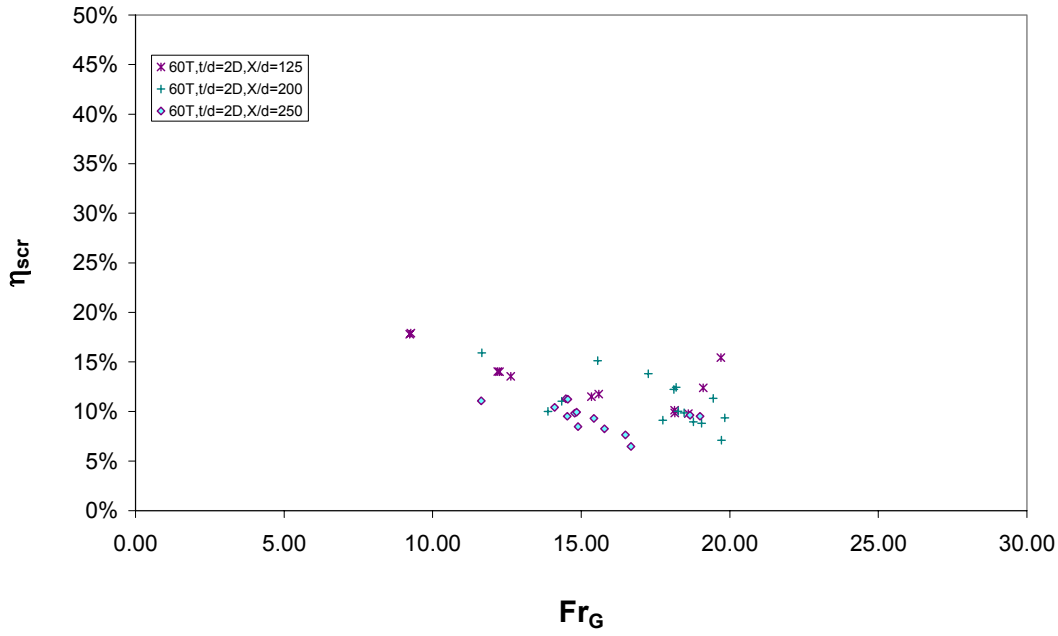

Figure D.32 η_{scr} vs. Fr_G at t/d=2D

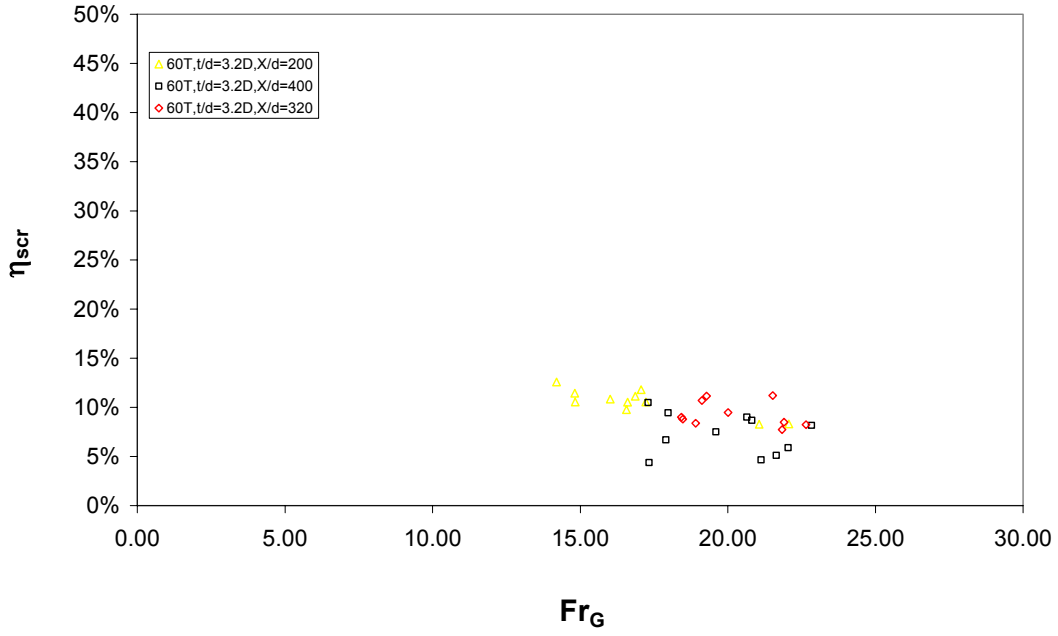

Figure D.33 η_{scr} vs. Fr_G at t/d=3.2D

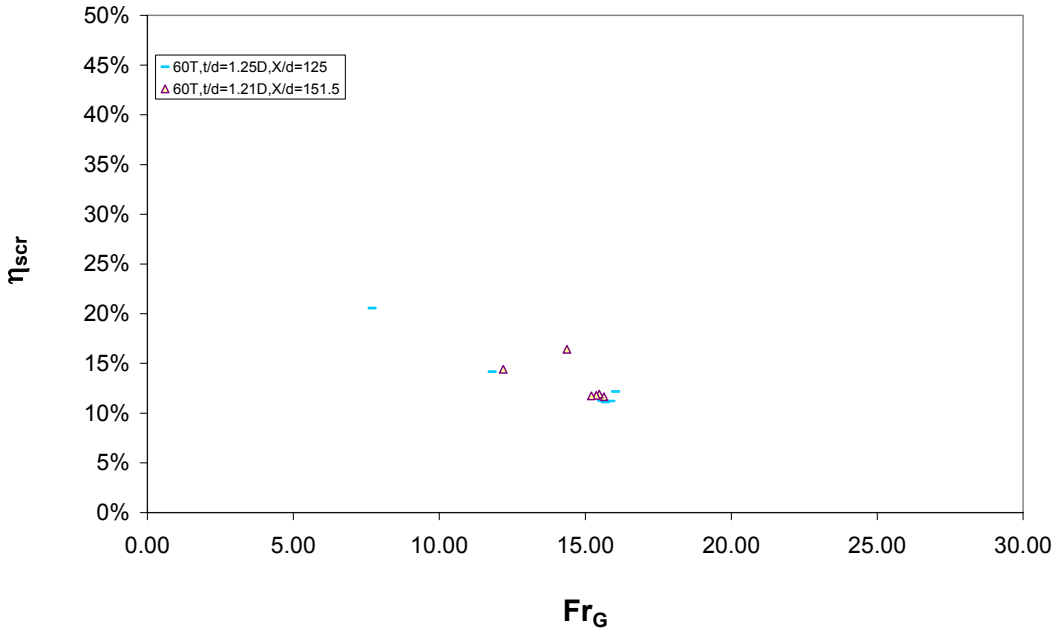

Figure D.34 η_{scr} vs. Fr_G at t/d=1.25D

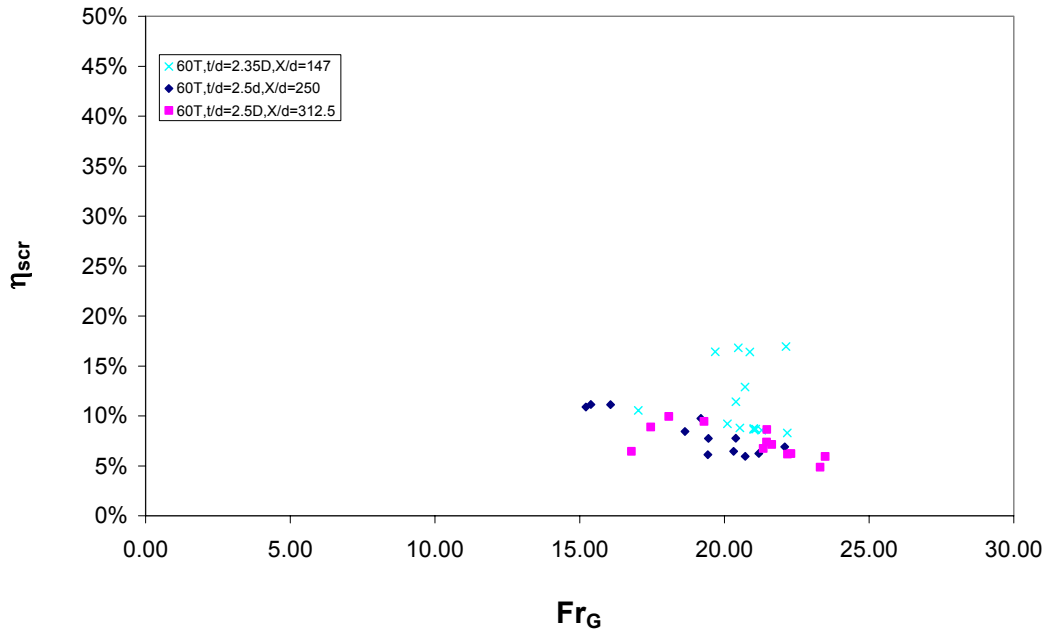

Figure D.35 η_{scr} vs. Fr_G at t/d=2.5D

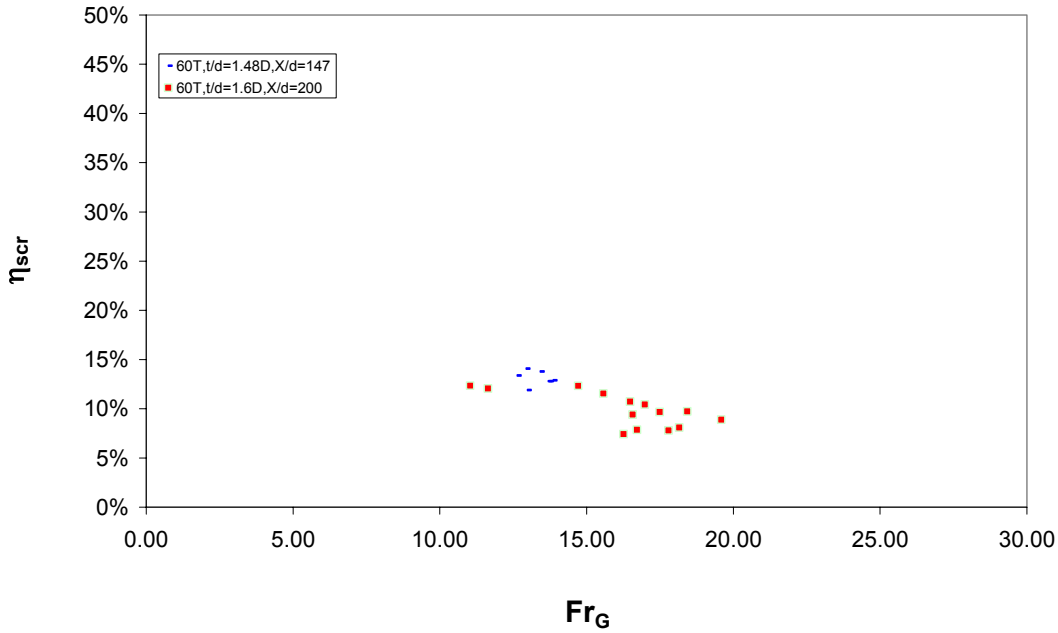

Figure D.36 η_{scr} vs. Fr_G at t/d=1.48D